Impacts of elevated temperature on the performance of compacted bentonite as a sealing material

A thesis submitted to the University of Manchester for the degree of

Doctor of Philosophy

in the Faculty of Sciences and Engineering

Linhua He

Department of Mechanical, Aerospace and Civil Engineering

2021

Contents

Word count: 34447

Nomenclature

A	the cross-sectional area (m^2)
a_s	Ca, Mg, K or Na in the extraction solution (mg/l)
a_{as}	the activity of the anhydrous smectite
a_{hs}	the activity of the hydrous smectite
a_{H_2O}	activity of the water
B	exchange capacity of the clay (meq/100 g)
b_l	Ca, Mg, K or Na in the blanks (mg/l)
C_0	groundwater at a dilute density (= 0.01 g/cm^3)
c	the volume of NH_4OAc used in extraction=(20)
D	dielectric constant of bulk fluid
D_r	the diffusion rate
d	half the distance between clay layers (m)
d_w	air-dried sample weight in gram
d_h	the average hydrodynamic diameter of the particles
e'	elementary electric charge (1.602×10^{-19} C)
e	the total void ratio
e_{macro}	macro pore ratio
e_{mirco}	micro pore ratio
G_s	the specific gravity
G_{xs}	excess mole Gibbs free energy of mixing
i	hydraulic gradient
i_0	threshold gradient
i_c	the critical hydraulic gradient
Q	the flux (m^3)
K	the diffuse double layer parameter(1/m)
K_h	the hydraulic conductivity (m/s)

K_{eq}	equilibrium constant of the interlayer hydration reaction
k_p	intrinsic permeability (m^2)
k	Boltzmann's constant (1.38×10^{-23} J/K)
mcf	moisture correction factor (=0.89)
m_{sm}	the molar mass of dry smectite (kg/mol)
n_0	the ionic concentration of the bulk fluid (number/m^3)
n	porosity of the clay
n_{micro}	micro porosity of the clay
n_c	number of moles of water in the interlayer adsorption or desorption reaction
n_s	the stacked layers of per particle
p	the swelling pressure (Pa)
R	gas constant (8.31 J/mol/K)
S	suction (MPa)
SSA_{tot}	total specific surface area measured by EGME
SSA_{ext}	the outer interlayer surface area
u	the nondimensional midplane potential
v_{il}	the specific molar volume of the interlayer water (m^3/mol)
W_{G1}	Margules parameter for the hydrous smectite
W_{G2}	Margules parameter for the anhydrous smectite
W_s	Margules parameter of the solid solution reaction
w	water content in percentage
X_{as}	mole fraction of the anhydrous smectite
X_{hs}	mole fraction of the hydrous smectite
X_{sm}	the mass fraction of smectite in the clay
y	the nondimensional potential at distance x from the clay surface
z	nondimensional potential at the clay surface
σ_{s1}	swelling pressure measured from free swell-compression test

σ_{s2}	swelling pressure measured from loading swell-compression test
σ_{cv}	swelling pressure measured from constant-volume test
θ_r	residual water content (-)
θ_{sat}	saturated water content (-)
ψ	the potential at distance x from the clay surface
ψ_0	surface potential of clay surface
ψ_d	the potential at distance d from the clay surface
μ_w	the dynamic viscosity of water ($Nm^{-2}s$)
γ_w	the unit weight of water (Nm^{-3})
ρ_d^{sm}	bulk dry density of smectite (kg/m3)
ξ	distance function
ε_0	$1/4\pi$ in the esu system
ρ_d	the bulk dry density of the clay (kg/m^3)
ρ_{im}	the density of the non-smectite minerals or impurities (kg/m^3)
$a,\ b,\ P_0,$ $\lambda,\ \eta,\ n_0^*,\ \alpha$	fitted parameters
$\Delta H_{r,T_0}^0$	the standard enthalpy of reaction at reference temperature
ΔC_p^0	he standard heat capacity of the reaction at constant pressure

List of Abbreviations

ATR	micro-attenuated total reflectance spectroscopy
CEC	cation exchange capacity
CCC	the coagulation critical concentration
DLS	dynamic lighting scattering
DDL	diffuse double layer theory
EBS	the engineered barrier system
EGME	ethylene glycol monoethyl ether adsorption method
EDXRF	energy-dispersive X-ray fluorescence
FTIR	fourier-transform infrared spectroscopy
HLW	high-level radioactive waste
SEM	scanning electron microscope
TEM	transmission electron microscopy
P&A	permanent plugging and abandonment for wells

Abstract

Compacted bentonite clays as engineered barrier can be exposed to elevated temperature (i.e., due to the decay heat from waste in HLW disposal, and the geothermal around oil and gas wells). Understanding the temperature effects on hydro-mechanical behaviour of bentonite is important for the design and performance assessment of engineered barrier systems and plugging and sealing the wells and boreholes. The clay barrier is expected to maintain a high swelling pressure, low hydraulic conductivity, and long-term integrity under elevated temperatures. This thesis presents an investigation of temperature effects on swelling pressure development, hydraulic conductivity, and erosion behaviour of compacted bentonite at a range of dry densities.

A bespoke high-pressure, high-temperature constant rate of strain system (CRS) was designed and constructed to conduct two series of investigations on: i) the hydro-mechanical properties of Volclay bentonite compacted at different temperature ranging from 20°C to 80°C during and after saturation; and ii) the erosion behaviour at elevated temperatures. The experiments of the first series were carried out on a range of compacted samples (dry densities 1.1, 1.4 and 1.7 Mg/m^3). The results showed that with the increase of temperature, the swelling pressure decreases whilst the hydraulic conductivity increased. Furthermore, the rate of swelling pressure development was found to be considerably enhanced at elevated temperatures. The results indicated that the hydro-mechanical response of the clay to elevated temperature is strongly linked with the exchange of pore water in clay microstructure, which is facilitated by the reduced retention capacity of water in the clay system and by changes to the viscosity and density of water.

The diffuse double layer theory (DDL) was revisited to include micro/macro aspect of clay system for the calculation of swelling pressure. A model for swelling pressure of compacted bentonite at different temperatures was proposed. It combined the regular solid-solution theory and the diffuse double layer theory into a thermodynamic framework for the evolution of hydrous and anhydrous smectite at different temperatures. This new model was assessed by comparing the predicted swelling pressure and experimental data for calcium bentonite and sodium bentonite. The results showed that the consideration of temperature effects on pore evolution and distance between clay aggregates improves considerably the prediction of the swelling pressure by DDL at elevated temperature. The research presented offers an improved method for assessing the swelling pressure development of compacted bentonite, which incorporates the evolution of micro/macro pore at elevated temperature.

The experimental results of erosion of compacted bentonite at elevated temperature showed that the concentration of the eroded bentonite particles increased with increasing temperature. The results indicated that bentonite erosion does not significantly reduce the physical stability of a generic bentonite plugs for applications in plugging and abandonments of wells. However, the temperature effects on chemical transport processes in compacted clay requires further studies to underpin safety assessment of bentonite plugs.

Declaration

I declare that no portion of this work referred to in this thesis has been submitted in support of an application for another degree or qualification of this or any other university or other institute of learning.

Copyright

Acknowledgements

The whole research in this thesis was supported by the joint scholarship of the China Scholarship Council and the University of Manchester. I sincerely thank the China Scholarship Council and the University of Manchester for providing financial support throughout my PhD study.

I must express my sincerely gratitude to my supervisors, Prof Andrey P Jivkov and Dr Majid Sedighi, Dr Mojgan Hadi Mosleh. I would like to sincerely thank to Dr Sedighi. The academic guidance and inspiration and firmly support he gave me help me cope with different issues that I met and realise this milestone. Without his contribution, I couldn't reach so far. I am grateful to Prof Jivkov for his extensive passion and invaluable academic guidance. That really inspired me no matter in academic work but also in daily life. I would like to express my thanks to Dr Mosleh for her technical comments and encouragement for my experimental work and write-up work.

A special thanks to Sonya and Ziheng Wang for their help in the preparation of laboratory work. Sincerely thanks to Ziheng who has contributed to the dynamic light scattering measurement. I am also grateful to Huaxiang Yan and Tian Chen for assisting me in computer programming and for their invaluable friendship.

I am thankful to the staff in Parsier building including Ross, Mel, Phill, Stuart, Alex, Alan for their help, care and advice in lab.

I would like to express my truly thanks to Dr Qingrong Xiong, Dr Chenyuan Lin, Dr Shanshan Qin, Dr Jiangmin Wang, Dr Kangpei Meng. Weiqiang Chen, Cong Yao, Puyu Shi, Siying Zhu, Chundi Feng, Dr Janis Castins, Fatemeh Shahbazi, Muhammad Omer, Suleyman Bulbul, Dr Bashar Ismael, Ogbonnaya Chukwuma, Amin Deyranlou, Dr Elijah Borodin.

Finally, a great thank to my family for their selfless support and love. Their continuous encouragement helped me through a lot in these years.

CHAPTER **ONE**

1. Introduction

1.1. Research background and motivations

The waste generated by extraction and mining, oil and gas production, and nuclear activities requires safe isolation to protect the geo-environment (IEAE, 1983; Yong et al., 2006). Without appropriate isolation, the migration of pollutants can result in huge cost of land remediation and incalculable consequences for the preservation of water resources. Therefore, it is necessary to develop a better understanding of the challenges in geo-environmental engineering and to improve the knowledge and technologies for management of geo-environmental resources (Yong et al., 2006; Sedighi, 2011; Bag, 2011).

Bentonite is a natural clay, which forms from volcanic ash and contains a large proportion of montmorillonite (Pusch and Yong, 2006). Montmorillonite is a typical smectite clay mineral with a three-layer crystalline structure. Bentonite has been recommended and used for plugging water wells, oil and gas wells, seismic shot holes, mining shafts and exploratory holes (e.g., James, 1996; Wheaton et al., 1994; Englehardt et al., 2001; Holl and Scheuermann, 2018; Holl, 2019; Towler et al., 2020). Bentonite-based materials are also considered for one of the engineered barriers in the geological disposal facilities for high-level radioactive waste (HLW) (SKB, 2011; ENRESA, 2000; JNC, 2000; NAGRA, 2002; AECL, 1994; ANDRA, 2005; NDA, 2010; CAEA, 2006). As shown in Fig.1.1, the multi-barrier sealing system is comprised of waste canister, clay buffer material, and host rock (natural geology). The gap between host rock and canister is filled with compacted clay buffer. At the time of emplacement, the clay buffer is partially saturated and undergoes a non-isothermal re-saturation phase at which the clay buffer exerts a relatively large swelling pressure to the canisters and the host rock.

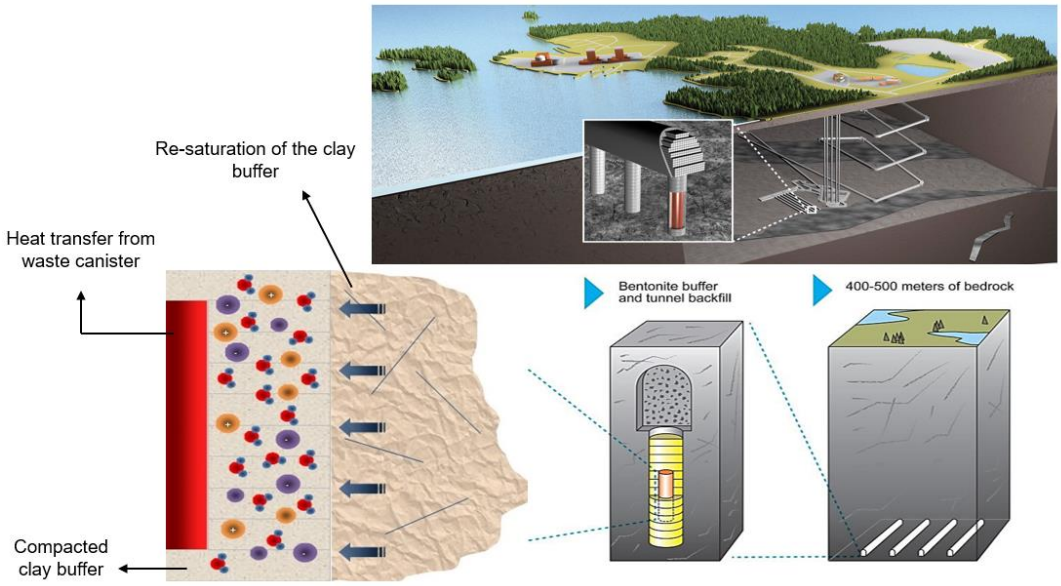

Fig. 1.1. The sealing system for geological disposal of high-level radioactive nuclear waste (Image from Posiva Oy, 2020).

Another application of bentonite as an engineered barrier is to seal abandoned oil and gas wells. Permanent plugging and abandonment (P&A) is necessary to minimise the leakage of hydrocarbons to the surrounding biosphere and atmosphere through the wellbore and preferential pathways. As shown in Fig.1.2, previous studies have revealed critical problems with the performance and integrity of cement due to potential cracking and corrosion under certain fluid composition, temperature and pressure conditions that can lead to the failure of isolation zone (e.g., Celia et al., 2005; Davies et al., 2014; Kiran et al., 2017; Ahmed and Salehi, 2021). Cement has been traditionally used for plugging of wells. However, this solution has been challenged due to insufficient knowledge of the integrity and long-term sustainability of such plugs (Flopetrol, 2019; Achang et al., 2020). There is a pressing need to develop new techniques and apply alternative sealing materials with efficiency in the complex downhole conditions for the abandonment of wells.

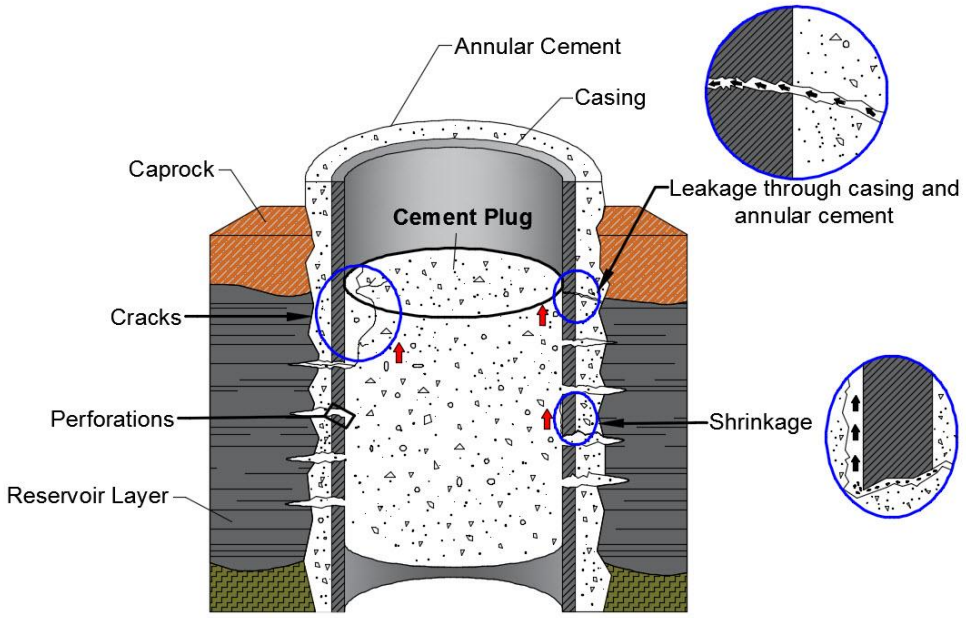

Fig. 1.2. Potential pathways for leakage along an abandoned well (after Celia et al., 2005).

At present, many hydrocarbon wells across the major fields such as North Sea and Golf of Mexico are approaching a stage that the production is no longer profitable or feasible (Davies et al., 2014; Celia et al., 2005; Kang et al., 2016). In the standard of NORSK (2004), alternative plugging materials are explored to meet the requirements for performance and safety prescribed for cement-based plugs. The success of field trials in many regions have introduced changes in the regulations by recommending bentonite as an alternative plugging material for well plugging (Englehardt et al, 2001; Carl, 2004; Towler et al., 2016). In terms of using clay plugs in well abandonment, bridging/clogging and early hydration during operational process are the challenges in the placement of the bentonite plugs (AMEC, 2016). The fundamental knowledge regarding the hydration process and swelling behaviour of compacted bentonite needs to be well understood for the use of bentonite plugs in different well conditions (e.g., high temperature and high-pressure wells).

The thermal, hydraulic, mechanical, and chemical phenomena in the sealing process are highly coupled (e.g., Dixon et al., 1999; Börgesson et al., 2001; Rutqvist et al., 2001; Singh, 2007; Pusch, 2008; Lloret and Villar, 2007; Cleall et al., 2013; Gens

et al., 2021; Pogacnik et al., 2016; Pandey et al., 2017; Li et al., 2021). The clay buffer in the disposal of HLW is expected to experience a period of 100 to 10,000 years under elevated temperatures arising from the radiogenic heating sources inside canisters (Pusch and Yong, 2006; Sedighi, 2011). The management of HLW needs to consider the implications caused by heating from waste. In the majority of geological disposal concepts, temperature is required to be maintained below 100°C through spacing between heat generating canisters (Bel and Bernier, 2001; JNC, 2000; SKB, 2006; ANDRA, 2005; Johnson et al., 1994; Sedighi, 2011). In the context of well plugging, the geothermal gradient is influenced by the depth of wells. Average temperature at 2000 m depth is likely to be approximately 60°C in the UK (Busby, 2010). Importantly, the natural geothermal gradient at the location of the plugs will influence the evolution and performance of a borehole seal following emplacement. Maintaining a high swelling pressure and very low permeability under elevated temperatures is a key performance criterion for the clay buffer to control the potential release and migration of highly toxic radionuclides to the surrounding biosphere. Elevated temperature is expected to affect the important hydraulic properties and mechanical behaviour of clays, which is associated with the evolution of sealing material.

In literature, there are two conflicting observations regarding the temperature effect on swelling pressure of compacted bentonite: i) swelling pressure increases with increasing temperature (e.g., Cho et al., 2000; Pusch et al., 1990; Bag and Rabbni, 2017; Ye et al., 2013); ii) swelling pressure decreases with increasing temperature (e.g., Lingnau et al., 1996; Villar et al., 2010). The swelling process and the associated swelling pressure dynamics under elevated temperature are not fully understood. For evaluating the feasibility and optimizing the performance of bentonite clay, it is important to develop a better understanding and improve the knowledge of temperature effects on the swelling behaviour of compacted bentonite.

The bentonite clay will swell instantly when subjected to water and fill the voids or cracks, providing sufficient sealing of the repository. Due to the restricted condition,

the generated swelling pressure acts uniformly on the surroundings, which may cause the rock failure in sealing repositories (Pusch and Yong, 2006; Sellin and Leupin, 2013). The development of swelling pressure is a key function of the barrier material. It requires to be high enough to ensure good sealing performance without disturbing the stability of the host rock (Karnland et al., 2010; Wang et al., 2012; Li et al., 2010; Delage et al., 2010). The swelling pressure of bentonite is dependent on many factors such as the density, the concentration in pore water, water content, and compaction method (Komine and Ogata, 1999; Wang et al., 2012; Karnland et al., 2008; Pedarla et al., 2012; Zhu et al., 2013; Bag, 2011). Several methods including empirical and semiempirical models, diffuse double-layer models, molecular dynamics simulation, and thermodynamic models have been developed for the estimation of the swelling pressure (Fredlund, 2006; Singhal et al. 2014; Tu and Vanapalli 2016; Sato, 2008; Schanz et al., 2013; Sun, 2017; Sun et al., 2015; Hsiao and Hedström, 2017; Du et al., 2021).

The pore structure of compacted bentonite can be altered during heating and drying processes, which impacts on the hydraulic properties and the mass transport (e.g., Ma and Hueckel, 1993, Saiyouri et al., 2000; Salles et al., 2009). The complex pore space, with pore sizes spanning several orders of magnitude, contributes to the differences in water types and their properties in bentonite (Kozaki et al. 2008; Bradbury and Baeyens, 2002; Bourg et al. 2003; Wersin et al. 2004). The pore size distribution is of great significance for understanding how transport by diffusion occurs in bentonite (Appelo, 2013). The evolution of the micro/macro fabric system of compacted bentonite at elevated temperature contributes to the change of pore size distribution.

The presence of groundwater flow can potentially erode bentonite because of generating colloidal particle of bentonite (Bessho and Degueldre, 2009; Albarran et al., 2014). The effect of bentonite colloids on contaminants transport has been studied for evaluating the stability of bentonite and performance assessment (Möri et al., 2003; Missana et al., 2008; Albarran et al., 2011; Bouby et al., 2011). Previous studies focused

on the surface erosion of bentonite particles caused by a groundwater flow at the interface of a compacted bentonite, i.e., considering the effects of the inflow rate and ionic strength of the groundwater (Baik et al., 2007; Missana et al., 2003), but without thermal effects that could exist in nearfield scenarios. The above overview reveals a knowledge gap: the effect of temperature on the sealing performance and erosion behaviour of bentonite with different dry densities is poorly understood, but of significant practical importance in geotechnical applications.

1.2. Aim and objectives

The aim of this research is to advance the understanding of the temperature effects on hydro-mechanical behaviour of compacted bentonite as a sealing material. The work consists of experimental and theoretical studies. The laboratory experiments involve the measurements of swelling pressure and hydraulic conductivity at various dry densities as well as the colloid generation from the erosion of compacted bentonite. Two immediate areas of applications of the new knowledge created in this research are:

(1) Compacted bentonite buffer in the context of geological disposal of high-level radioactive waste; and

(2) Compacted bentonite as alternative plug for hydrocarbon well abandonment.

The experimental programme of research aims to develop the fundamental knowledge required on the performance of the bentonite-based sealing in these two applications. The specific objectives of the project are as follows:

(1) To quantify the swelling pressure development and the evolution of hydraulic conductivity of compacted bentonite during hydration and under different temperatures through laboratory tests;

(2) To develop an understanding of the effects of microstructure evolution of compacted bentonite under different temperatures on swelling pressure and hydraulic performance;

(3) To develop an assessment model for swelling pressure by integrating the regular solid solution model into the diffuse double layer model;

(4) To evaluate the micro/macro evolution of saturated clay and the swelling pressure development under elevated temperature.

(5) To investigate the erosion behaviour at elevated temperature.

1.3. Outline of the thesis

Chapter 1 summarizes the research background, the aims and objectives of the study, and outlines the structure of this thesis.

Chapter 2 provides a detailed literature review on the nature of bentonite, hydration of compacted bentonite, the measurements of swelling pressure of compacted bentonite, the temperature effects on swelling pressure and hydraulic conductivity, the theoretical method for the prediction of swelling pressure, and colloid generation for compacted bentonite.

Chapter 3 presents the properties of Voclay (SPV) bentonite used for this research and the experimental methods. Physical properties including natural water content, specific gravity, particle size distribution, Atterberg limits are described. The development of compaction methodology to achieve the targeted uniform density is presented. Physico-chemical properties including total specific surface area, external specific surface area, cation exchange capacity and mineralogy and chemical composition of clays are presented. The determination of total specific surface area using ethylene glycol monoethyl ether (EGME) adsorption method was adopted. The determination of external specific surface area is based on BET theory by using nitrogen gas. The detailed description of the experimental program for the tests is presented.

Chapter 4 presents the hydro-mechanical test results. In the first test series, the swelling pressure of compacted bentonite samples at different dry densities were measured by increasing temperature from 25°C to 80°C. In the second test series, the compacted bentonite samples were saturated at different temperature. The elapsed time against swelling pressure and calculated hydraulic conductivity are presented. The influence of hydraulic gradient on hydraulic behaviour were also studied.

Chapter 5 presents the result of improved model for the prediction of swelling pressure at ambient temperature based on Gouy-Chapman diffuse double layer (DDL) theory. The theoretical prediction considers the effects of the clay particle size and the evolution of micro/macro pores for compacted bentonite. This improved model was applied to the prediction for ten different products of bentonite. The comparisons between theoretical prediction and experimental values are presented.

Chapter 6 presents the prediction of swelling pressure of three different types of bentonites at elevated temperature based on DDL theory. The estimated swelling pressure is compared with the results from classic DDL theory and the experimental data from literatures. The regular solid solution model is introduced to characterise the hydration of smectite. The suction variations at different dry densities are estimated. The evolution of micro/macro pore at elevated temperature and the temperature effects on the formation of clay particles for different compacted bentonite are presented.

Chapter 7 shows the results of surface erosion of compacted bentonite at isothermal conditions. During the tests, the samples at the same dry density were subjected to different temperature, respectively. The analysis of the turbidity of the collected outflow solution was conducted. The chemical analysis of the concentration of the eroded solution was completed by conducting dynamic light scattering measurement. The elapse time against the concentration of the eroded solution is presented.

Chapter 8 lists the main conclusions of this thesis and suggestions for further work. The references and the appendix are listed at the end of thesis.

CHAPTER **TWO**

2. Literature review

2.1. Introduction

Compacted bentonite is being considered as an important component of the engineered sealing system in many repositories designs, i.e., H12 repository concept (JNC, 2000) and Posiva's KBS-3V disposal concepts (SKB, 2006). due to its favourable physical and chemical properties. For example, a key component of the engineered barrier system (EBS) in the disposal of high-level waste in crystalline rocks is clay buffer. It has critical functions in the overall safety and performance of the disposal system, including: i) reducing the water percolation around nuclear waste canisters and the associated reduction of corrosion rates of the canisters, ii) providing a stable mechanical environment for canisters via its high swelling potential, and iii) retarding radioactive nuclides (e.g., Pusch and Yong, 2006; SKB, 2006). In many repository concepts, compacted bentonite bricks are stacked around the waste canisters in the EBS (Andra, 2005; Martin et al., 2006; Juvankoski, 2010; Wang et al., 2013) with initial small cavities or voids between the bricks (Gatabin et al., 2016; Chen et al., 2017; Jia et al., 2019). In general, the voids are filled with pellets. That would require a choice of sealing material with impermeable properties to ensure these engineering voids would not be potential pathway for fluids.

In repositories, the compacted bentonite is subjected to elevated temperature and the intrusion of groundwater, with the associated physico-chemical processes during the operational period. This chapter presents a literature review of the physico-chemical processes in compacted bentonites, including swelling mechanism, swelling pressure tests, temperature effect on hydro-mechanical behaviour, swelling pressure prediction for compacted bentonite, and the surface erosion of compacted bentonite.

2.2. Nature of bentonite

Bentonite as a sealing material is widely available in many product forms (pellets, chips, gravel, grout, and powder) due to its ability to reshape to the surroundings and heal any cracks which may occur. Bentonite clay will expand and form a nearly impermeable barrier once in contact with water. The permeability of bentonite is remarkably low, less than 10^{-13} cm/s, with specific value depending on the fabric. In addition, the latent hydration characteristic of swelling, which is a critical parameter in the design, can cater to the change of environment around the formation. The water absorption ability of bentonite is controlled by the charge, hydration energy and the properties of exchange cations, and its swelling ability depends on the size of small particles, high surface area, and porosity. The main mineral composition of bentonite is montmorillonite, and the accessory components can be other clay minerals (e.g., kaolinite or illite), quartz, feldspars, gypsum, calcite, pyrite, and different iron oxides/hydroxides. The chemical and physical properties of bentonite are mainly determined by the montmorillonite.

2.2.1. Characteristics of montmorillonite

The structure of montmorillonite comprises an alumina octahedral sheet sandwiched between two silica tetrahedral sheets. The centre cation of the octahedron is Al^{3+} with six hydroxyls at each corner, whereas the centre cation of the tetrahedron is Si^{4+} with four oxygen atoms at each corner. The process of replacement of one structural cation with another cation without modifying its chemical structure is referred as isomorphous substitution (Uddin, 2018). For example, Si^{+4} may be replaced by Al^{3+} in tetrahedra and the replacement of Al^{3+} by Mg^{2+}, Fe^{2+}, Fe^{3+} may occur in octahedra. The substitution results in a net of negative charge for montmorillonite. As shown in Fig. 2.1, the space between layers contains exchangeable cation and water. This characteristic enables the bentonite to swell many times its original volume. Due to the variety of cations between interlayer regions in bentonite, it has developed several kinds

of products such as sodium bentonite and calcium bentonite.

Swelling contributes to decreasing the size and connectivity of pores, thus physically impeding the convective transport of solutes and gases. Subsequently, the length of the diffusive flow path or the tortuosity would increase, and the tortuous flow path promotes the contact and reaction of contaminants with interlayer surfaces once completely hydrated (Gates et al., 2009).

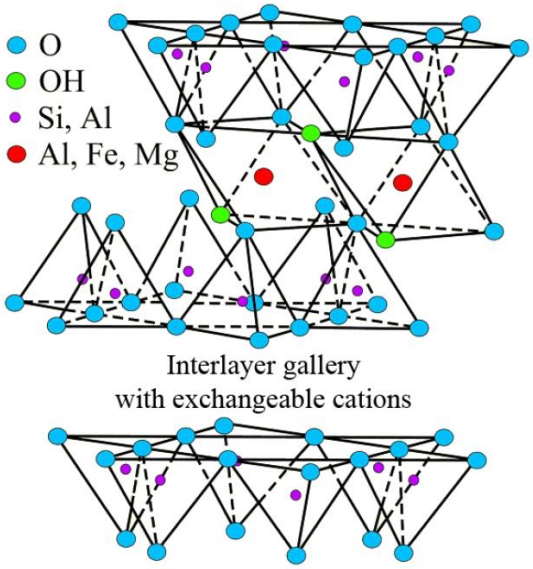

Fig. 2.1. Diagram of the unit structure of montmorillonite (Steinmetz, 2007).

2.2.1. Structure of compacted bentonite

The pore system of compacted bentonite can be simplified by two scales of porosity (Pusch, 1982; Gens and Alonso, 1992; Delage et al., 2006): i) the interlayer porosity that includes the spaces between the unit layers of montmorillonite (microstructure) and ii) the macro porosity that represents the pore spaces between the particles and aggregates of particles (macrostructure). The interlayer hydration or dehydration process can only alter the distance between the clay microstructure units (interlayer distance) by adding or removing discrete layers of water (Push and Yong, 2006). In a steady state or equilibrium, the amount of water in micro pores of compacted bentonite has a negligible contribution to the macroscopic flow and is considered to be immobile (Pusch and Yong, 2006; Chen et al., 2020).

The behaviour of compacted bentonites is determined by the interactions between the aggregates and particles (Pusch, 2001; Lloret et al., 2003). Montmorillonites are organized in quasicrystals that consists of multiple stacked unit layers. From the observations by transmission electron microscopy (TEM), it is suggested that quasicrystals are dynamic and flexible (Laird, 2006). Large quasicrystals may break up into several smaller ones, and this process is reversible. The number of layers per clay particle varies with the amount of water content (Delage et al., 2006).

There are different statements about the number of unit layers in a stable particle of smectite, eg.: 1 to 16 (Sposito,1984); 2 to 3 (van Olphen,1977); 4 to 10 (Marcial et al., 2002); 3 to 50 (Schanz and Tripathy, 2009). The number of clay platelets per particle was found to be ranging from 3 to 7 for Na-montmorillonite in compact materials (Pusch, 2001; Melkior et al., 2009). Liu (2013) assumed this value ranges from 1 to 3.5 for Na and Ca dominated compacted bentonite in the prediction. The formation of clay particle is related to the specific surface area, affecting the interactions force between layers as well as the adsorption and reaction. The specific surface area of edges of a particle has been reported to be approximately 1 to 5 % of the external surface area (Holmboe et al., 2012, Tournassat et al., 2003), which has a negligible effect on the calculation of total external surface area. The total specific surface area of smectite (SSA_{total}) can be established based on the lamellar structure of smectite (Chen et al., 2020):

$$SSA_{total} = SSA_{ext} + SSA_{int} + SSA_{Edges} \tag{2.1}$$

where, SSA_{Edges} is the surface area of the layer edges; SSA_{ext} is the external specific surface area; SSA_{int} is the internal specific surface area. SSA_{total} can be measured through Ethylene Glycol Monoethyl Ether (EGME) technique. SSA_{ext} is measured by the gas sorption test or the calorimetric methods. SSA_{Edges} can be estimated by the Atomic Force Microscopy (AFM) (Cadene et al. 2005).

2.3. Swelling mechanisms of bentonite clays

During the hydration of bentonite clays when exposed to aqueous solution, the breakdown of the clay particles was observed by using SEM (Scanning electron microscope), FTIR (Fourier-transform infrared spectroscopy), and ATR (micro-attenuated total reflectance) spectroscopy (Katti and Katti, 2001). The reduced particle size was related to increased misorientation of the clay platelets. For instance, Saiyouri et al. (2004) observed that the particle size decreased from 350 to 10 layers with a decrease of suction. In confined condition, the swelling of montmorillonite clays is characterised by an increase in the interparticle spacing and a reduction of the interaggregate pores (Delage et al., 2006).

This hydration process is influenced by many factors such as relative humidity, temperature, pressure, net layer charge, substitution location, and interlayer cation (Zhang et al., 1993; Laird, 2006; Anderson et al., 2010; Sun et al., 2015; Villar and Lloret, 2004; Segad et al., 2013; Smith et al., 2006). Two mechanisms for the swelling of bentonite clays are reported: (i) crystalline swelling and (ii) osmotic swelling (Zhang and Low, 1989; van Olphen, 1977; Hensen and Smit, 2002; Anderson et al., 2010; Pusch, 2015; Sing et al., 2006), and these are described below.

2.3.1. Crystalline swelling

Initially, water uptake occurs due to the clay surface hydration. Cations and water molecules enter the interlayer space, resulting in increasing the space eventually. This process is referred to as the crystalline swelling. It was reported that the crystalline swelling was in the range of 9 to 20 Å from interlayer spacings (Anderson et al., 2010). For instance, the basal spacing for Na-montmorillonites increased from 9.7 Å in the dry state to 12.6 Å, 15.6 Å and 18.6 Å corresponding to one, two, or three water layers, respectively (Holmboe et al., 2012; Villar et al.2012). The results from simulations (e.g., Hensen and Smit, 2002) also confirmed that the crystalline swelling occurs in the interlayer region. The thickness and volume of water that can be absorbed on the clay

surface is determined by the properties of exchangeable cations and the charge density of clay surface.

Crystalline swelling is affected by interlayer cation nature, relative humidity or water activity, dry density and swelling conditions (free or confined) (Imbert and Villar, 2006; Karnland t al., 2011; Komine et al., 2009; Lloret et al., 2003; Schanz and Tripathy, 2009; Villar et al., 2012; Villar and Lloret, 2008). Using analysis from X-ray peaks, Pusch et al. (1990) presented the hydrate thickness for different types of cations as shown in Table 2.1. Using this data, Khan (2012) estimated the water content of bentonite with the same specific surface area and found that the Na-type bentonite absorbed more water compared to other bentonites. This might explain the high swelling capacity for sodium-type bentonite. The presence of multivalent (e.g., Ca^{2+}, Mg^{2+}) exchangeable cations in the interlayer of montmorillonite leads to an increase of attractive force. On the other hand, for monovalent (e.g., Na^{+}) exchangeable cations, the interlayer attractive force decreased (Wilson and Wilson, 2014; Anderson et al., 2010).

Table 2.1 The evaluation of thickness in Å (1Å=10 nm) for dehydrate montmorillonite and hydrate layers (Pusch et al.,1990)

Cations	0 hydrate	1 layer	2 layers	3 layers
Mg^{2+}	9.52	12.52	15.55	18.6
Ca^{2+}	9.61	12.5	15.25	-
Na^{+}	9.62	12.65	15.88	19.36
K^{+}	10.08	12.5	16.23	-

2.3.1. Osmotic swelling

The osmotic swelling results from the concentration difference between the clay surface and the bulk solution. This phenomenon is induced by the repulsion between the formed diffuse double layers on platelet surfaces. Although most of the total surface

charge of montmorillonite is located within the interlayer region, DDL is unable to form due to the limited space. Part of the total charge is located on the external surfaces of quasicrystals (Laird, 2006), where DDL can be formed.

As the cations move close to the negatively charged surface, the difference in concentration results in cations diffusing from regions of high concentration to regions of low concentration. The separation of basal spacing is limited for Ca-type montmorillonites (Holmboe et al., 2012; Michot et al., 2013). Due to osmotic forces that may exist on the outer surfaces of particles, water molecules that cannot enter the interlayer spaces are attached to outside particles. This phenomenon is called "inter-particle osmotic swelling" (Madsen and Müller-Vonmoos, 1989; Segad et al., 2010). It has been discussed that the external surface of clay particles also plays an important role in the swelling behaviour of clay (Laird, 2006; Liu, 2013; Madsen and Müller-Vonmoos, 1989).

The osmotic swelling is strongly influenced by the type of cations. If monovalent cations enter the interlayer space, distances between clay platelets can be larger than 40 Å due to osmotic swelling (Meleshyn and Bunnenberg, 2005; Michot et al., 2004). While for divalent cations, the influence of osmotic swelling seems to be limited due to ion-ion correlation forces, and the repulsion in the diffuse double layer water reduces (Kjellander et al., 1988). As discussed earlier, this might explain the superior swelling capacity of sodium-type bentonite compared to calcium-type bentonite.

2.4. Swelling pressure tests for compacted clay

The use of bentonite-sand mixture is often preferred for the reason of increasing heat transfer and mechanical strength (Cui, 2017). Compared with pure bentonite, the mixture of bentonite and sand yields the same void ratio at higher yield stress (Wang et al., 2013). In situ stress state is the original stress status in the rock before excavations or other perturbations. The maximum swelling pressure of bentonite-based material must be lower than the in situ minor stress. For instance, this minor stress is 7 MPa in

the underground research laboratory of Bure site, France (Delage et al., 2010; Tang et al., 2011), 3-4 MPa at Tournemire site, France (Barnichon and Deleruyelle, 2009), and 4-5 MPa at Mol site, Belgium (Li et al., 2010). The magnitude of swelling pressure depends on the final dry density of bentonite in the mixture (Wang et al., 2012, Cui, 2017).

The prevailing method for measuring the swelling pressure of compacted bentonite is a constant-volume test where no volume change is allowed during saturation. The method has been used in many experimental investigations on the swelling pressure of compacted bentonite (Pusch, 1982; Komine and Ogata, 1994; Villar and Lloret, 2004; Karnland et al., 2007; Villar and Lloret, 2008; Komine et al., 2009; Schanz and Tripathy, 2009; Pusch et al., 2003; Cho et al., 2000; Villar et al., 2004; Lee et al., 2010; Ye et al., 2014). As shown in Fig. 2.2, the measurement of swelling pressure of compacted clays can be achieved by conducting free swell-compression test, loading swell-compression test and constant volume test (Sridharanet al., 1986; Li and Wang, 2003). These three experimental methods can be carried out in the consolidation apparatus.

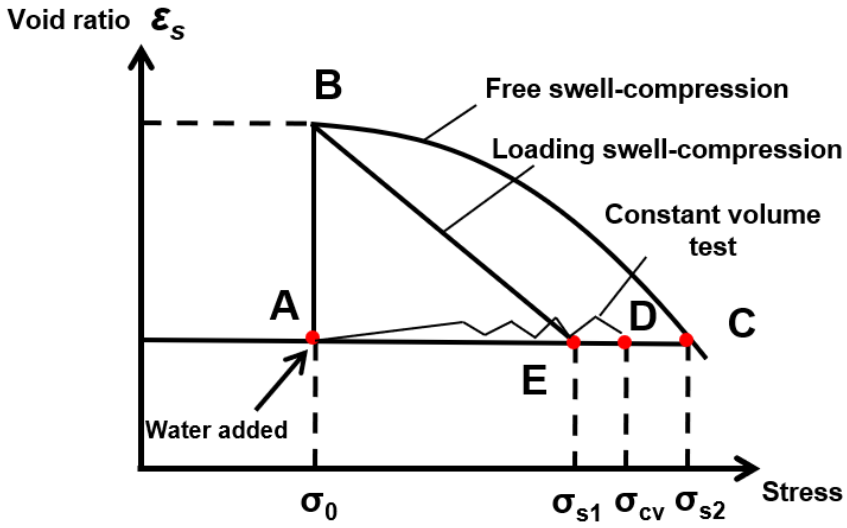

Fig. 2.2. The measurement of swelling pressure of compacted bentonite by using different methods (after Sridharan et al., 1986, and Schanz and Al-Badran, 2014).

In the free swell–compression experiment (A-B-C), water is added at point A, the sample swells fully until point B, and load is applied until the void ratio returns to the

initial value at point C as shown in Fig. 2.2. Then the measured vertical stress is marked as the swelling pressure (σ_{s1}). The second method is the loading swell–compression test (A-B-E). Several identical samples are required by applying different loads. After swelling, different void ratio will be obtained under different loads. The intersection of the straight line connecting the points of the corresponding tests with the horizontal line representing the initial void ratio in the void ratio; vertical pressure space gives the swelling pressure (σ_{s2}). The third method is the constant volume test (A-D). To prevent the volume change of the sample at phase AD, the vertical stress is kept adjusted until no vertical deformation is measured (σ_{cv}), which is equivalent to the magnitude of swelling pressure. Sridharan et al (1986) compared the results and found no definite relation from these three methods. Constant volume test is widely used in laboratory due to its merit, i.e., a single specimen is needed, and the test is relatively rapid.

2.5. Temperature effect on swelling pressure of compacted bentonite

A large body of research has shown that elevated temperatures have considerable effect on hydraulic and mechanical behaviour of compacted clay buffer (Villar et al., 2010; Bag and Rabbani, 2017; Ye et al., 2013; Ye et al., 2014, Tripathy et al., 2015; Villar and Lloret, 2004; Cho et al., 2000; Zihms and Harrington, 2015; Tang et al, 2008; Pusch et al, 1990; Daniels et al., 2017; Kalea and Ravi, 2019).

Early studies by Pusch (1980a) showed a drop of swelling pressure of compacted MX-80 bentonite (Na-montmorillonite) at 90°C compared to that at 20°C. This was explained by reduction of water in interlayer and inter-particle spaces of the clay system at elevated temperature. Tripathy et al. (2015) reported similar observations and suggested that the decrease of swelling pressure of compacted MX-80 bentonite at elevated temperature was associated with induced changes in the electrical potentials. By comparing bentonites with different dominant cations, Pusch et al. (1990) suggested that the effect of temperature on swelling pressure of compacted bentonite depends largely on the type of the dominant cation. For example, in Ca-dominated bentonite the

swelling pressure decreases with temperature, while in compacted Na-bentonite the swelling pressure increases with temperature. The latter observation conflicts with the previous work by Pusch (1980a). In the experimental study by Ye et al. (2013), the swelling pressure of a compacted Na-bentonite (GMZ01) was found to increase between 20°C and 40°C, in partial support of the work by Pusch et al. (1990). Villar et al. (2010) studied the swelling pressure of compacted FEBEX bentonite (Ca/Mg-type) and reported a reduction of swelling pressure between 30°C and 40°C, but insignificant changes between 60°C and 80°C, an observation which did not fully support the findings by Pusch et al. (1990). Similar observations were reported by Cho et al. (2000) who studied the swelling pressure of Ca-bentonite at the range of 20°C to 80°C. However, a recent study by Bag and Rabbani (2017) showed that the swelling pressure of a Ca-type compacted bentonite (Bikaner bentonite) increases at higher temperatures.

Experimental investigations of temperature effects on swelling pressure of compacted bentonite provide rather conflicting observations when associated with the type of dominant exchangeable cation in smectite minerals. Some observations on compacted sodium-rich smectite bentonite, e.g., MX-80, indicate that by increasing temperature the swelling pressure decreases (Pusch, 1980a; Tripathy et al., 2015), while others indicate increasing swelling pressure (Pusch et al., 1990; Shirazi et al, 2010, Pusch et al, 2003). Similarly, experimental studies on compacted bentonite where divalent cations (Ca^{2+} and Mg^{2+}) are the dominated exchangeable ions indicate that swelling pressure can either increase or decrease with increasing temperature (Villar et al., 2010; Cho et al., 2000; Ye et al., 2013). Apart from the decrease of swelling pressure at elevated temperature, it was found that the amount of water uptake was less than that at the ambient temperature, and the heating contributed to the reduction of test duration (Daniels et al., 2021). These opposing observations suggest the need for further experimental investigations, coupled with suitable explanations of the effect of temperature on swelling pressure in clays.

2.6. Temperature effect on hydraulic conductivity of compacted bentonite

In this section, the method for the calculation of hydraulic conductivity of bentonite clay is presented. The flow through clay as a fine-grained soil is commonly accepted as Darcian. In addition, the hydraulic conductivity of compacted bentonite can be related to hydraulic gradient. The temperature effect on hydraulic conductivity of compacted bentonite is discussed.

2.6.1. Hydraulic properties at different hydraulic gradients

Darcy's law is the most widely used formulation for the flow in coarse-grained natural soils. This is illustrated by the black line in Fig. 2.3. It has been found that Darcy's law is not a sufficiently accurate description for the flow in some fine-grained soils containing highly active clay minerals, such as montmorillonite (Alabi et al., 2012). A more appropriate flow relationship is described by the red line shown in Fig. 2.3, where Q is the flux (m^3); A is the cross-sectional area (m^2); K is the hydraulic conductivity (m/s); i is hydraulic gradient; i_0 is defined as an apparent threshold, below which no flow occurs; and i_c is defined as the critical hydraulic gradient, below which flow occurs but non-Darcian (Yong and Warkentin, 1975). The main difficulty in obtaining such a relationship is in the long time required for measuring clay's permeability, particularly for compacted clays. The application of high hydraulic gradient may be a solution to overcome the problem. However, the applied hydraulic gradients may be far from those anticipated in actual conditions. Dixon et al. (1999) showed a summary of applied hydraulic gradients at the range of 10^{-4} to 10^6 for the tests of low permeability soils. To investigate the hydraulic conductivity of bentonite, Dixon et al. (1992) adopted the high initial hydraulic gradients and the data did not support the concepts of threshold and critical gradients. Furthermore, dry densities at 0.76 Mg/m^3 and 1.09 Mg/m^3 and hydraulic gradients at the range of 2.5 to 400 were taken (Dixon et al., 1999). There were no critical or threshold gradients.

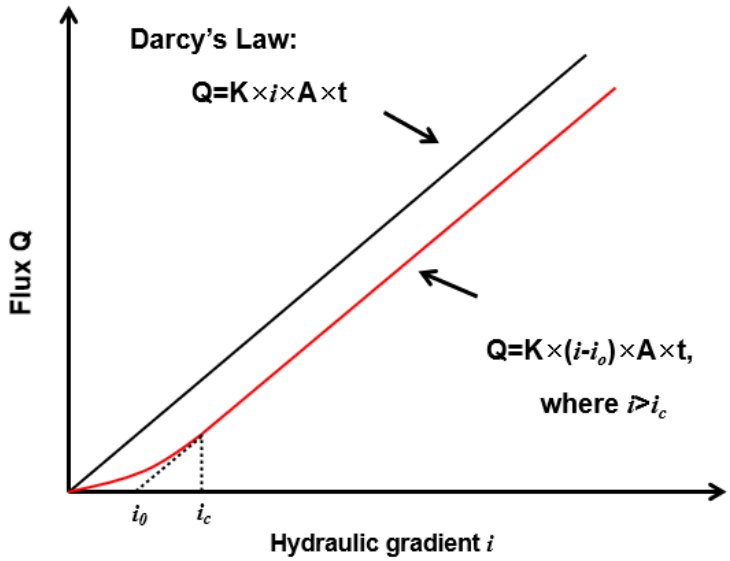

Fig.2.3. The graphical definition of critical gradient i_c and threshold gradient i_0 (after Dixon et al., 1992).

2.6.1. Temperature effect on hydraulic conductivity

Pusch (1980b) reported that the saturated hydraulic conductivity of compacted bentonite increased when temperature increased to 70°C. Similarly, Cho et al. (1999) reported that for compacted bentonite samples with dry densities ranging from 1.4 Mg/m^3 to 1.8 Mg/m^3, the hydraulic conductivity at 80°C was 3 times larger than that at 20°C. Zihms and Harrington (2015) investigated the hydraulic performances of bentonite by conducting a series of thermal cycles and found hydraulic conductivity to be sensitive to temperature changes. Pusch et al. (1990) discussed that the changes in microstructure of montmorillonite at elevated temperature had strong influence on the hydraulic conductivity of compacted bentonite. It was found that temperature could induce changes in the clay fabric and porosity redistribution (e.g., Romero et al. 2001; Sedighi et al., 2018). Other researchers suggested that the changes in water properties such as water density and water viscosity at elevated temperature could influence the observed hydraulic conductivity of compacted bentonite (Hopmans and Dane, 1986; Cho et al., 1999; Delage et al., 2000). By combining the effects of flow channels (fabric)

and water properties, Ye et al. (2013) developed a satisfactory prediction of variations of saturated hydraulic conductivity with temperature. In their model, the predicted values are overestimated compared with experimental values by assuming that the temperature effect on intrinsic hydraulic conductivity is ignored. Suggestions were presented that temperature affects the pore structure of bentonite as well.

2.7. Theoretical prediction of swelling pressure

The magnitude of swelling pressure of compacted bentonite is related to the nature of the bentonite material including the mineralogy, the specific surface area, the cation exchange capacity, and the characteristics of pore water (i.e., solution concentration present in the pore water). It is known that physico-chemical forces are responsible for the development of swelling pressure in saturated bentonite. There are several approaches for the prediction of swelling pressure of compacted bentonite including the Gouy-Chapman diffuse double layer model, empirical models, and thermodynamic models. The most popular theory for ionic distribution was developed by Gouy (1910) and Chapman (1913), referring as the Gouy-Chapman diffuse double layer theory. It states that the interaction force between two double layer depends on the ion concentration at the midplane, which is given by the osmotic pressure (Bolt, 1956). This approach has been widely used for the description of clay compressibility in the clay-electrolyte system (Sridharan and Rao, 1973; Sridharan and Jayadeva, 1982; Mitchell, 1993 Marcial et al., 2002).

Komine and Ogata (1996) applied a theory that the swelling pressure is caused by the repulsive and attractive forces between two parallel layers and proposed a new model for predicting the swelling pressure of compacted sodium bentonite. Their result showed this method could only be applied when the swelling pressure was below 3 MPa. One assumption of the Gouy–Chapman DDL theory is that the attractive forces between layers are ignored. Many researchers focused on predicting the swelling

pressure by employing the Gouy–Chapman DDL theory (e.g., Pusch et al. 1990; Yong and Mohamed, 1992; Sridharan and Choudhury, 2002; Tripathy et al. 2004). Based on the established relationship between swelling pressure and void ratio for clays (Sridharan and Jayadeva,1982; Tripathy et al., 2004), Schanz et al. (2013) found out the prediction was acceptable at low dry densities (below 1.4 Mg/m^3), but underestimated the experimental data at higher density. Therefore, an attempt to establish the relationship between the total void ratio and theoretical void ratio from diffuse double layer in the calculation was made, and the comparison showed a good agreement with experimental data for six other bentonites.

Low (1979) demonstrated that the relationship between swelling pressure and the mass ratio of montmorillonite to water agreed with an empirical equation and its validity was examined through laboratory investigations (Viani et al, 1983). Although the simplicity, the effects of ion concentration doesn't embody in this empirical equation for the prediction of swelling pressure.

Sposito (1972) suggested the swelling pressure at equilibrium could be calculated from the thermodynamic properties of clay, governed by the difference in vapour pressure between the clay-system and the solution. Karnland (1997) expanded the conservative thermodynamic model with an additional osmotic term considering the ions might enter the clay water system along with the saturating solution and change the partial free energy of water. The improved thermodynamic model is available for predicting swelling pressure in saturated sodium chloride solution. Agus and Schanz (2008) developed a method for predicting swelling pressure of bentonites based on thermodynamic relationships between swelling pressure and suction. The sorption isotherm of bentonite is required to be known in their model, which is applicable only for samples saturated with distilled water (the effect of ion concentration was not considered).

Liu (2013) proposed a mechanistic model to predict the swelling pressure of compacted bentonite-based materials in distilled water or diluted saline solutions. The

advantage of this model comes from the combined use of a thermodynamic relationship to describe the crystalline swelling and diffuse double layer model for the osmotic swelling. Considering the presence of the salinity condition in repositories and its influences on swelling pressure, Navarro et al. (2017) proposed an approach based on the macro- and microstructure characteristics to describe the behaviour of MX-80 bentonite, but its applicability required improvement for high salinities.

2.8. Colloid erosion from compacted bentonite clay

When in contact with flowing groundwater, clay particles may detach from the surface and be dispersed in the form of colloidal suspension in cavities of fractures. This process is generally referred to as the bentonite erosion as it results in a loss of material (Pusch, 1983; Alonso et al., 2018). The erosion of compacted bentonite reduces the sealing material as it is accompanied with decrease of density. If the bentonite is allowed to swell, swelling pressure of compacted bentonite decreases. Another concern is that advection in the sealing material can increase the transport rate of radionuclides, resulting in shortening of the lifetime of the barriers (Baik et al., 2007; Missana et al., 2008; Schaefer et al., 2012).

In the context of HLW disposal, the free swelling of bentonite into fractures could reduce the buffer density, which in turn could decrease the swelling pressure between canisters and host rock. As shown in Fig. 2.4, the diffusion of bentonite colloids into the flowing groundwater occurs from a solid state to a liquid form. The erosion is affected by many factors such as flow velocity, water chemical composition and fracture conditions (Birgersson et al., 2009; Missana et al., 2011; Pusch, 1999; Schatz et al., 2013). Considering the scenario of bentonite-rock interface, Pusch (1983) found that the penetration rate of the bentonite into a fractured rock is related to the density and the fracture width. The erosion of the bentonite gel depends on its shear strength and the groundwater flowing rate in the fractures. The dominated force will be the

diffusion if there is no hydraulic gradient for the separation of colloid particles (Kallay et al., 1987).

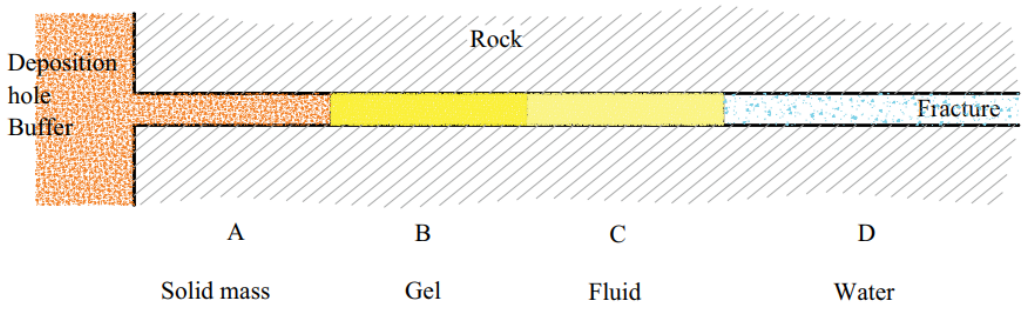

Fig. 2.4. Conceptual model of bentonite that swells from the deposition hole and penetrates into a fracture (Birgersson et al.,2009).

Pusch (1999) performed a study on the colloid formation from compacted MX-80 buffer that had penetrated fractures although this work was focused on colloids with a relatively larger size between 2 and 50 μm. The erosion of sodium bentonite and calcium bentonite, namely Kunigel-V1 and Kunibond, respectively, can happen at flow velocities ranging from 10^{-5} to 10^{-4} m/s (Kurosawa et al., 1999). It was concluded that the effect of bentonite colloids on radionuclide transport can be negligible for the performance assessment of geological disposal of radioactive waste in Japan. Missana et al. (2003) studied the colloid formation of FEBEX bentonite in a confined system and found the concentration of particles increased with increasing the water flow rate. Similar conclusions were obtained from the study of Baik et al. (2007).

The erosion rates were estimated under various chemical conditions in colloid generation experiments (Missana et al., 2011; Albarran et al., 2014; Baik et al., 2007). The eroded amount of clay seems to be higher in saline water compared with that of in non-saline water (Börgesson and Sandén, 2006). Neretnieks et al. (2009) found that the release of bentonite particles stopped and ended up with the coagulation in high ionic concentration. In a low ionic concentration, the repulsive forces caused by the cations in the diffuse layer dominate over the attractive forces between particles. While at higher ionic strength, the development of the diffuse double layers was restricted and the attractive van der Waals force can become stronger than the repulsive force at some

distance.

2.9. Summary

In this chapter, the structure of montmorillonite and the microstructure of compacted bentonites were presented. The swelling mechanisms of bentonite including crystalline swelling and osmotic swelling during the hydration process were described. The laboratory methods for the determination of swelling pressure of compacted bentonite were discussed. The parameters affecting the swelling pressure of compacted bentonite were reviewed. The current knowledge of temperature effects on swelling pressure and hydraulic conductivity of compacted bentonite was reviewed. Previous theoretical work on the estimation of swelling pressure of compacted bentonite were presented. It was found that these models did not provide satisfactory predictions for the swelling pressure of compacted bentonite at different temperature. Further, the factors that affect the erosion of bentonite were discussed. It was noted that the understanding of bentonite erosion at elevated temperatures was limited, despite its importance in the context of HLW disposal and P&A. Overall, the review demonstrated knowledge gaps in the hydro-mechanical behaviour of compacted bentonite. This thesis addresses some of these gaps and provide an improved understanding of hydro-mechanical behaviour of compacted bentonite as engineered barrier considering the thermal effects.

CHAPTER **THREE**

3. Material and Methods

3.1. Introduction

This chapter presents the properties of bentonite, and the details of bentonite characterisation and methods of constant-volume swelling pressure tests and erosion tests for compacted bentonite. In section 3.2, the physical properties of studied bentonite are presented, and the relationship between suction and water content of compacted bentonite is described. To investigate the hydro-mechanical behaviour of compacted bentonite at different temperature, a bespoke experimental setup was designed and developed which is presented in section 3.3. The setup includes i) a stainless-steel load cell, ii) a pressure controller that controls injection pressure and fluid flow, iii) a temperature control system, and iv) a data logging system. Section 3.4 describes the details of compaction of clay samples. The testing methods of swelling pressure and erosion are presented in section 3.5 and section 3.6, respectively. A summary is presented in section 3.7.

3.2. Characterisation of bentonite

A commercially powdered bentonite (Voclay SPV200) supplied by AMCOL (UK) was used in this study. The properties of the Voclay bentonite are presented in Table 3.1. The bentonite soil used was a mixture of dioctahedral montmorillonite with smaller amounts of quartz, plagioclase, K-feldspar, pyrite, gypsum, opal-C/cristobalite and a trace of kaolinite. The analysis of the chemical compositions of bentonite powder was undertaken using Energy-dispersive X-ray fluorescence (EDXRF). The clay fraction less than 2 μm of bentonite is a mixture of dioctahedral montmorillonite with traces of illite/mica and kaolinite. The hygroscopic water content was determined by oven drying at 105°C.

Table 3.1 Physical and chemical properties of the bentonite used in this study

Properties	Value
Clay fraction (%)	56
Montmorillonite content (%)	86.8
Accessory minerals (%)	
Quartz	3.9
Plgogioclase	5.6
K-feldespar	0.9
Pyrite	0.2
Gypsum	Trace
Compositions (%)	SiO_2= 62.30, Al_2O_3 = 19.13, Fe_2O_3= 10.31, CaO = 3.70, K_2O = 1.39, MgO =1.52, P_2O_5 = 0.38, TiO_2= 0.39
Hygroscopic water content (%)	12
Liquid limit (%)	409
Plastic limit (%)	52
Specific gravity	2.74
External surface area (m^2/g)	20.0
Total surface area(m^2/g)	528
CEC (meq/100g)	94
Exchangeable cations (meq/100g)	Na^+= 56, Ca^{2+}= 30, Mg^{2+}= 7, K^+=1.0

Particle size distribution

As shown in Fig.3.2, the particle size distribution was obtained by dry sieving and hydrometer test. Clay powder samples were size distributed by using a series of sieves from 0.075 mm to 4.25mm as shown in Fig. 3.1a. Hydrometer tests were conducted according to ASTM D422-63. According to the different settling rates, the estimated size of clay particles at various intervals were recorded. Fig. 3.1b presents the hydrometer test that the graduated cylinder with the cloudy liquid contains the clay sample in the water-dispersant solution. This was prepared by dissolving 33 g of sodium hexametaphosphate and 7 g of sodium carbonate in distilled water to make 1 L of solution. The temperature in the bath was monitored to ensure measurements are taken at a constant temperature.

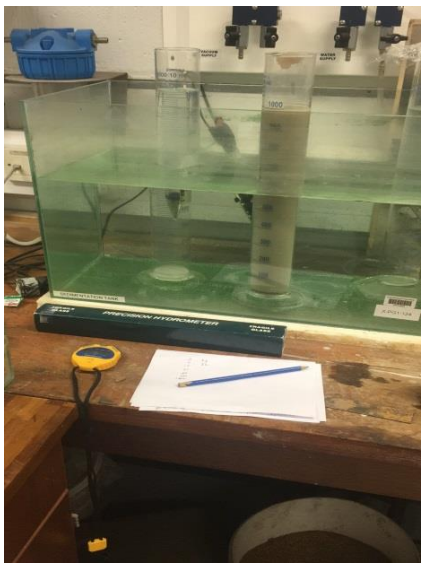

(a) clay powder and sieving (b) hydrometer test

Fig.3.1. The tests for the determination of particle size distribution of Voclay. bentonite

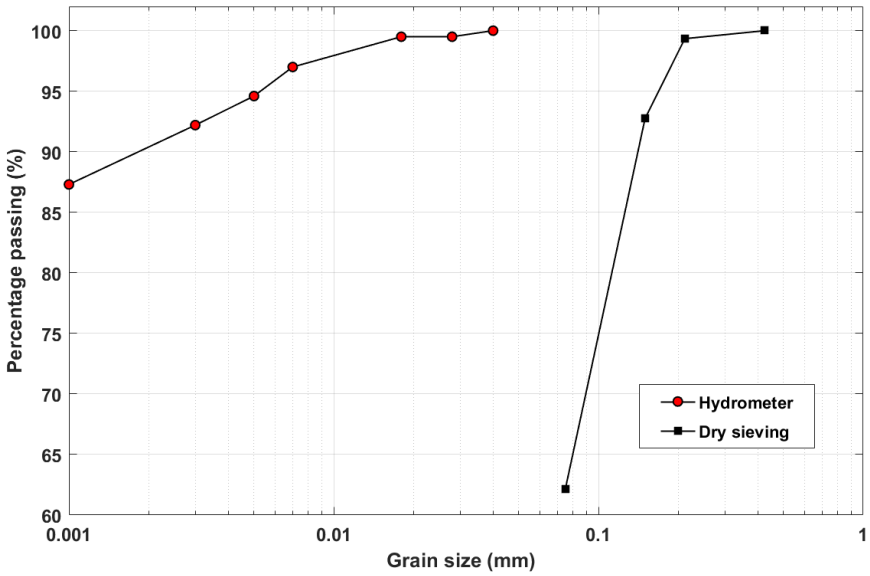

Fig. 3.2. The particle size distribution of Voclay bentonite in this study.

Liquid limit and plastic limit tests

The liquid limit and the plastic limit of clay samples were determined by fall-cone test and dynamic shear test, respectively, based on BS 1377-2(1990). The liquid limit is defined as the moisture content at which a soil passes from the liquid to the plastic state. There are two types of methods for the measurement of the liquid limit of soil.

The first is Casagrande test, where a paste of soil and water are placed in a shallow cup, the paste is cut into two parts with a deep groove and the cup is then dropped repeatedly in a standard manner until the groove has closed owing to the flow of the paste. The second one is a cone penetrometer test. This is a static test allowing for more reproducible results, while the Casagrande test is more susceptible to discrepancies due to operators. Therefore, the method of fall-cone test was adopted.

For the fall-cone test, the paste was prepared by mixing the bentonite powder (with particles smaller than 0.425mm) with water and leaving it to saturate for 24 hours. Care was taken in placing the penetrometer by ensuring smooth surface of the soil paste and the positioning the tip of the cone as close to the surface as possible. The cone was released from this position and the penetration value was recorded. The amount of water was altered to allow for a range of penetration values between 15 mm to 25 mm to be recorded and the result was shown in Fig. 3.3. The liquid limit of the soil was determined from the graph at a cone penetration of 20 mm.

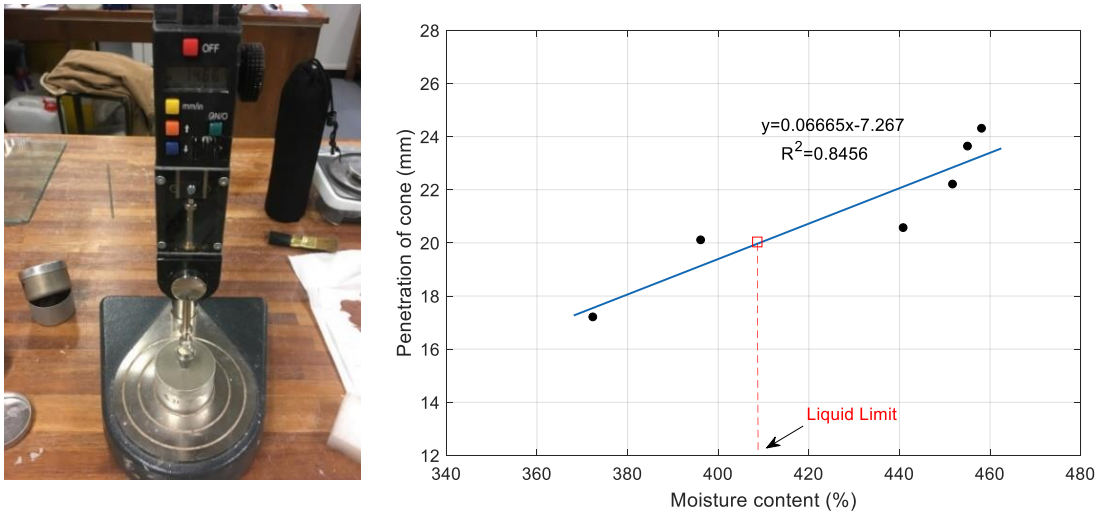

(a) (b)

Fig. 3.3. Fall-cone test (a)The penetrometer setup with sample; (b) Results of liquid limit.

The plastic limit is defined as the moisture content at which a soil becomes too dry to be in a plastic condition. For determining the plastic limit, approximately 20 grams

clay powder was added to water, leaving the mixture in room temperature until the mass become plastic enough to be shaped into a ball. Approximately 8 to 12 grams of the moistened soil was used to roll the ball by hand. If the soil could be rolled to a thread 3 mm thick without crumbling, the process was continued until the soil crumbled. The crumbled parts were collected and placed in a tared aluminium, oven dried at 110°C to a constant weight to estimate the water content. The measured water content provided the plastic limit.

Specific gravity

The particle density of the bentonite clay was obtained by pycnometer tests according to BS 1377-2(1990). Fig. 3.4 presents the equipment for vacuuming the bottles. The amount of powder was around 5 grams. To make sure the clay powder completely contacting with water, one should be cautious when adding as the clay powder might stick to the neck of bottle. To obtain reliable results, the soil was left under vacuum for at least 48 hr until the height no longer changed. According to BS 1377-2(1990), the air was gradually evacuated by using the desiccator until no more air bubbles were observed.

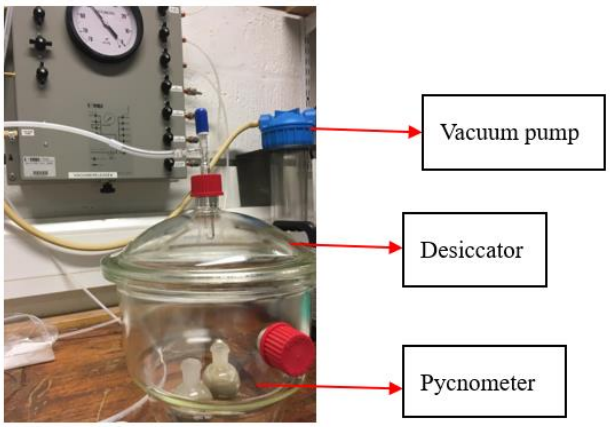

Fig. 3.4. The setup for the measurement of the particle density of clay powder.

Specific surface area

Specific surface area (SSA) exhibits a significant influence on the properties of

clays, such as liquid limit (Warkentin 1972; Churchman and Burke 1991) and swelling potential (Dasog et al. 1988). Generally, there are two approaches used to determine specific surface area of clays: (1) to measure external surface areas by the adsorption of simple molecules, such as the application of BET theory by using nitrogen as the adsorbate (Brunauer et al. 1938), and (2) to measure the total surface area by the adsorption of polar liquids (Tiller 1990).

The Gemini 2360 Surface Area Analyser was used to measure the external surface area of clays with the use of nitrogen based on Brunauer-Emmett-Teller (BET) theory. Since the molecular dimension of nitrogen are known, the surface area of the sample in the unit of m^2/g can be obtained by calculating the number of molecules of nitrogen required to form a monolayer.

The measurement of the total surface area was determined by the adsorption of ethylene glycol monoethyl ether (EGME) (Tiller, 1990; Cerato and Lutenegger, 2002). The arrangement of the setup is presented in Fig. 3.5. Before mixing with 20 mL of EGME desiccant, approximately 110 grams of 40-mesh anhydrous calcium chloride was placed in an oven for 1 hour to remove any residual moisture. The clay powdered sample was oven-dried at a temperature of 120 °C for 24 hours. Around one gram of clay soil was spread into the bottom of the aluminium tare, and the mass of the clay soil was determined with an accuracy of 0.001 g. Then, 3 mL of EGME was added and mixed with a gentle hand swirling motion to ensure full contact with the sample and create a uniform slurry. The tares were placed in a glass sealed vacuum desiccator and left for 20 minutes. Finally, the desiccator was evacuated by using vacuum pump providing a vacuum of 760 mm Hg. The tares were weighed after 8 hours. One measurement was taken 16 hours after the first evacuation, and again after 24 hours. If the difference between two readings was larger than 0.001 grams, the sample was put back and evacuated again for another 2 hours.

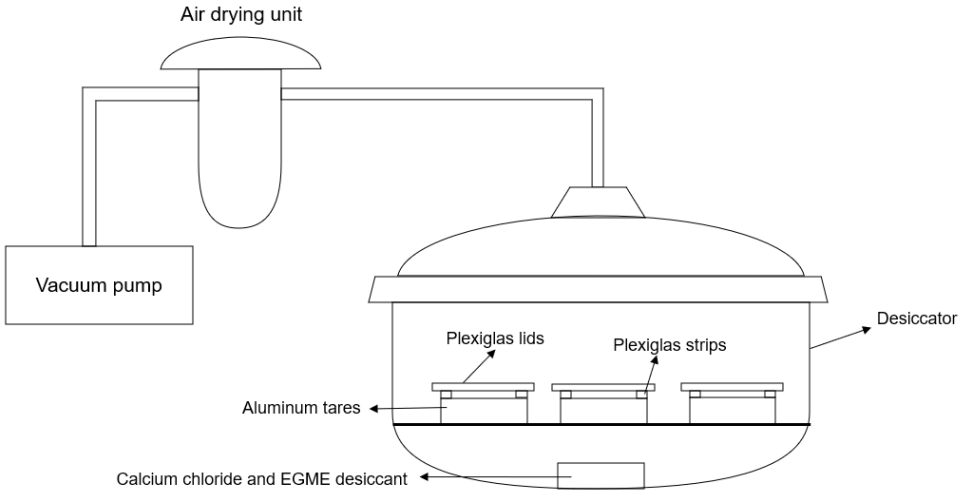

Fig.3.5. The setup for the EGME tests.

Cation exchange capacity

The bentonite clays have cation exchange capacity (CEC) that is able to hold positively charged ions due to its negatively charged surface. The cation exchange capacity and exchangeable cation composition of the clay was obtained by displacing the exchangeable cations by 1 M ammonium acetate (NH_4OAc) at pH=7.0 which was prepared by dissolving 375 g NH_4OAc in distilled water and making up to 5 litres and adjusting pH to 7.00 with acetic acid 10% (Reeuwijk, 2002). 20 mL of 1 M NH_4OAc was mixed with 2 grams of air-dry clay powder. The soil-solution slurry was shaken for 2 h in the shaker. The solution was then separated from the solid by a centrifuge until the samples were clear for 15 minutes. The concentrations of Na, K, Ca and Mg were subsequently analysed by inductively coupled plasma optical emission spectroscopy (ICP-OES). The calculation of CEC is followed by:

$$Exch.\ Ca=\frac{(a_s\text{-}b_l)*c*mcf}{10*20*d_w} \quad (3.1)$$

$$Exch.\ Mg=\frac{(a_s\text{-}b_l)*c*mcf}{10*12.15*d_w} \quad (3.2)$$

$$Exch.\ K=\frac{(a_s\text{-}b_l)*c*mcf}{10*39*d_w} \quad (3.3)$$

$$Exch.\ Na=\frac{(a_s\text{-}b_l)*c*mcf}{10*23*d_w} \quad (3.4)$$

where, a_s (mg/l) is Ca, Mg, K or Na in the extraction solution. b_l (mg/l) is Ca, Mg, K or Na in the blanks. d_w is air-dried sample weight in gram. mcf (=0.89) is moisture correction factor. c (=20) is the volume of NH_4OAc used in extraction.

Water retention curves

As shown in Fig.3.6, the chilled-mirror hygrometer (WP4C) was used for the measurement of total suction of clay with controlled water content. The instrument WP4C was supplied by the METER GROUP. WP4C directs the light beam onto a mirror, which reflects into the photodetector. When condensation occurs on the reflector, the photodetector senses the change in reflectivity. Then, a connected thermocouple to the mirror records the temperature at which condensation occurs. A green LED flashes and beeps when it reaches the final values.

There are three modes including the precise, continuous, and fast modes. The precise mode ensures accurate water potential readings through repeated operations. Typical reading time is between 10 and 15 minutes. The continuous mode can be used for long-term monitoring of samples that take a particularly long time to reach vapor equilibrium, such as plant samples and wet soil samples with water potential greater than -0.5 MPa. In fast mode, the measurement takes 3 to 5 minutes with a reduced accuracy. Though the temperature control of this WP4C is ranging 15°C to 40°C, large temperature differences between sample and block needs longer reading times.

Before conducting the measurement, it is necessary to make sure the cleanness inside chamber that would affect the readings. Verification standards provide salt solutions that have a specific molality and water potential. In this way, the reading can be checked and the error can be avoided. The potassium chloride (KCl) verification standards are available to be used with very high accuracy The reading of the KCl standard at 20 °C should be −2.19±0.05 MPa MPa, and at 25 °C the reading should be −2.22 ±0.05 MPa MPa.

Seiphoori et al. (2014) applied a microcell for the determination of the total suction at a given void ratio. For this study, a similar microcell was made of brass that contains specimens 5 mm high with a diameter of 30 mm. A thread lid was screwed tight with a solid base to provide constant volume conditions. The top of the lid was perforated to provide the possibility of water exchange in vapour form with the surrounding environment. A standard ASTM steel mesh number 200 (opening equal to 75 μm) was placed at the top of the specimen to prevent migration of the fine material particles. The mixtures of clay powder with different amount of water were sealed in plastic containers for two days to ensure the homogenisation of the water in the specimen.

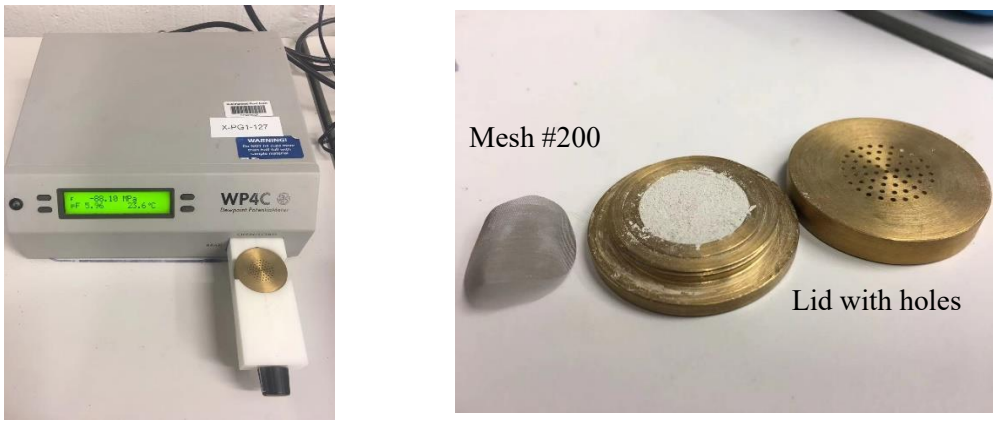

(a) (b)

Fig. 3.6. (a) WP4C dew point chilled mirror hygrometer; (b) Microcell component with a compacted sample.

The generated points were recorded by the measured suctions at different dry densities. The van Genuchten's relationship (van Genuchten, 1980) was adopted for the description of the relationship between water content and suction:

$$\theta = \theta_r + \frac{\theta_{sat} - \theta_r}{[1+(a_0 S)^{\frac{1}{1-m}}]^m} \tag{3.5}$$

where, a_0 and m are fitting parameters, s is suction (MPa). θ_r and θ_{sat} are residual water content (-) and saturated water content (-), respectively. In Fig. 3.7, the van Genuchten model is used to plot with experimental data. The parameters required to fit with experimental data are provided in Table 3.2.

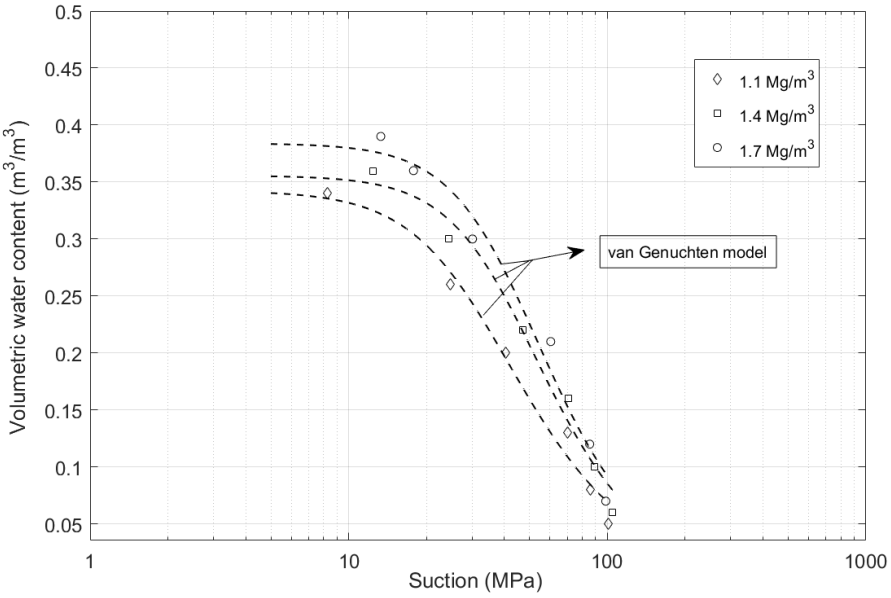

Fig. 3.7. The volumetric water content with suction for compacted Voclay bentonite

Table. 3.2 Parameters for the water retention curves of compacted Volclay bentonite.

	Dry density (Mg/m^3)		
Parameters	1.1	1.4	1.7
a (1/MPa)	0.030	0.020	0.022
M	0.585	0.626	0.630
θ_s	0.342	0.356	0.384
θ_r	0	0	0

3.3. The experimental setup

A bespoke constant strain rate consolidation (oedometer) setup was designed and constructed. The development was commissioned by the GDS Instruments. Instead of applying stress increments manually with a typical oedometer, this equipment is capable of gradually applying the load at a constant rate under controlled temperature. Water injection and drainage are allowed through either the top or the base of the apparatus, so that constant head permeability tests can be performed. Drainage is through the base of the apparatus, thereby controlling the excess pore pressure. The main advantage of this apparatus is that the completion time for a one-dimensional

consolidation test can be shortened significantly for low permeability materials by reduction of the excess pore pressure.

Fig.3.8 presents a schematic diagram of the experimental setup and pictures of the complete cell. The equipment consists of i) a stainless-steel load cell, ii) a pressure controller that controls injection pressure and fluid flow, iii) a temperature control system, and iv) a data logging system.

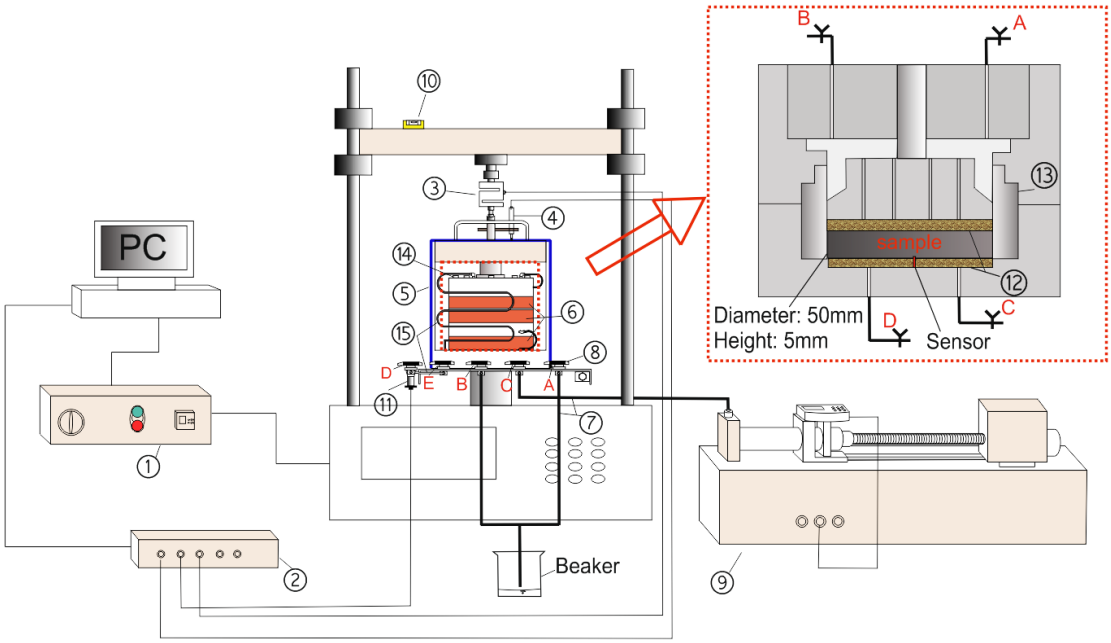

① Watlow temperature box ② data logger ③ external S-beam load cell ④ displacement transducer
⑤ steel cover ⑥ heating pads ⑦ coil tube ⑧ switches ⑨ pressure controller ⑩ level spirit
⑪ pore pressure transducer ⑫ porous plates ⑬ O' ring ⑭ screwers ⑮ steel tube

(a)

(b) (c)

Fig. 3.8. Experimental equipment: (a) schematic diagram of the developed setup: constant strain high temperature, high pressure system; (b) the oedometer cell with heating mats; (c) the oedometer cell with heat resistance cover mounted on the load frame.

The loading system

The loading system consists of a load frame and a load cell. The cell rests on the circular bottom plate that can move upward or downward when applying load. The load frame is able to operate in velocity and displacement control mode via keypad or software. In the technical specifications, the speed range can be controlled between 0.00001mm/min and 89.9999mm/min. The load range is up to 50 kN. The measurement components include a linear displacement transducer at the top of the steel cover, and a load ram that connects with external S-Beam load cell and internal sample.

The Linear Variable Differential Transformer (LVDT) local strain transducers manufactured by GDS Instruments was used to measure the vertical volumetric deformation of the sample with accuracy better than 0.1% of Full Range Output. The range of LVDT is up to 50mm.

High pressure controller

To provide a constant injection pressure, a high-pressure volume controller (200 cm^3 volumetric capacity and 0 to 20 MPa pressure range with an accuracy of 0.1%) was used. The resolutions of pressure and volume are 1 kPa and 0.1 mm^3, respectively. The pressure controller can measure the amount of water injected into the specimen during the infiltration process.

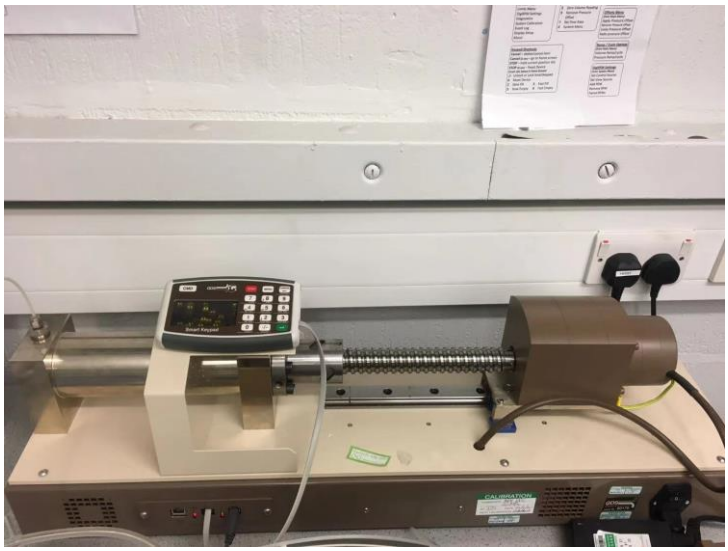

Fig.3.9 Advanced pressure controller

Temperature control system

To ensure isothermal conditions during the tests, three heating pads were attached at the top, middle, and bottom of the external surface of the sample holder. The changes in cell temperature were monitored via a thermocouple fitted into the base of porous plate. The temperature control system can maintain the isothermal temperature from ambient temperature up to 80°C. The temperature equilibrium in the entire system is usually achieved in a couple of hours. The expansion of the metal parts during heating (usually for temperatures higher than 40°C) can affect the load cell readings, so an increase of axial load ranging from 20 kPa to 170 kPa may be observed. These changes in axial load were accounted for during calibration of the system.

3.4. Sample preparation

Compacted bentonite samples were formed by compacting the powder to the target

dry densities using a specimen ring and a compaction mould. The compaction mould has four parts including a base, a collar, a spacer, and connecting ring. The specimen ring was placed on the base of the compaction mould. The collar and the connecting ring were attached and tightened with bolts. Fig.3.9a shows the assembled compaction mould.

In order to minimise the friction, the internal surface of the specimen and the spacer were lubricated with silicon grease. The testing machine as shown in Fig.3.10 was used to compact the samples by lowering down the cylinder to the pointed height, thus achieving the target dry density. Vertical pressures in the range of 7 kN to 50 kN were applied to the samples at a constant displacement rate of 0.2 mm/minute. Once a sample reached the target height, the load was maintained for 10 minutes in case of potential immediate rebound and internal fabric changes. Each compacted sample was then immediately emplaced in the constant-rate consolidation cell for testing.

(a) Compaction mould (b) Testing machine

Fig. 3.10. The setup for the compaction of samples.

3.5. Swelling pressure tests

The swelling pressure of expansive clays was measured after a completion of saturation from oedometer tests. There are three kinds of experimental methods to measure the swelling pressure of clays, including free swell compression test, the

loading swell compression test and constant volume test (Barckley, 1975; Sridharan et al., 1986; Xianmin and Wang, 2003; Ye et al., 2014). In this study, the constant volume test was used to determine the swelling pressure due to time-saving.

Calibration of the load cell against temperature

For calibration of the swelling pressure tests of compacted bentonite, a sample with a dry density of 1.4 Mg/m^3 was used. Figure 3.12 presents the monitored temperature of heating pads and inner sample with time. It takes around 1 hour to reach the target temperature of sample (40°C). The temperature of heating pad kept increasing until the monitored temperature of the inner sample reached 40°C. When increasing temperature to 60°C and 80°C, the average heating pad temperature are accordingly 64°C and 87°C.

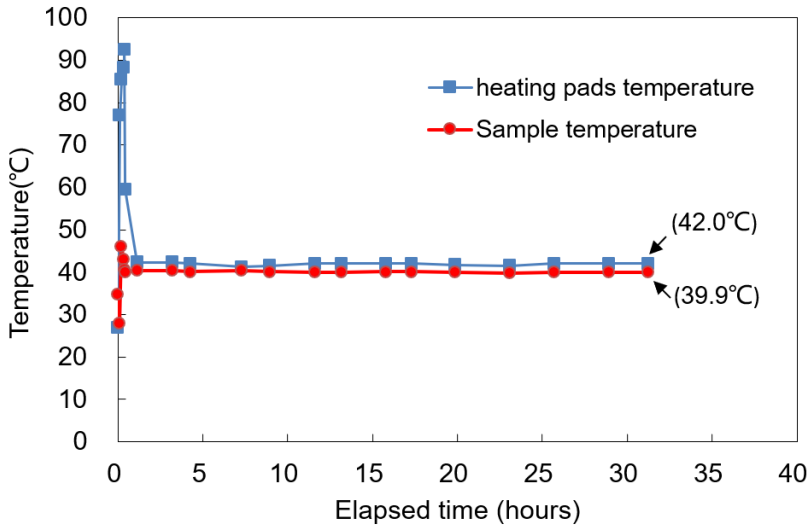

Fig. 3.12. The evolution of temperature against time.

The swelling pressure tests were conducted for compacted samples at three different dry densities of 1.1, 1.4, and 1.7 Mg/m^3. After the compaction, the specimen ring with compacted sample was placed in the chamber and confined between two porous plates as shown in Fig.3.8. The external S-Beam load cell was fixed with the restrained bar of the load frame. The load cell was placed at the position connecting the top of the loading ram and the S-Beam load cell. Fluid inlet and outlet tubes at the base of the cell were connected to the pressure controller. Two test series were conducted in

this study. The first test series focused on studying the effects of temperature on the swelling pressure using pre-saturated samples of compacted bentonite. For the second test series of experiments, each sample was saturated at different temperatures while the swelling pressure development was monitored.

3.6. Erosion tests

The generation of colloid bentonite is much closer to the realistic conditions in the applications of HLW disposal and P&A. To identify the erosion process of confined bentonite, the bottom porous plate was replaced by sintered stainless-steel filters with the bespoke oedometer described in section 3.3. The sintered stainless-steel plate was supplied by Mott Corporation. The average or nominal pore size of this plate is 100 μm. Two top openings were closed, and filter paper and thin film were placed on the top of the specimen to ensure there was no outflow through top. As shown in Fig. 3.13, the deionised water flow from the left bottom opening, the collected solution from the right bottom opening was used for dynamic lighting scattering (DLS) measurement. The DLS measurement is used to determine the concentration of the collected solution. There was no volume change during the whole process. In this case, the development of swelling pressure was monitored.

The Zetasizer NANO ZSP device from Malvern shown in Fig. 3.14a was used to measure the Brownian motion of the particles to determine the size of particles. The angle of scattering are 173 degrees. The single measurements lasted 60 s. The range of measured sizes was from 0.3 nm to 10 μm. The particles or molecules in the suspension cause the laser light to be scattered at different intensities. By using the Stokes-Einstein relationship to analyse these intensity fluctuations, the speed of Brownian motion can be obtained and hence the particle size. The proportionality of light counts measured by the method of dynamic lighting scattering can be utilised for the concentration determinations (Ledin, et al, 1993; Missana et al., 2003; Baik et al., 2007). The count rate is determined by the number of particles in the scattered volume. The relationship

between the concentration and the count rate for bentonite colloids was found to be linear (Missana et al, 2008; Niemiaho, 2013). To obtain the calibration curve, the bentonite suspensions were prepared with a known concentration from Voclay (SPV200) bentonite.

Turbidity was measured in the unit of NTU (Nephelometric Turbidity Units), which is correlated to the amount of particles in suspension and to their mean size. The turbidimeter was used to measures the intensity of the light scattered at 90 degrees when the beam passes through the water sample. The HI98703 turbidimeter is produced by Hanna Instruments, which has an accuracy of ±2% of reading plus 0.02 NTU with the reading ranges from 0 to 1000 NTU. As shown in Fig. 3.14b, the right four bottles with known turbidity (<0.1 NTU, 15 NTU, 100NTU, 750 NTU) were used to calibrate the turbidimeter. The calibration can be performed with two, three or four points, which means two, three or four bottles of standard solution were used for calibrating. The light passes through the cuvette to reach the sample and the measurements may be affected by flaws, dirt, dust, scratches, or fingerprints on the cuvette surface. To ensure accurate measurements the outer surface of the cuvette was cleaned by silicon gel to remove imperfections and scratches.

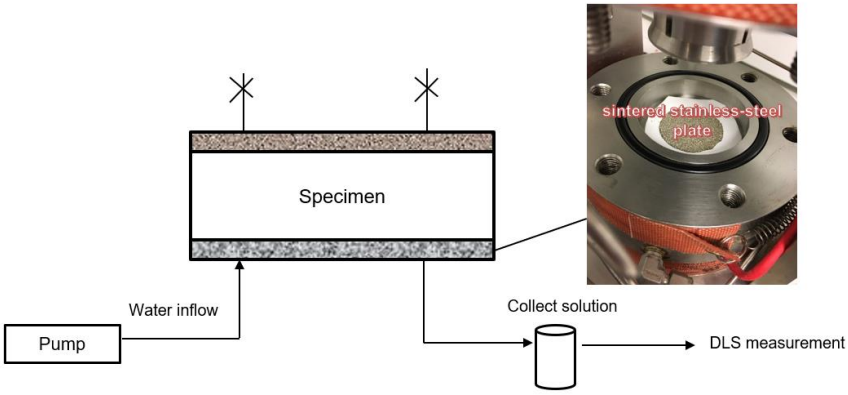

Fig. 3.13. A schematic of the erosion tests.

(a) (b)

Fig. 3.14. The analysis of colloid solution: (a)The Zetasizer NANO device from Malvern in DLS measurement (b)The setup for measurement of turbidity.

3.7. Conclusions

The properties of Voclay (SPV200) bentonite were presented in this chapter. The physical and chemical properties of the bentonite, such as liquid limit, plastic limit, specific gravity, specific surface area, cation exchange capacity and weighted average valence of exchangeable cations are presented.

A compaction module was developed for specimen preparation. The relationships between suction and water content at different dry densities were obtained from chilled-mirror hygrometer. By applying van Genuchten model, the results indicated that the sample with higher dry density contains more water compared with the sample with lower dry density. In order to investigate the temperature effects on hydro-mechanical behaviour of compacted bentonite, a bespoke oedometer with temperature control was built for conducting swelling pressure tests and erosion tests. Both tests were carried out at confined condition, i.e., no deformation was allowed. In erosion tests, the chemical analysis was conducted after collecting the solutions. The designed setup allowed for monitoring the evolution of swelling pressure. Details of the procedures for sample preparation, constant volume swelling pressure tests, and erosion tests at different temperatures were presented.

CHAPTER **FOUR**

4. Elevated temperature effects on swelling and hydraulic properties of compacted bentonite

4.1. Introduction

Previously reported observations of swelling pressure development in compacted bentonite-sand mixture at elevated temperature have led to opposing conclusions. Unambiguous answer to temperature effects on swelling behaviour of clays is critical in the context of geological disposal of-high level nuclear waste, where the clay barrier is expected to maintain high swelling capacity and low hydraulic conductivity for a significant time under elevated temperatures. With the aim to address this knowledge gap, this chapter presents an experimental investigation of temperature effects on swelling and hydraulic properties of bentonite-sand mixture for a range of dry densities and temperatures up to 80°C.

The aim of this study is to develop an improved understanding of the effects of elevated temperature on two key engineering properties of the clay buffers, namely swelling pressure and hydraulic conductivity. It is important to understand the hydro-mechanical response of compacted bentonite to temperature increases, and the extent to which such responses are interlinked with soil compaction and microstructure. In section 4.2, detailed procedure for conducting two test series using the bespoke high-pressure high-temperature constant strain oedometer is described. In section 4.3, the results of two series of laboratory experiments are presented which are based on two approaches for investigating the effects of temperature. The first set of experiments focuses on investigating how temperature increase can influence the swelling and permeability of saturated samples at ambient temperature. The second set of experiments explores the clay response to a range of elevated temperatures during saturation process. Swelling pressure development is recorded for both series of

experiments. The hydraulic conductivity of samples is also measured at a number of stages during the test to provide an understanding of the temperature effects on hydraulic properties. The discussions and summary are presented in section 4.4 and 4.5, respectively.

4.2. Experimental programme

Two series of experimental tests were conducted in this study:

Series A: In this series, the samples were first saturated at ambient temperature and the swelling pressure resulting from the saturation process was allowed to reach steady state before increasing the temperature. The swelling pressure development was monitored until water intake and swelling pressure were stabilised. The temperature was then increased from 25°C to 40°C and maintained until swelling pressure reached new steady state. Temperature was subsequently increased to 60°C and to 80°C following the same process and measurements. Fig. 4.1a presents a schematic diagram of the controlled temperature procedure applied for the first test series. The hydraulic conductivity of the sample was measured at each temperature after the steady-state swelling pressure was reached, by creating a pressure gradient across the sample and measuring the water flow rate. The hydraulic gradient was created by increasing the base pressure while the top valves were kept open to atmospheric pressure. The procedure applied here was similar to that adopted by Ye et al. (2013), Ye et al. (2014), and Huasmannonva and Vasicek (2014). Darcy's law was then applied to calculate the hydraulic conductivity of the samples from the measured flow rate and the applied hydraulic gradient. The range of hydraulic gradients created between the bottom (injection point/upstream) and the top (downstream) of the sample was varied from 2000 to 20,000 (m/m), corresponding to increasing injection pressure from 100 kPa to 1 MPa. The GDS advance pressure controller was used to accurately record the volume of water injected into the sample with time.

Series B: In this series, each sample was saturated at different temperatures, and the swelling pressure development was monitored. The experiments were conducted on three samples compacted at dry densities of 1.1, 1.4, and 1.7 Mg/m^3. The aim was to study bentonite behaviour under a range of low to high densities for which the contribution of interlayer water to total water was known to change approximately linearly (Sedighi and Thomas, 2014). The saturation was conducted under restrained deformation (confined saturation).

Fig. 4.1b presents a schematic diagram of the controlled temperature procedure applied for both types of experiments. The procedure of saturation was similar to that described by Bag and Rabbani (2017) and Villar et al. (2010). During the tests, the evolution of swelling pressure and volume of injected water were monitored and recorded for given temperature. The hydraulic conductivities of the samples were then measured after the swelling pressure stabilised at each temperature.

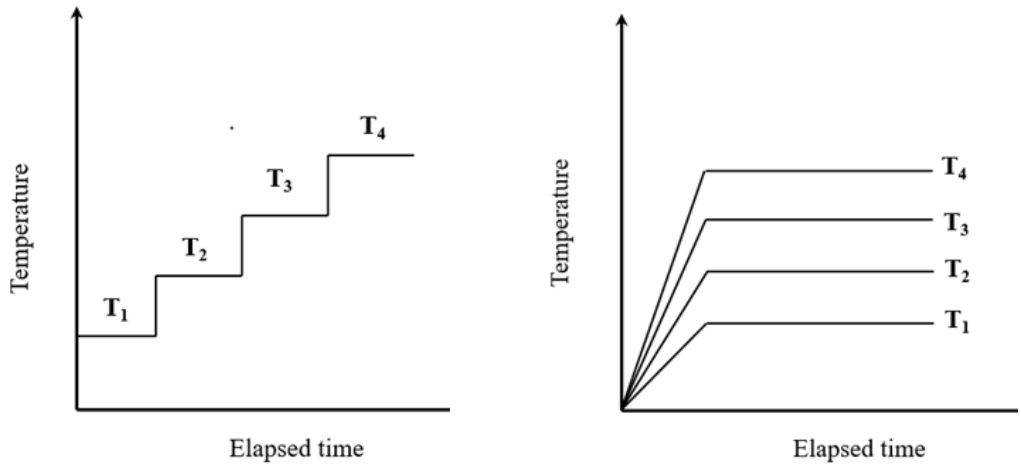

(a) (b)

Fig. 4.1. Temperature control with time for the two sets of experiments carried out: (a) response of the saturated clay to temperature increase; (b) saturation at different temperatures.

4.3. Results

4.3.1. Temperature effects on swelling pressure

This section presents the results of swelling pressure under the effects of elevated temperature from the experiments outlined in Section 4.1 as *Series A* and *Series B*. The saturation of compacted bentonite is considered to be completed which is based on the stabilisation of water intake and swelling pressure development (Villar et al., 2010). The equilibrium of swelling pressure is defined as increasing up to a constant value (Ye et al., 2013). In *Series A*, the equilibrium at different stages have been maintained for at least 24 hours. In *Series B*, the measured pressure is registered as the maximum swelling pressure after remaining constant. In addition, the final water content of each sample at 25°C were measured by oven drying and found to be 51.2 % for 1.1 Mg/m^3, 37.3% for 1.4 Mg/m^3, and 32.2% for 1.7 Mg/m^3. Accordingly, the calculated degrees of saturation are 94%, 106%, and 144%, which are considered to be completely saturated.

The magnitude of swelling pressure largely depends on the content of smectite in compositions (Komine, 2004). The partial dry density of smectite can be obtained from the dry density of clay and the smectite content (Idemitsu et al., 1996, Liu et al., 2003):

$$\rho_d^{sm} = X_{sm}\rho_d \left[1 - (1 - X_{sm})\frac{\rho_d}{\rho_{im}}\right]^{-1} \tag{4.1}$$

where, X_{sm} is the mass fraction of smectite in the clay (dimensionless), which is equal to the clay fraction times the smectite content. ρ_d represents the bulk dry density of the clay (kg/m^3). ρ_{im} denotes the density of the non-smectite minerals or impurities (kg/m^3) which is close to the density of smectite. Therefore, it is assumed to be around 2.8 Mg/m^3 for simplifications (Bourg et al., 2006). In this work, the comparison was made with data of swelling pressure against dry density of smectite for different bentonite clays at ambient temperature in existing literature (JNC, 2000; Schanz andAl-Badran, 2014; Lee et al., 2012; Schanz et al., 2013; Bucher and Müller, 1989; Schanz and Tripathy, 2009; ENRESA, 2000; Madsen, 1998; Imbert and Villar, 2006; Komine,

2004;). The measured values of swelling pressure are relatively lower due to a smaller dry density of smectite. The swelling pressure tends to be larger with a high dry density of smectite at the dry density (i.e., 16.3 MPa for FEBEX at a bulk dry density of 1.7 Mg/m^3 and the calculated dry density of smectite is 1.36 Mg/m^3, 3.5 MPa in this work at the same dry density and the calculated dry density of smectite is 1.2 Mg/m^3).

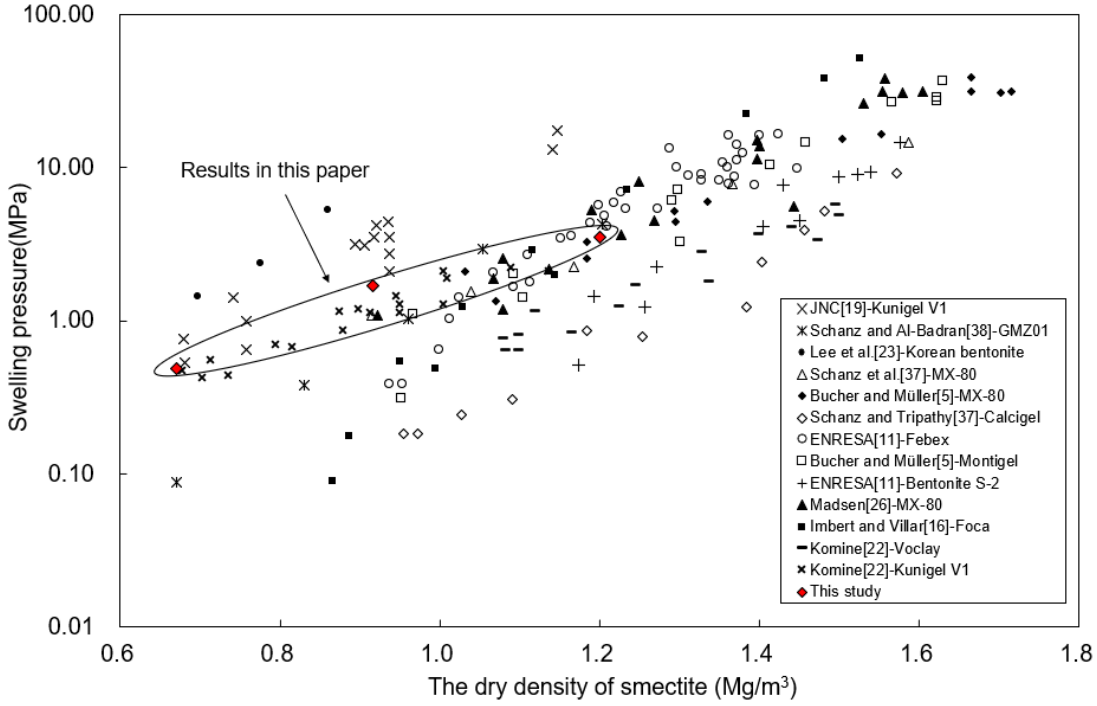

Fig. 4.2. Experimental data for swelling pressure of different bentonite clays at different dry density of smectite.

Figure 4.3 presents the results of swelling pressure of compacted bentonite when temperature increases stepwise from 25°C to 80°C (*Series A*). CB1, CB2, and CB3 represent the samples with dry densities of 1.1, 1.4 and 1.7 Mg/m^3, respectively. The results show that the steady-state swelling pressure during saturation (at 25°C) increases with the increase of the dry density of compacted bentonite, which is compatible with observations reported in the literature (e.g., Tripathy et al., 2015; Cho et al., 2000). The results also show that the swelling pressure decreases from the initial value with increasing temperature.

At the initial saturation stage, only one peak in the swelling pressure evolution is observed for CB3 (high dry density), corresponding to the steady-state, while two peaks

appear for both CB1 and CB2 (lower dry densities), the second corresponding to the steady-state. These observations agree with the study by Komine and Ogata (1994) that the first peak does not exist at high dry densities but appears at relatively low dry densities. In general, the high dry density yields high initial suction, i.e., larger water absorbing capacity, which dominates in water uptake process, thereby showing a continuous rise. For low density samples, the presence of the first peak is due to the loss of shear strength at the aggregate level (Pusch, 1982). The two peaks for low densities potentially result from the change of soil fabric. Before reaching the first peak, the swelling of aggregates induces an increase of interparticle distance which in turn generates a swelling pressure and shear stresses between the aggregates. Due to the high water-adsorption capacity of bentonite, water molecules enter the interlayer space between aggregates. The thick quasicrystal split into thinner ones, and deformable aggregates are repositioned and divided, resulting in a slight decrease of swelling pressure (Pusch, 1980a; Cui et al., 2000; Zhu et al., 2013). Matric suction dissipation is dominated at the stage of first peak, while second peak develops slower controlled by the osmotic suction (Singh et al., 2006).

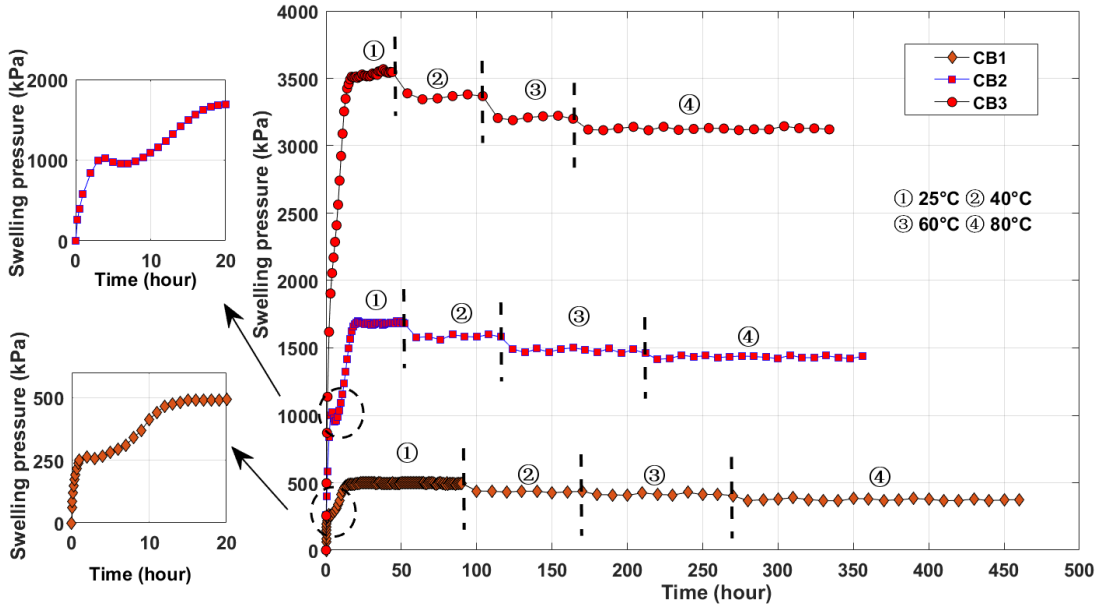

Fig. 4.3. Variations of swelling pressure of compacted bentonite with time for experiments *Series A*.

For the case of CB1 and CB2 samples, the swelling pressure decreases slightly after the first peak, and as the hydration process continues, it increases again towards the second peak. The phenomenon of double peak has been further reported in the swelling pressure tests conducted by Ye et al. (2013) with GMZ01 bentonite compacted to a dry density of 1.5 Mg/m^3 at 20°C and 40°C and Villar and Lloret (2008) using the compacted FEBEX bentonite with a dry density of 1.7 Mg/m^3 at room temperature.

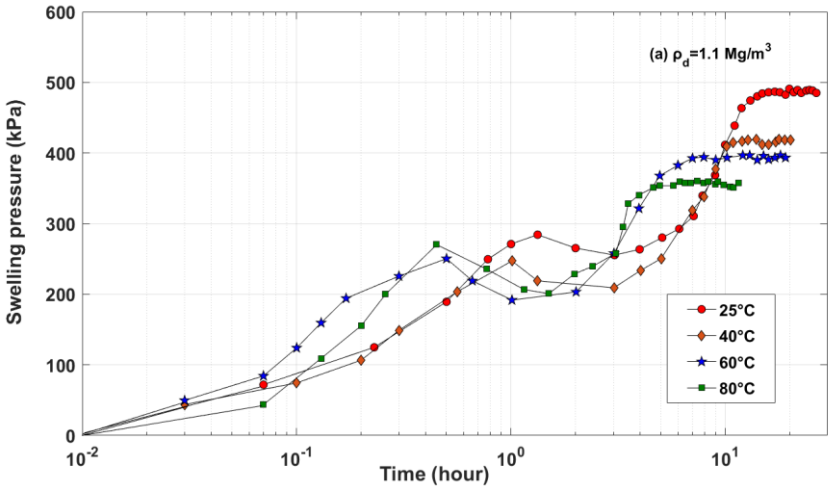

(a)

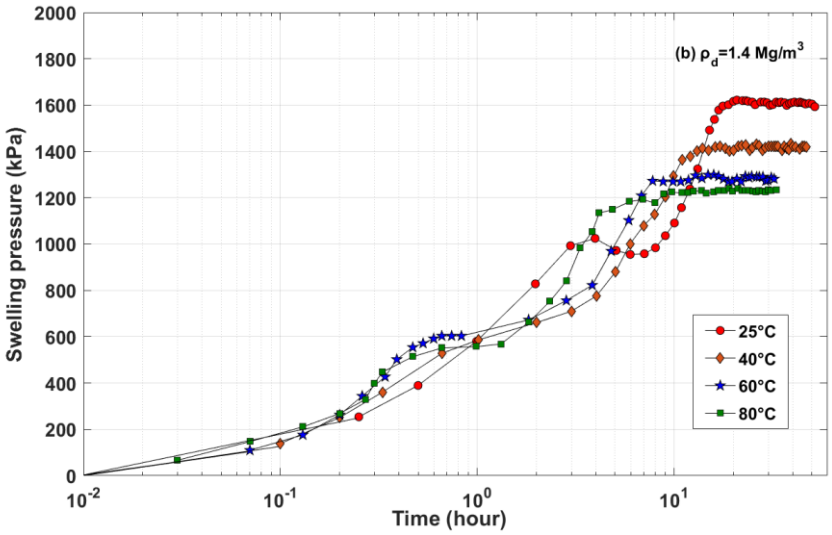

(b)

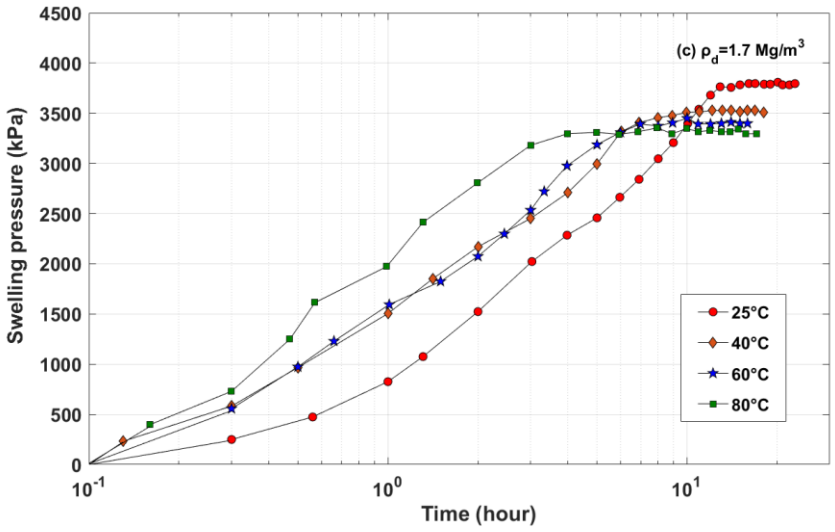

(c)

Fig. 4.4. The development of swelling pressure of compacted bentonite at different dry densities with time from test *Series B.*

For CB3 sample, which has a higher density however, the rate of swelling pressure development with time is smaller before reaching the final equilibrium. The overall reductions of swelling pressure due to temperature increase from 25°C to 80°C for samples CB1, CB2 and CB3 are 120, 250 and 440 kPa, respectively. This shows that swelling pressure reduction is much larger for samples with higher densities.

Fig. 4.4 a-c presents the results of the experimental tests in *Series B* which were focused on studying the swelling pressure development at different isothermal temperature values. At higher temperature, the swelling pressure shows a decrease for the samples with the same initial dry densities. For instance, the swelling pressures of the sample with dry density of 1.7 Mg/m^3 are 3.8, 3.6, 3.4 and 3.3 MPa at isothermal temperatures of 25°C, 40°C, 60°C, and 80°C, respectively. The results show that the swelling pressure decreases with temperature. These observations are compatible with data published by Villar et al. (2010) on compacted FEBEX bentonite.

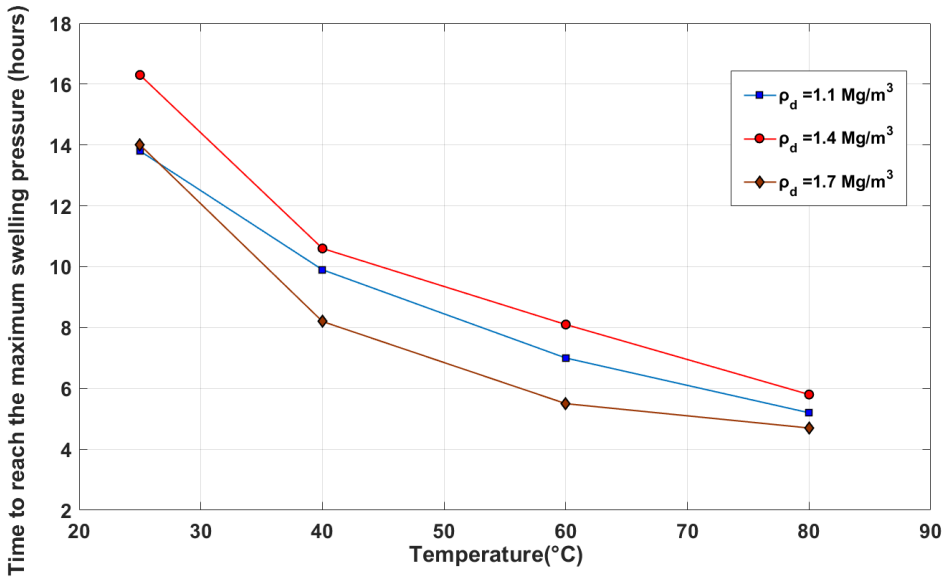

Fig. 4.5. Hydration time to reach the maximum swelling pressure at different temperature.

The results of experiment *Series B* show that by increasing temperature the hydration rate accelerates which is presented in Fig. 4.5. The rate of swelling pressure development is found to be much smaller at lower temperature. The time to reach the maximum swelling pressure, which is considered to be the end of saturation, is longer at low temperature than that of at higher temperature (e.g., for a dry density of 1.4 Mg/m^3, 16.2 hours at 25°C, and 5.8 hours at 80°C). The time to reach the steady-state of swelling pressure is the shortest for samples with the highest dry density. The variation of the swelling pressure with temperature (Fig. 4.6), show an overall decrease of the swelling pressure. These observations are consistent for both experimental *Series A* and *B*.

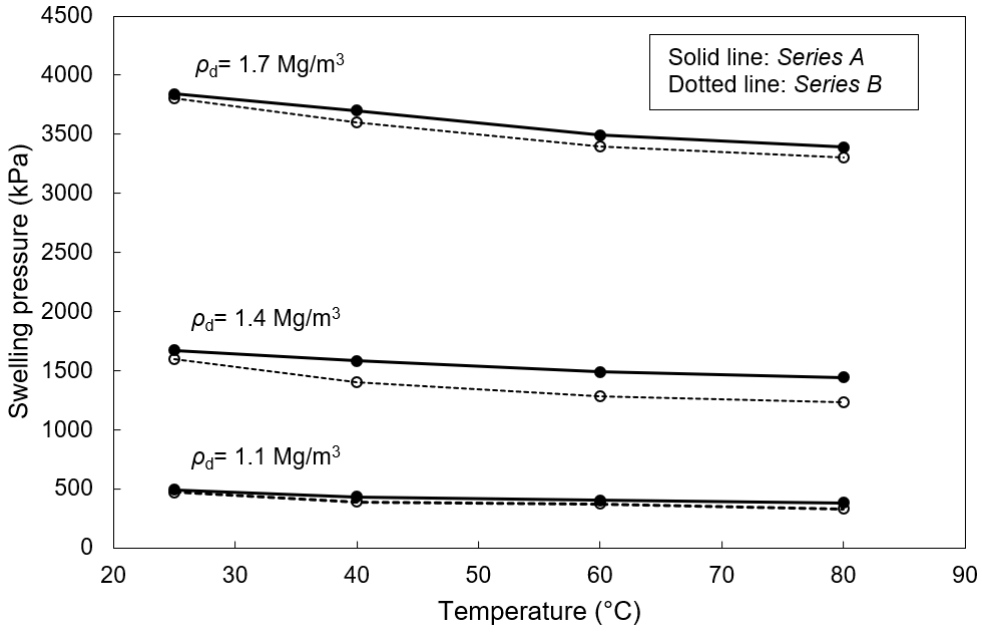

Fig. 4.6. Variations of swelling pressure with temperature for compacted bentonite for *Series A* and *Series B.*

4.3.2. Temperature effects on hydraulic conductivity

For both series of experiments *Series A* and *Series B*, once the swelling pressure reached steady-state at a given stage of the test, the hydraulic conductivity of the sample was measured under isothermal temperature. A linear relationship between flux and time was observed at each equilibrium for all the test (i.e., the injected volume versus elapsed time for CB1 is presented as shown in Fig. 4.7). The slight drop of volume between different stages is possible due to an increase of the water pressure at base interface when increasing temperature. The pressure controller automatically proceeds from the feedback and further reduces the injected volume. The saturated hydraulic conductivity was calculated based on Darcy's law:

$$Q = K_h i A \tag{4.2}$$

where, Q is the water flux (m^3/s), K_h is the hydraulic conductivity (m/s); i is the hydraulic gradient (m/m) and A is the cross-section area (m^2). The variations of hydraulic conductivity with water properties can be presented by:

$$K_h = \frac{\gamma_w}{\mu_w} k_p \tag{4.3}$$

where, k_p is intrinsic permeability (m^2), γ_w is the unit weight of water (Nm^{-3}), and μ_w is the dynamic viscosity of water ($Nm^{-2}s$). As shown in Fig. 4.8, with an increase of dry density of smectite, the presence of the reduction of permeability can be observed by comparing the data from literatures. Increasing dry density of smectite means the width of flow channel is much reduced. The decrease of permeability at higher dry density is related to the increase in viscosity caused by the main fraction of pore water is mineral-adsorbed (Pusch, 1980b).

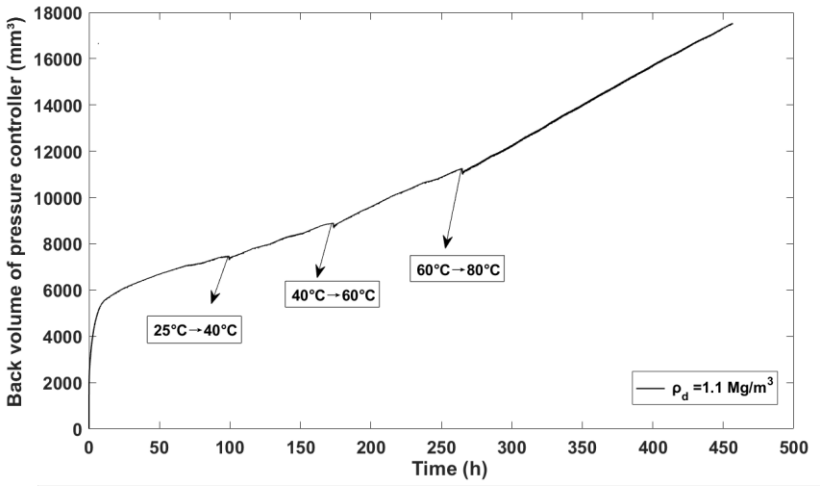

Fig. 4.7. Evolution of the injected water volume at different temperature for CB1 in *Series A*.

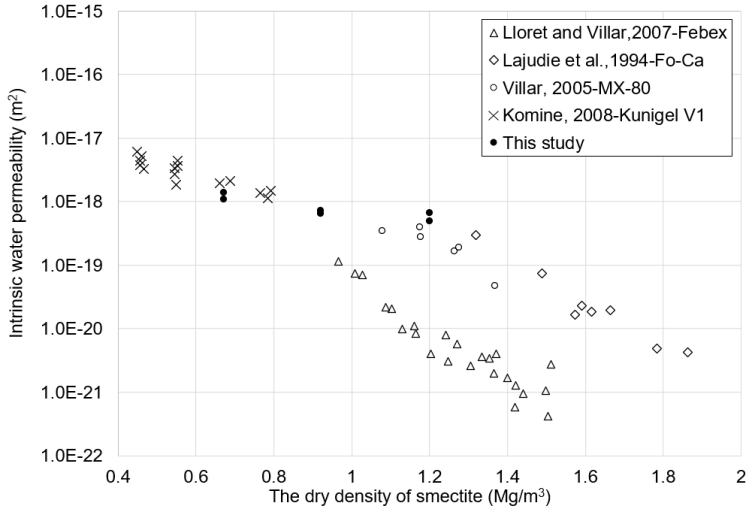

Fig. 4.8. Experimental data for intrinsic water permeability of different bentonite clays at different dry density of smectite.

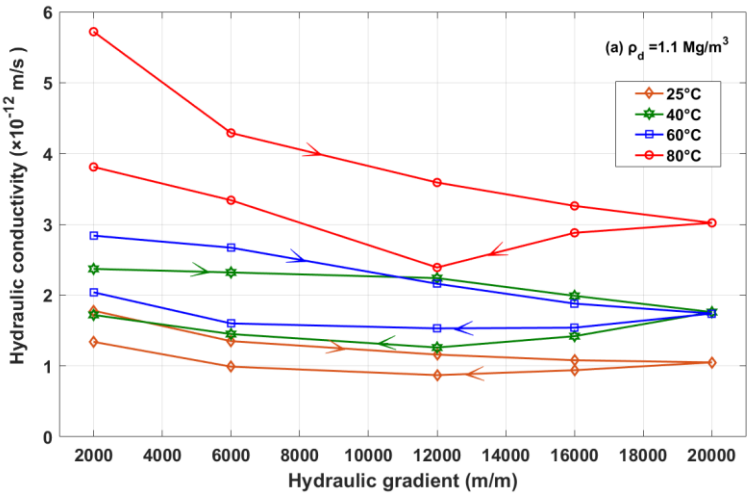

(a)

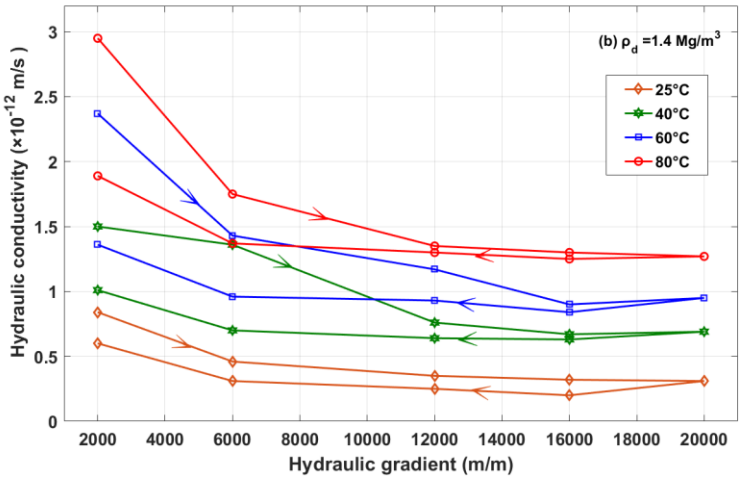

(b)

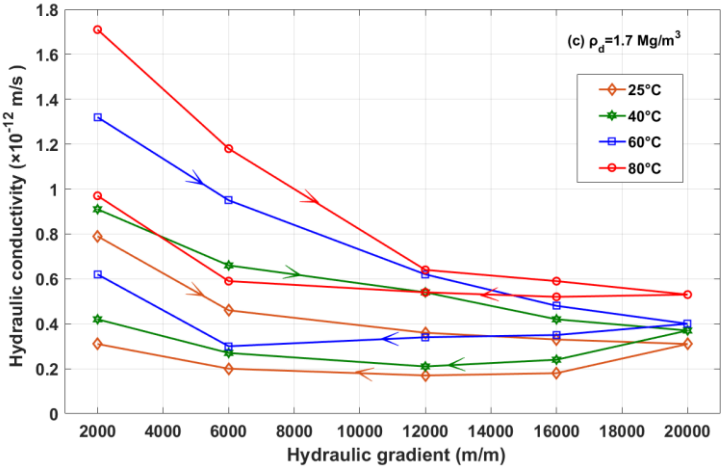

(c)

Fig. 4.9. Variations of hydraulic conductivity with hydraulic gradient at different temperature and dry densities for experiments *Series B*.

In *Series A*, the results show that temperature has larger effects on the hydraulic conductivity at low dry density (for the sample CB1, k increased from 1.2×10^{-12} m/s at ambient temperature to approximately 2.5×10^{-12} m/s as shown in Fig. 4.10.). The increases of hydraulic conductivity at 40°C and 60°C are found to be limited for CB2 and CB3 compared to the values measured at 25°C. However, the increase of temperature has less impact on the hydraulic conductivities for CB2 and CB3 compared to that observed for CB1 when temperature is increased from 60°C to 80°C.

In *Series B*, the hydraulic conductivity was measured at different hydraulic gradients as shown in Fig. 4.9. The hydraulic gradient was first increased for each sample and then reduced gradually to the initial value. During each step the hydraulic conductivity was calculated by knowing the flow rate and hydraulic gradient. The aim was to establish an understanding of whether the hydraulic gradient caused changes to the fabric and to what extent temperature would be important in this process.

Figure 4.10 presents the variations of hydraulic conductivity with temperature for the two series of tests. For the case of CB1 (dry density of 1.1 Mg/m^3), the overall increase of hydraulic conductivity at 80°C is found to be much more significant in comparison with that of the samples with higher dry densities (i.e., CB2 and CB3 with dry densities of 1.4 Mg/m^3 and 1.7 Mg/m^3, respectively). Less compactive effort is needed for CB1, and the bonding between particles is the weakest. The force generated by the accelerated flow might affects the stability of soil matrix, especially for CB1.

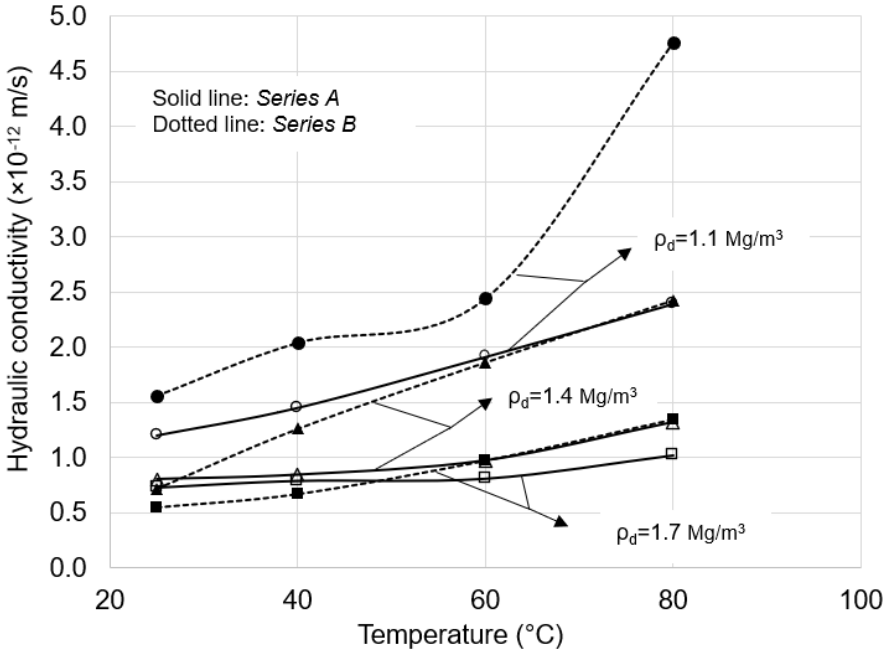

Fig. 4.10. Variations of hydraulic conductivity with temperature for *Series A* and *Series B*.

Fig. 4.10 presents the variations of hydraulic conductivity with hydraulic gradient for different samples studied under *Series B*. The average values of hydraulic conductivities were obtained based on starting values and final values through a cycle of gradient path. A level of irreversibility can be observed with regards to the hydraulic response of the samples to hydraulic gradients applied. These observations are consistent with those reported by Dunn et al. (1984) on fine-grained soil samples. The hydraulic conductivity of compacted bentonite clays decreases with the increase of hydraulic gradient, while it is subsequently found to be irreversible and by decreasing the hydraulic gradients from 20,000 to 2,000, the hydraulic conductivity is increased.

As already mentioned, the hydraulic gradient in our study was firstly increased from low to high value, and then decreased back to the original low value. However, Pusch (1980b) adopted different path, reducing the gradient from 10,000 to 1000 and observed different hydraulic behaviour. They found that the hydraulic conductivity of compacted bentonite was influenced by hydraulic gradients and decreased with the decrease of hydraulic gradients at low bulk density. For denser samples, the behaviour

was different, and the hydraulic conductivity remained unchanged when decreasing the hydraulic gradient. Dixon et al. (1999) investigated this phenomenon and indicated that the hydraulic conductivity is gradient dependent. Increasing the hydraulic gradient led to an increase of hydraulic conductivity of bentonite sample in low dry densities (0.76 Mg/m^3 and 1.09 Mg/m^3). The experimental results from Al-Taie et al. (2014) showed that the reduction of hydraulic conductivity appeared when hydraulic gradient was beyond certain value. The shear stresses raised by the increase of injected pressure could induce aggregate breakdown, particularly for the prominent parts with weakened bonding. In addition, the impacts of applying high hydraulic gradients may also cause migration of particles, resulting in clogging the pore spaces and subsequently reduction of permeability.

4.4. Discussion

Microstructure of compacted bentonite changes with temperature and such effects can explain the changes in the swelling pressure and hydraulic conductivity of compacted bentonite with temperature. The system of compacted bentonite can be described as an assemblage of particles with sizes at different length scales and the associate multiscale pores. Fig. 4.11 presents a schematic of the compacted bentonite and its microstructure. At least two scales of porosity can be described in compacted bentonite which include micro porosity and macro porosity. Micro porosity constitutes the pores between the clay layers (it is also called interlayer porosity) and macro porosity includes the spaces between aggregates (inter-aggregate and intra-aggregate pores are included within macro porosity) (Delage et al., 2006; Romero et al., 2011; Massat et al., 2016).

The pore water in the system includes: i) the interlayer water which exists in the micro pores, ii) the water affected by the electrical surface charges (DDL water) which exists in macro pores and iii) free water in macro pores for which the properties of bulk

or free water can be assumed (Bradbury and Baeyens, 2003; Appelo, 2013).

The clay-water-chemical system responds to the temperature changes to establish a new equilibrium in the clay system which is ultimately reflected in the evolution of swelling pressure and hydraulic conductivity. Those responses and processes can be categorised as below:

- Temperature effects on the properties of water
- Changes to the water clay interactions and retention
- Re-distribution of water between micro and macro structure

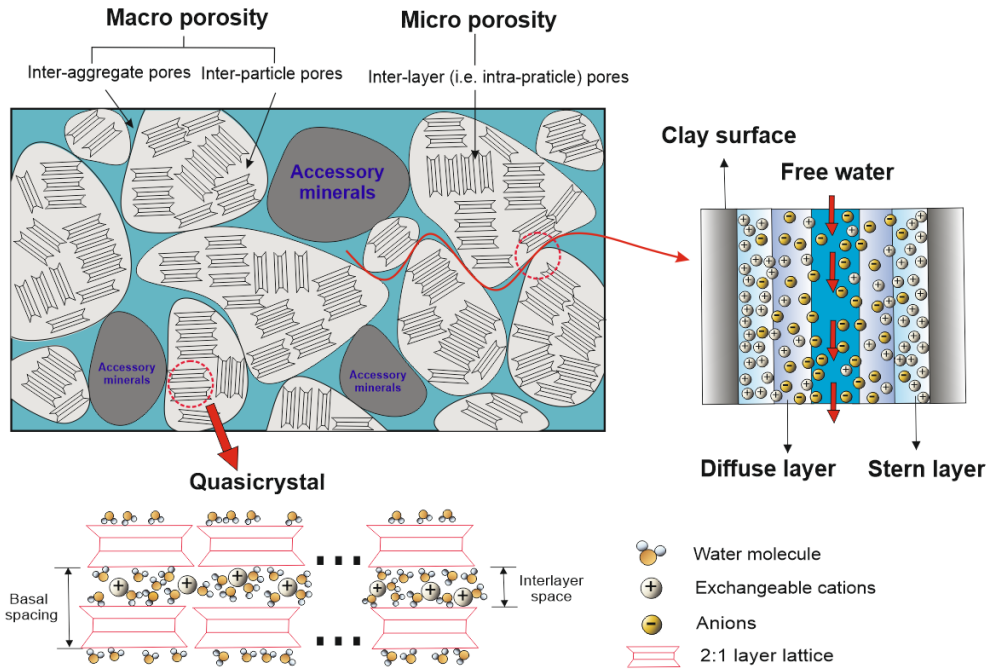

Fig. 4.11. Microstructure of compacted bentonite at saturation.

4.4.1. Temperature effects on the properties of water

The physical properties of water, e.g., density (unit weight) and viscosity, vary with temperature. The changes on water viscosity and density contributed to the evolution of hydraulic conductivity with temperature (Villar et al., 2010). If intrinsic permeability is assumed to be temperature independent (which is only the case of coarse-grained materials and not compacted bentonite), the variations of hydraulic conductivity with temperature could be calculated purely based on temperature

dependency of water density and viscosity by using Eq. (4.3). Figure 4.12 presents the variations of hydraulic conductivity with temperature calculated using Eq. (4.3), i.e., $K_h = \frac{\gamma_w}{\mu_w} k_p$, for experiments series *A* together with the experimental data points.

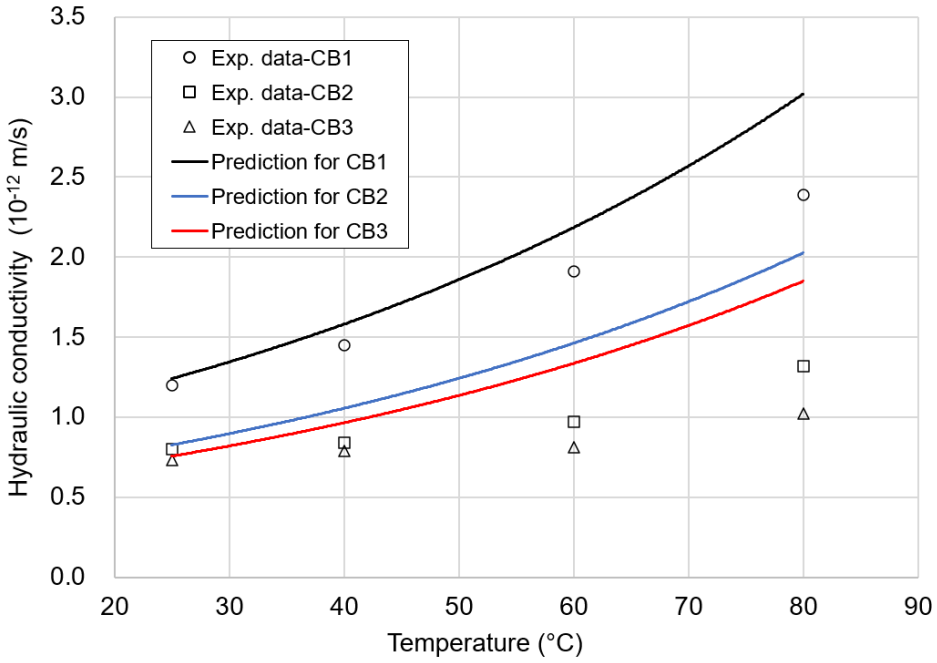

Fig. 4.12. Variations of hydraulic conductivity with temperature for experiments *Series A* according to water viscosity and density changes.

The measured variations of conductivity with temperature cannot be attributed to the changes in water properties alone, as the calculations based on Eq. (4.3) over-predict the temperature effect for all clay densities. The results presented agree with similar calculations for compacted FEBEX bentonite (Villar and Lloret, 2004). The discrepancies between the calculation and experimental observations are related to i) the fact that the intrinsic permeability in compacted bentonite is strongly controlled by microstructure (e.g., Chen et al., 2020), and ii) the physical states of water in micro (interlayer) and macro pores are different. It has been shown that the viscosity of absorbed water on mineral surfaces is higher than that of bulk water under normal hydraulic gradient (Pusch and Yong, 2006). Therefore, the mobility of interlayer pore water is considered to be limited and the interlayer water can be regarded as an immobile phase. The exchange of water between the micro pores and macro pores can

in principle increase the potential flow at elevated temperature as the ratio of mobile water to the total water increases. It has also been shown that the interlayer water density can be larger than that of free water (Lloret and Villar, 2007). Skipper et al. (1991) estimated the interlayer water density to be 1.4 Mg/m^3 for Mg-smectite and 1.1 Mg/m^3 for Na-smectite. Jacinto et al. (2012) calculated and obtained the range which is from 1.17 to 1.09 Mg/m^3 for MX 80 bentonite compacted at 1.6 Mg/m^3 dry density. Fernández and Rivas (2005) have shown that the interlayer water density is ranging from 1.1 to 1.5 Mg/m^3 in compacted FEBEX bentonite. Wang et al. (2014a) indicated that the interlayer density was 1.1 Mg/m^3 for the saturated MX-80 sample at a dry density of 1.6 Mg/m^3, which increases with increasing dry density.

The extent to which the temperature effect on water viscosity and density is important in controlling the hydraulic conductivity has been studied by Villar and Lloret (2004). They have shown that if only temperature dependency of water viscosity and density are considered as controlling mechanisms for hydraulic conductivity, an over-prediction of the experimentally measured values can be expected. The results in this work support their conclusions and suggest that the intrinsic permeability of the clay cannot remain the same at elevated temperature. The microstructure evolution with temperature is complex and involves changes to the soil fabric and tortuosity which ultimately affects the intrinsic permeability (e.g., Chen et al., 2020).

4.4.2. Changes to the clay water interactions and retention properties

The overall retention of water in the clay system is affected by temperature and subsequently the main mechanisms of swelling pressure development in bentonite (i.e., crystalline swelling and osmotic swelling) are affected. It has been shown that the water retention capacity of bentonite reduces at elevated temperature (Villar et al., 2010). It is partly related to the fact that surface tension of water varies with temperature and affinity of water to surfaces reduces as temperature increases. The osmotic effects are rather more complicated as they involve the complex geochemical behaviour of multi-

ionic system of pore water in macro pores including the activity of water, ionic species, precipitation/dissolution processes.

Experimental observations of water retention behaviour of compacted bentonite at elevated temperature indicate an overall decrease of water retention capacity at higher temperature (Jacinto et al., 2009). At higher temperature, the total water content (after saturation) tends to be lower. On the other hand, and as shown in Fig. 4.4, the time to reach equilibrium (or reach the maximum swelling pressure) is longer at lower temperature than that of elevated temperature. Such effects can induce changes to the equilibrium and kinetics of water adsorption in the system which is therefore reflected in the overall swelling pressure and hydraulic conductivity.

Temperature affects the properties of diffuse double layer where osmotic swelling is dominating. As shown in Fig. 4.11, the diffuse double layer contains three types of water: Stern layer water, diffuse layer water, and free water. The dielectric constant of pore fluid and the Debye length (i.e., the maximum possible diffuse double layer thickness) can change with the increase of temperature (Michell and Soga, 2005). Tripathy et al. (2015) have shown that the decrease in the swelling pressure of compacted MX-80 at elevated temperature is in several ways related to temperature effects on the major parameters embedded in the electrical triple-layer (i.e., the clay surface, the Stern-layer, and the diffuse double layer) theory. However, this prediction of swelling pressure only fits well with the samples whose density is under 1.45 Mg/m^3 when compared with experiment. In principle changes to the water interaction with surfaces and chemical system, induce mobility and water exchange between the microstructure which are discussed further below.

4.4.3. Re-distribution of water between micro and macro pores

It has been shown that the proportion of micro porosity (interlayer porosity) in saturated compacted bentonite increases almost linearly with dry density (e.g., Bourg et al., 2003; Sedighi and Thomas, 2014). For the sodium rich MX-80 bentonite,

compacted at dry densities above 1.6 Mg/m^3 more than 50% of pore water is in the micro porosity (Sedighi, 2011; Sedighi and Thomas, 2014). A large proportion of pore water in macro pores is affected by the electrical diffuse layer at high dry densities and thus there is a limited amount of bulk or free water. Bradbury and Baeyens (2003) estimated that the free water only accounted for 1.1% of total pore water at a dry density of 1.8 Mg/m^3 when compacted MX-80 bentonite was saturated under constant volume. Similarly, Fernández et al. (2004) reported that only 1.5% of total pore volume was available for free water in compacted FEBEX bentonite at dry density 1.65 Mg/m^3. At lower densities (below 1.6 Mg/m^3), the largest proportion of water is in macro pores. For example, only 20-30% of pore water at dry density of 1.2 Mg/m^3 is located in micro pores (Sedighi and Thomas, 2014). Elevated temperature induces an exchange of pore water between the interlayer and macro pores (Ma and Hueckel, 1992; Lloret and Villar, 2007; Sedighi et al., 2018). It has been shown that the interlayer porosity can shrink by approximately 20% when temperature increases from 20ºC to 80ºC for a fully saturated MX-80 bentonite at dry density 1.6 Mg/m^3 (Sedighi, 2011). Such exchange of water between the micro pore and macro pore can reduce the contribution of the crystalline swelling in the overall swelling pressure at elevated temperature. The effect is less pronounced at lower densities as most of the water locates in the macro porosity.

The three key processes described above are strongly interlinked and assessing the contribution of each process on the experimental observations may not be fully accurate based on existing theoretical developments. It is anticipated that the exchange of water between micro pores and macro pores play a significant role in the observed behaviour, as this process can increase the potential flow at elevated temperature due to the increase of the fraction of mobile water. From the experimental results it can be observed that the swelling pressure drops more considerably in denser samples in both *Series A* and *Series B*. For all densities at which hydration tests were carried out, an acceleration of hydration at elevated temperatures are observed. This is largely related to the fact that a larger proportion of water exists at macro pores and the mobility of

water is facilitated at elevate temperature. The overall increase of water mobility is also reflected in the hydraulic conductivity measured.

It is recognised that the clay particles shrink at elevated temperature due to the decrease of interactions between surfaces and water (Jacinto, 2009; Sedighi et al., 2018), but understanding of how the particles evolve (i.e., the number of individual clay layers forming a particle) at elevated temperature is limited. The loss of absorbed water into macro pores results in the decrease of crystalline component of swelling pressure. Meanwhile, the proportion of mobile water in macro pores increases and the effects of osmotic processes can be further enhanced.

The increase of hydraulic conductivity observed is partially related to the reconfiguration of microstructure and porewater in the system. For the denser sample, the volume of bulk water is lower after saturation, which explains why the change of hydraulic conductivity is smaller than that of the looser sample. Furthermore, the change of hydraulic gradient can result in the breakdown of aggregate with weak bond and subsequently block the flow path (the appearance of clogging in macro pores) which is evident in the variations of hydraulic conductivity observed in cycles of analysis.

The evolution of swelling pressure and hydraulic conductivity with temperature is controlled by a set of complex and strongly interlinked microstructural processes. Overall, the exchange of water between the different pore scales which is facilitated by the reduction of water retention properties of clay at elevated temperature is a critical controlling process. Understanding how these processes are interlinked requires further theoretical insights into the problem. The gap in knowledge is particularly evident at particle level, i.e., how temperature affects the particle system (e.g., number of layers forming a particle).

4.4.4 Implications for plugging and abandonment of oil and gas wells

Compacted bentonite as an alternative plugging material to cement in the forms of small pellets and large bullet shapes (Englehardt et al., 2001; Towler et al., 2016) have been used for plugging of onshore well. At the depth of deployment of clay plugs, the mechanical stability of plugs mainly depends on the magnitude of swelling pressure of bentonite as the generated friction force against the casing wall. This is also related to the length of a plug which prevents the plugs from moving upward or downward. The guidelines of laboratory qualifications of bentonite clays recommend the shear bond strength of larger than 1 MPa which is originally generated by swelling pressure (Oil and Gas UK, 2012). Based on a series of successful field trial tests, an optimum range of swelling pressure has been found to be between 0.69 MPa and 3.45 MPa so that sufficient friction force can be generated to keep the plugs in place without damaging the wellbore casing (Carl, 2004). Our study has generated new insights to the impacts of temperature on the final swelling pressure and also the kinetics of swelling pressure development which are important in the context of well plugging application. Specifically:

1. It has been shown that the increase of temperature (representing the temperature increase of the sample from ground level to the emplacement depth) generates a maximum 30% reduction in the swelling pressure from 20°C to 80°C.

2. The hydration time (time to reach maximum swelling pressure) is considerably reduced at elevated temperature. This observation has two implications: i) rapid sealing of the well by bentonite plug at depth which is an advantage (when setting time is important) ii) accelerated hydration during emplacement which can cause unforeseen friction with the wall.

3. The results show that for the case of the bentonite used, the magnitude of swelling pressure and hydraulic conductivity at dry density of 1.1 Mg/m^3, might not be sufficient for the purpose of wellbore plugging. The swelling pressure for the samples compacted at 1.4 Mg/m^3 provides an adequate level of swelling pressure and hydraulic

conductivity in this research. For further application, one aspects of future investigations need to focus on the shear bond strength as required with a higher dry density.

4. From the swelling pressure point of view, the use of dry unit weight of smectite instead of gross dry unit weight (as it was used in Fig. 4.2) can provide a guidance for the preliminary selection of the suitable commercial bentonite from plugging.

It is noted that the swelling pressure is only one of the key properties of a bentonite-based plug and other properties such as hydraulic conductivity are equally important and this requires further investigation. In addition, further research to examine the behaviour under the specific fluid conditions of the plugging depth is critical (e.g., salinity impact).

4.5. Conclusions

The effects of elevated temperature on swelling pressure and hydraulic conductivity of sodium-rich bentonite compacted at three dry densities were studied. A bespoke high pressure, high temperature constant strain oedometer was designed and commissioned to develop an understanding of i) the swelling pressure response of pre-saturated compacted bentonite to the increase of temperature and ii) the swelling pressure development during saturation at elevated temperature. The measurements were extended to evaluate the effects of elevated temperature on hydraulic conductivity of samples studied for both series of experiments.

The results showed an overall decrease of swelling pressure with temperature increase from 25°C to 80°C for all three dry densities studied. The swelling pressure reduction was much larger for higher density samples, indicating a larger exchange of pore water in the microstructure system of the clay. The response of samples saturated at elevated temperature indicated an acceleration of the hydration rate to reach the new pressure equilibrium. An increase of hydraulic conductivity with temperature was

consistently observed across the densities studied. Larger increase of hydraulic conductivity was observed for lower density samples. An enhanced hydraulic conductivity was observed with increasing hydraulic gradient, which was further pronounced at elevated temperatures. The responses observed were explained with the rearrangement of pore water in the microstructure and with changes to water mobility due to changes of its physical and retention properties with temperature.

CHAPTER **FIVE**

5. Prediction of the swelling pressure of compacted bentonite

5.1. Introduction

Prediction of the swelling pressure of compacted bentonite in the engineered barriers system is important in all sealing concepts. The ion distributions adjacent to the charged clay surfaces is an important factor for understanding the swelling behaviour of bentonite clay. In this chapter, a model for predicting the swelling pressure of compacted bentonite is proposed and presented which is based on regular solid-solution theory and diffuse double layer theory. The procedures used to establish the variation of swelling pressure with dry density of smectite and at elevated temperature in compacted bentonite are presented.

In section 5.2, the diffuse double layer (DDL) theory is introduced and applied for the prediction of swelling pressure. In section 5.3, an improved model for swelling pressure calculation based on DDL theory is proposed. In section 5.4, the calculated values of swelling pressure from the proposed model are compared with the experimental data for ten different types of bentonite from literature. The applicability of the proposed method is tested, and the influence of the formation of clay particles on the dry density of smectite against swelling pressure of compacted bentonite were also studied. A conclusion is presented in section 5.5.

5.2. Theoretical background

5.2.1. DDL theory

Bentonite clays have a high swelling potential which is mainly due to the presence of a high proportional montmorillonite clay mineral (Pusch and Yong, 2006). Montmorillonite is negatively charged as the result of isomorphous substitutions. An

electrical double layer is formed when the surface of clay is exposed to a fluid (Bolt, 1956; Mitchell 1993). The closer to the clay surfaces, the higher concentration it exhibits due to the absorbed cations. Hence, the difference in concentration leads to the cations diffuse away from the clay surfaces for the charge balance. Water molecules and the exchangeable cations move towards the clay surface and into the interlayers space, driven by the equalization of potential and charge deficiencies between the clay surface and solution.

According to the Gouy-Chapman diffuse double layer theory (DDL), the interaction force between two clay layers depends on the ion concentration at the midplane and is equivalent to the osmotic pressure in that plane (Bolt, 1956). The swelling pressure is the difference between the osmotic pressure in the midplane and the osmotic pressure in equilibrium solution (Bolt, 1956). Bolt (1956) and van Olphen (1964) proposed a method for calculating the swelling pressure in a clay–water electrolyte system. Sridharan and Jayadeva (1982) improved the procedure given by Bolt and van Olphen and the equations are as follows:

$$p = 2n_0 kT(\cosh u - 1) \tag{5.1}$$

$$\sqrt{(2\cosh z - 2\cosh u)} = \left(\frac{B}{S}\right)\sqrt{\frac{1}{2\varepsilon_0 D n_0 kT}} \tag{5.2}$$

$$\int_z^u \frac{1}{\sqrt{(2\cosh y - 2\cosh u)}}\,dy = -Kd \tag{5.3}$$

$$K = \sqrt{\frac{2n_0 v^2 e'^2}{\varepsilon_0 DkT}}\ (m^{-1}) \tag{5.4}$$

$$e = G_s \gamma_w SSA_{tot} d \times 10^6 \tag{5.5}$$

where p is the swelling pressure (Pa), n_0 is the ionic concentration of the bulk fluid (number/m^3), k is Boltzmann's constant (1.38 × 10^{-23} J/K) and T is the absolute temperature (K). u is the nondimensional midplane potential, x is the distance from the clay surface, y is the nondimensional potential at distance x from the clay surface, ξ is the distance function and z is the nondimensional potential at the clay surface. γ_w is the unit weight of water, SSA_{tot} is the total specific surface area of soil (m^2/g), B is the exchange capacity of the clay (meq/100 g), d is half the distance between clay

layers (m), K is the diffuse double layer parameter (1/m), e' is the elementary electric charge (1.602×10^{-19} C), ε_0 is the permittivity of vacuum and is equal to $1/4\pi$ in the esu system (Partheniades, 2010). D is the relative dielectric constant of bulk fluid (80.4 for water), the n_0 (ionic concentration of bulk fluid) value is considered as 10^{-4} M (Schanz et al., 2013), which refers to distilled water, e is the void ratio, G_s is the specific gravity of solid particles. As shown in Fig. 5.1, ψ_0 means surface potential. ψ and ψ_d means the potential at distance x and d from the clay surface.

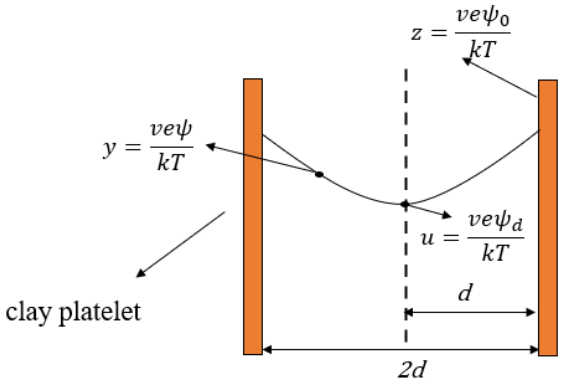

Fig. 5.1 A simplified schematic of the diffuse double layer formed between two parallel surfaces of clay platelets.

The simplified model with two single clay platelets is presented in Fig.5.1. The determination of the swelling pressure using Eq. (5.1) requires the nondimensional midplane potential function, u. For the given properties of the bentonite (i.e., e, B, SSA_{tot}, n_0 , and v) and the corresponding values of d values were calculated from Eq. (5.5). From Eq. (5.1), the magnitude of swelling pressure depends on the value of d (half the distance between parallel clay layers). K is calculated from Eq. (5.4). The values of z and u can be determined from Eq. (5.2) and Eq. (5.3).

5.2.2. Swelling pressure calculation by DDL theory

In this section, the predictions of swelling pressure of compacted MX-80 bentonite and FEBEX bentonite are presented by applying the DDL theory from Eq. (5.1) to Eq. (5.5). The parameters for the determination of the relationship between swelling

pressure and dry density are shown in Table. 5.1. The deviation between experimental data and predicted values for swelling pressure is disused below.

Table 5.1 Physic characteristics of two kinds of bentonite

Name	MX-80[a]	FEBEX[b]
Dominated cations	Na	Ca
Specific density (Mg/m^3)	2.76	2.7
Montmorillonite content (%)	75	92
CEC (meq/100g)	0.73	1.02
Specific surface area (m^2/g)	562	725
Weighted average valency of cations	1.14	1.67

[a] Data from Bucher and Müller, 1989; [b] and [c] Data from ENRESA, 2000

Figure 5.2 presents the variations of swelling pressure and the dry density of MX-80 and FEBEX bentonite. For compacted MX-80 bentonite, the prediction seems to fit well the experimental data when the dry density is smaller than 1.5 Mg/m^3. The deviation between predicted swelling pressure and experimental values turns into larger at relatively high dry densities (ranging from 1.5 to 1.7 Mg/m^3). For compacted FEBEX bentonite, the predicted values were overestimated compared with the measured values when the dry density is smaller than 1.4 Mg/m^3. However, there was an overestimation when the dry density is denser than 1.4 Mg/m^3, and the deviation between predicted swelling pressure and experimental values becomes larger.

The deviations between experimental swelling pressure and theoretical swelling pressure in Fig. 5.2 might be caused by many reasons which can be concluded as follows: (i) poorly developed or partially developed diffuse double layer, (ii) reduced specific surface area because of formation of clay particles, (iii) surface and ion hydration at close particle distances,(iv) non-uniform size of clay plates, (v) existence of electrical attractive forces, (vi) presence of multivalent cations, (vii) effect of ion size, (viii) anion adsorption, and (ix) particle size (Bolt, 1956; Sridharan and Jayadeva, 1982; Mitchell, 1993; Schanz and Tripathy, 2009; Schanz et al., 2013). Efforts have been made to develop an appropriate relationship between the u and Kd by obtaining

the empirical equation from experimental data (Schanz and Tripathy, 2009; Schanz et al., 2013; Sun, 2017). Using the model proposed by Sridharan and Jayadeva (1982), the result shows that it also does not truly represent the conditions present in a clay-water system. The influence of hydration force between interlayers cannot be neglected. As cations and water molecules enter the interlayer space, the overlapping double diffuse layers is not the reason that contributes to the repulsive force between clay layers but rather by the existence of structurally modified water in the vicinity of clay surfaces (Low, 1991). Yong and Mohamed (1992) stated that the repulsive forces arising due to interaction of clay layers at close particle spacing are primarily caused by the hydration of ions. At higher dry densities, the interlayer hydration force between clay platelet surfaces and exchangeable cations is dominated (Schanz and Tripathy 2009). For dry densities of the clay greater than 1.4 Mg/m^3, the development of swelling pressure can primarily be due to the hydration forces, and the predicted values from the diffuse double layer theory are much greater than the measured ones.

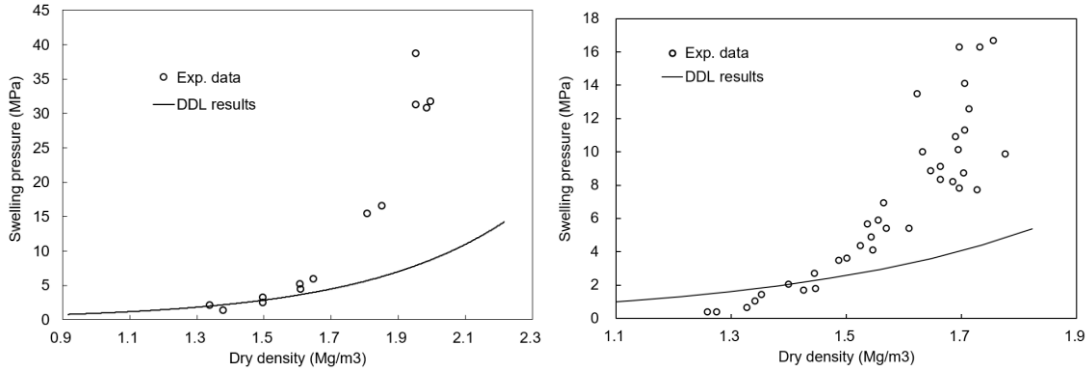

(1) MX-80^a (2) FEBEX^b

Fig. 5.2. Comparison of experimental and theoretical swelling pressures from DDL theory of sodium and calcium bentonites ([a] Data from Bucher and Müller, 1989; [b] Data from ENRESA, 2000).

5.3. Revisiting the DDL model for the prediction of swelling pressure

In DDL theory, the simplified two clay platelet model has been used to predict

swelling pressure by assuming that the clay particles consist of a single unit layer. The original model has a number of assumptions that contribute to over or under-estimation of swelling pressure of compacted bentonite. The model is revisited:

(i) The formation of tactoids can influenced the surface area of the montmorillonite as a much larger particle with the diffuse double layer only fully manifesting itself on the outside surfaces (Manassero et al, 2016). A possible reduction of the specific surface area due to the formation of the clay particles has not been considered in the DDL theory (Schanz and Tripathy, 2009). A relationship between external specific surface area (SSA_{ext}) and total specific surface area (SSA_{tot}) can be established based on lamellar structure of bentonite, and the SSA_{ext} can be expressed as Eq.(5.6) for bentonite (Tournassat et al. 2011, Chen et al., 2020),

$$SSA_{ext} = \frac{SSA_{tot}}{n_s} \tag{5.6}$$

where SSA_{ext} is the outer interlayer surface area (i.e., effective specific surface area). SSA_{tot} is a constant which can be measured by experimental techniques such as EGME (Ethylene Glycol Monoethyl Ether). n_s is the stacked layers of per particle.

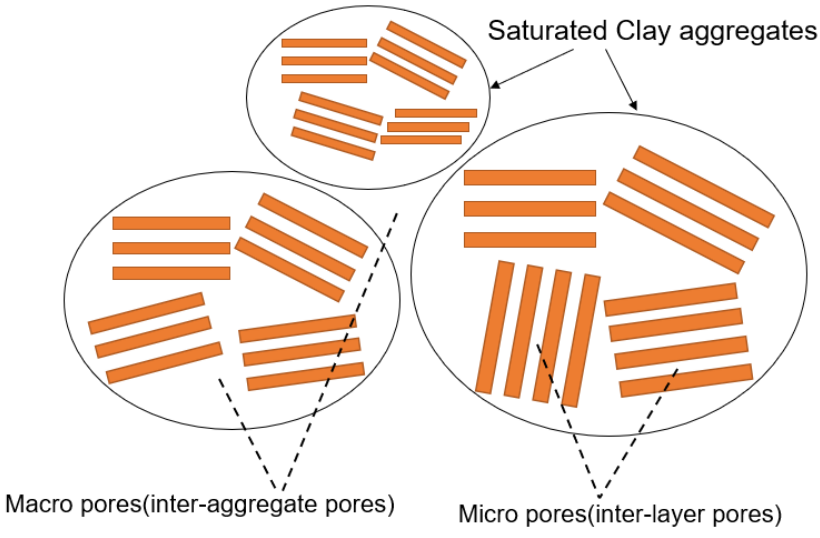

Fig. 5.3. Schematic of pore system of compacted bentonite

(ii) The DDL water forms the transition zone from the clay surface to free pore water (Appelo, 2013), which appears in macro pores as shown in Fig. 5.3. The amount

of diffuse layer water poorly developed due to the limited interparticle space (Ben et al.,1987; Marcial et al., 2002). The total void ratio (e) in the improved model given by Sridharan and Jayadeva (1982) can be modified by using the macro pore ratio e_{marco}. The total void ratio is presented as follows (Sedighi and Thomas, 2014):

$$n = 1 - \frac{\rho_d}{G_s} \tag{5.7}$$

$$n_{macro} = n - n_{micro} = \frac{e_{macro}}{1+e_{macro}} \tag{5.8}$$

$$n_{micro} = X_{hs} \frac{n_c v_{il}}{m_{sm}} \rho_d^{sm} \tag{5.9}$$

$$\rho_d^{sm} = X_{sm}\rho_d[1 - (1 - X_{sm})\frac{\rho_d}{\rho_{im}}]^{-1} \tag{5.10}$$

where n is porosity, G_s is the specific gravity of the clay, ρ_d represents the bulk dry density of the clay (kg/m^3). ρ_{im} denotes the density of the non-smectite minerals or impurities (kg/m^3). n_{macro} and n_{micro} are macro micro porosity of the soil, respectively. ρ_d^{sm} represents the dry density of smectite (kg/m^3). v_{il} denotes the specific molar volume of the interlayer water (=17.22 m^3/mol). m_{sm} means the molar mass of dry smectite (=378.79 kg/mol). n_c means moles of the adsorbed interlayer water. In fact, the hydration state of the interlayer is related to multiple factors such as the type of absorbed cations, the water activity, and the temperature. With the presence of crystalline swelling, it is considered that smectite display basal spacings normally determined by X-ray diffraction represents water layer hydration states. For example, the basal spacing is 1 nm, which is equivalent to no water layer. The basal spacing is 1.25 nm when there is 1 water layer. The crystalline swelling of homoionic Na- or Ca-montmorillonites seems to be unable to exceed three water layers (Norrish, 1954; Kozaki et al., 1998). The value of n_c is equal to 4.5 corresponding to two interlayers water. X_{hs} means the total amount of interlayer water with respect to the hydrate state of smectite when relative humidity is equivalent to 100%, X_{sm} is the mass fraction of smectite in the clay (dimensionless). Ransom and Helgeson (1994) described the mass action law as:

$$log\ K_{eq} = log\left(\frac{1-X_{hs}}{X_{hs}}\right) + \frac{W_s}{2.303RT}(2X_{hs} - 1) + n_c log\alpha_{H_2O} \quad (5.11)$$

where K_{eq} represents the equilibrium constant of the reaction. W_s denotes the Margules parameter for the binary regular solid-solution of hydrous and anhydrous smectite components at reference temperature (25 °C) and pressure (1 bar) which is independent of pressure and temperature (Ransom and Helgeson, 1994). R is gas constant. T is the temperature (K). In this model, the Eq. (5.5) can be modified as follows:

$$e_{macro} = G_s\gamma_w \frac{SSA_{tot}}{n_s} d \times 10^6 \quad (5.12)$$

Assumed the properties of bentonite (i.e., e, B, SSA_{tot}, n_0 , and v) are known, the procedures can be concluded to predict the swelling pressure as shown in Fig. 5.4:

(i) To obtain the hydration fraction of smectite X_{hs} through thermodynamic parameters W_s and K_{eq}.

(ii) Given that the smectite content is known, the micro porosity can be calculated from Eq. (5.9).

(iii) According to the previous studies of the formation of the clay particles, the unit layer per particle n_s can be assumed. The half the distance between clay layers d can be obtained by Eq. (5.12).

(iv) The physical characteristics of bentonite are known. The nondimensional midplane potential u and the nondimensional potential at the clay surface z can be calculated from Eq. (5.2) and Eq. (5.3).

(v) From Eq. (5.1), the theoretical swelling pressure can be determined.

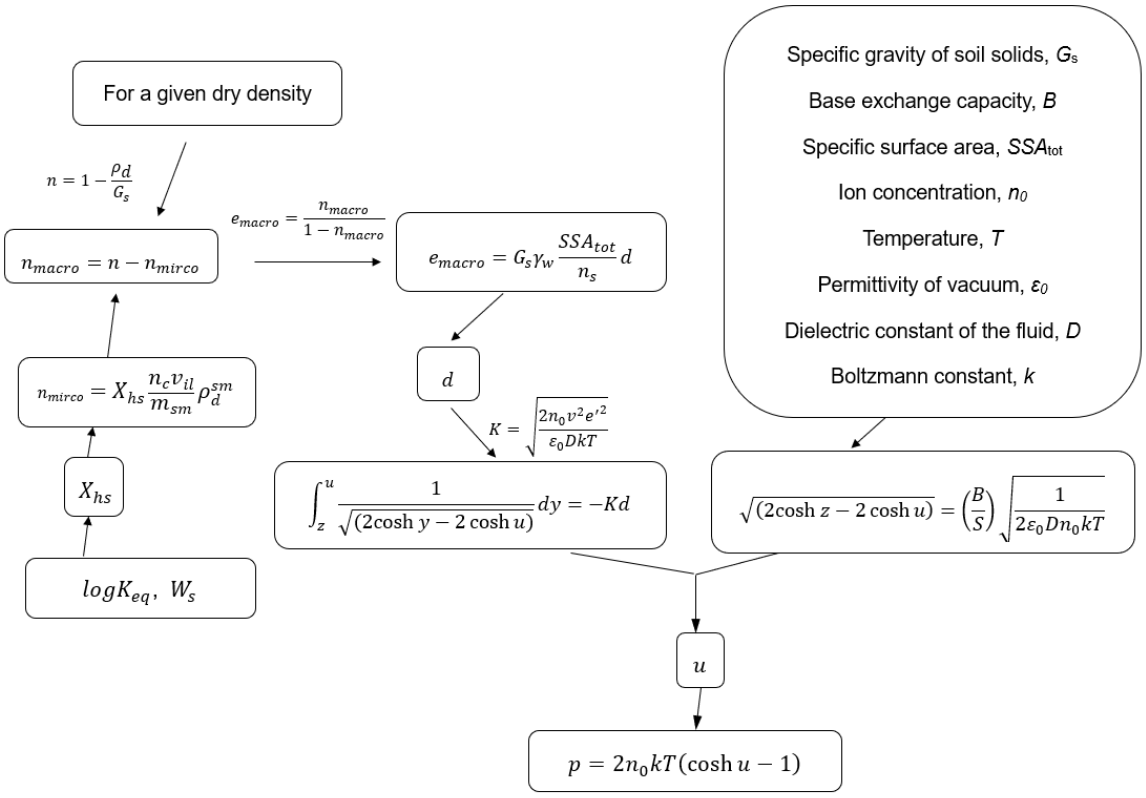

Fig. 5.4. The procedure for calculation of the swelling pressure for a given dry density with the proposed method.

5.4. Validation of the proposed model

To examine the accuracy, the improved model was applied to the prediction for the swelling pressure of ten kinds of bentonites which can be classified into sodium bentonite and calcium bentonite. The type of bentonite is named after the respective dominant absorbed cation in the smectite. The characteristics of those bentonite including specific density, CEC, specific surface area, montmorillonite content and weighted average valency of cations are shown in Table 5.2. At ambient temperature (=20°C), the thermodynamic parameters X_{hs} for MX-80 (sodium bentonite) and FEBEX (calcium bentonite) obtained by Eq. (5.11) are presented in Table 5.3 (Sedighi and Thomas, 2014). In this model, due to the lack of experimental data for the determination of X_{hs}, it is assumed that the hydrous fractions of smectite for sodium and calcium bentonite are 0.76 and 0.88, respectively.

Table 5.2 Physic characteristics of different types of bentonite

Name	Bentonite S-2[c]	Calcigel[d]	Kunigel-V1[e]	Kunigel[f]	Voclay(SPV200)[g]	Voclay[h]	MX-80[i]	GMZ-01[j]
Dominated cations	Ca	Ca	Na	Ca	Na	Na	Na	Na
Specific density (Mg/m^3)	2.78	2.8	2.70	2.79	2.74	2.84	2.88	2.71
Montmorillonite content (%)	92	80	48	48	56	71	80	75
CEC (meq/100g)	0.97	0.74	1.04	0.76	0.94	1.05	1.35	0.78
Specific surface area (m^2/g)	615	650	525	389	528	560	615	570
Weighted average valency of cations	1.66	1.90	1.46	2	1.39	1.43	1.49	1.47

[c] Data from ENRESA, 2000; [d] Data from Schanz and Tripathy, 2004; [e] Data from Japan Nuclear Cycle Development Institute, 1999; [f] Data from Komine and Ogata, 1996; [g] Data from this research; [h] and [i] Data from Komine et al., 2009; [j] data from Schanz and Al-Badran, 2014

Table 5.3 Thermodynamic parameters related to the water retention calculations of compacted clays (Sedighi and Thomas, 2014)

Name of bentonite	Type of bentonite	$LogK_{eq}$	W_s	X_{hs}
MX-80 bentonite	Sodium	-1.42	-2420	0.76
FEBEX bentonite	Calcium	-2.79	-3330	0.88

The theoretical swelling pressure for different bentonite are presented with comparison with the experimental data at various dry densities of smectite in Figure 5.4. The swelling pressure of compacted bentonite increased with dry density of smectite corresponding to dry density of samples, which is consistent with the observations in previous study (Komine and Ogata, 1999; Zou et al., 2018). The results from DDL theory cannot be used to explain the swelling behaviour for highly compacted bentonite. While the calculations of swelling pressure show a good correlation with the measured swelling pressure at different dry densities of smectite after considering the influence of the formation of clay particles. Especially in high dry density of smectite (corresponding to high dry densities), the predictions of swelling pressure are well improved the experimental data compared with the DDL theory. By modifying the specific surface area due to the formation of particles and void ratio, the results show that the prediction of swelling pressure at high dry densities is well improved with a comparison of experimental values.

For calcium bentonite including Calcigel bentonite, FEBEX bentonite, Bentonite S-2, and Kunigel, when the dry densities are smaller than 1.4 Mg/m^3, the predictions by adopting a higher $n_s$value show a better agreement with experimental data. For dry density of smectite larger than 1.4 Mg/m^3, taking a lower $n_s$value exhibits a better correlation.

For sodium bentonite like MX-80（Bucher and Müller, 1989）, the prediction fits well with experimental data when dry density is smaller than 1.45 Mg/m^3 by assuming n_s is equal to 2, while the calculations seem to have a better agreement with experimental data by taking a higher value of n_s than 3 at higher densities. Interestingly, for Kunigel bentonite, in the case of assuming n_s=4, the prediction fits well when the dry densities are smaller than 1.3 Mg/m^3. Based on the prediction, it should be taken a high value of n_s when the bentonite is denser than 1.5 Mg/m^3. The above predictions prove that the value of n_s changes with dry density of smectite. For the rest bentonite in this research, the speculation is not thoroughly presented due to the

lack of data in a wider range of dry density of smectite.

In general, sodium bentonite has a greater swelling potential than calcium bentonite, and the sodium bentonite contains a number of small tactoids, while calcium bentonite has a few large tactoids (Segad et al., 2012; Black and Miller, 1961). The fraction of interlayer water in the compacted calcium bentonite found to be smaller than that of in the compacted sodium bentonite (Warr and Berger, 2007). In addition, the drive force between clay platelets during hydration might be the reason for the difference in swelling behaviour of sodium bentonite and calcium bentonite. In clay dispersion, monovalent counterions always lead to a monotonic repulsion between the clay particles, while an attraction due to ion-ion correlations presents with divalent counterions (Segad et al., 2010). That might be the explanation for the formation of clay tactoids with void ratio for compacted bentonite.

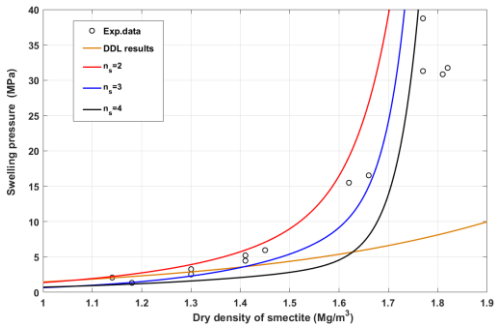

(1) MX-80[a]

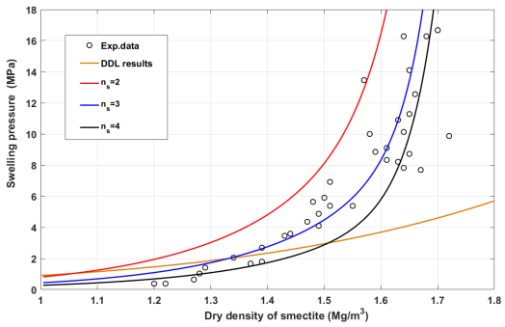

(2) FEBEX[b]

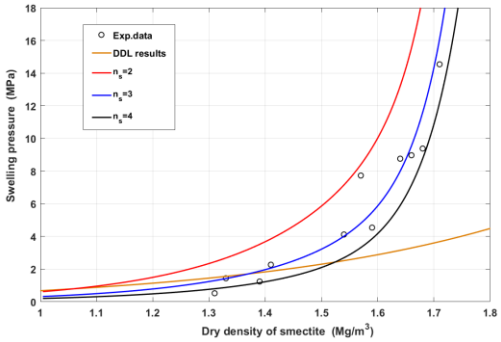

(3) Bentonite S-2[b]

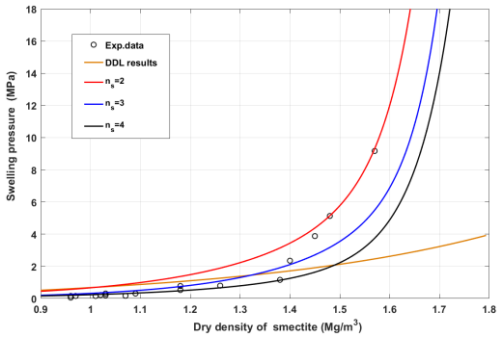

(4) Calcigel[d]

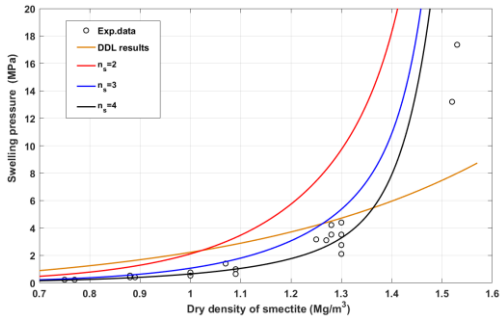

(5) Kunigel-V1[e]

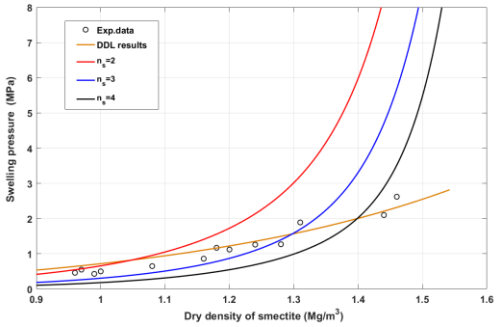

(6) Kunigel[f]

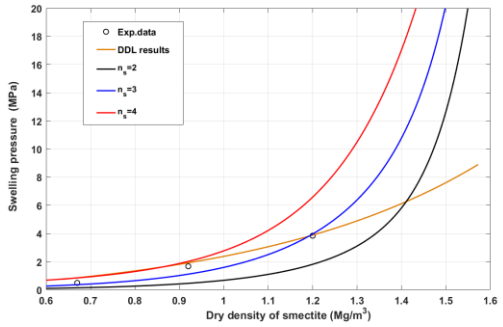

(7) Voclay(SPV)[g]

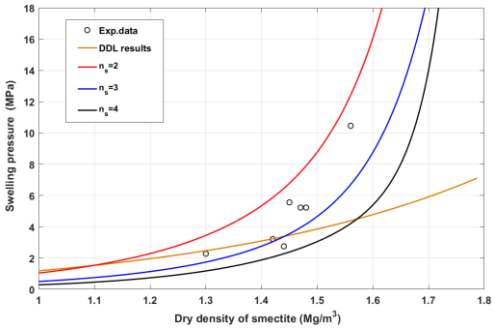

(8) Voclay[h]

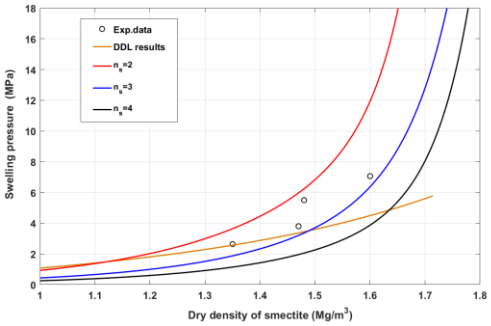

(9) MX-80[i]

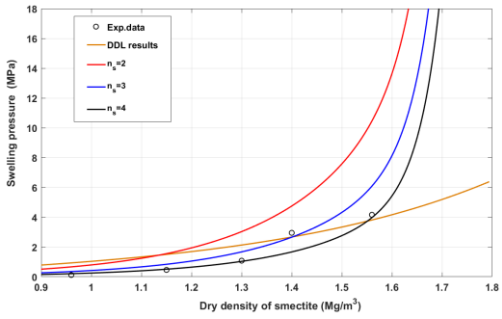

(10) GMZ-01[j]

Fig. 5.4. The predicted swelling pressure and measured swelling pressure of compacted bentonite.

5.5. Conclusions

In this chapter, a model to predict the swelling pressure of compacted bentonite was developed by combining the regular solid-solution theory and the diffuse double layer theory. The thermodynamic parameters Margules parameter (W_s) and logarithm of the equilibrium constant K_{eq} were used to characterise the adsorption of interlayer

water in sodium bentonite clay and calcium bentonite clay. Therefore, an improved understanding of how micro/macro pore was developed for the prediction of swelling pressure of compacted bentonite at different dry densities of smectite. Modified equations were suggested in terms of the relationship between void ratio and the number of unit layers per particle of clay. A close agreement between the computed swelling pressure and the reported experimental data was demonstrated for both sodium and calcium bentonite. The results showed considering the crystalline swelling improved the prediction of swelling pressure, particularly at relatively higher dry density of smectite. Only considering the osmotic pressure at diffuse double layers is inadequate as the crystalline swelling can be dominating. The reduced specific surface area was used in the proposed model since the formation of particles has a significant influence on the swelling pressure. The average number of clay platelets was found to be in the range 2 to 4 when the dry density of smectite was below 1.7 Mg/m^3. The variations in clay platelets size and the interaction between absorbed cations might result in the difference in the swelling behaviour for sodium bentonite and calcium bentonite. Future work can be focused on the transport parameters, e.g., hydraulic conductivity, obtained from macroscopic measurements for the characterisation of tactoids formation (Manassero et al., 2016).

CHAPTER **SIX**

6. Prediction of swelling pressure at elevated temperature

6.1. Introduction

In the context of the engineered barrier system (EBS) in geological disposal concepts for HLW, the clay buffer can be exposed to an elevated temperature sourcing from the heat generated by the HLW (JNC, 2000; SKB, 2006; ANDRA, 2005;) and the water intrusion at the interface with the host rock as result of hydration. Elevated temperature can affect the equilibrium state of water in the interlayer and induce an exchange of water between the interlayer porosity and macro porosity (Villar and Lloret, 2004). The combined effects of temperature on the mechanical properties of bentonite clays need to be investigated to ensure the safety of both geotechnical structures and the surrounding environments.

Currently, theoretical studies considering the temperature effect on the swelling behaviour change of bentonite are limited. In this chapter, an improved model based on the diffusive double layer theory is presented to predict the swelling pressure of compacted bentonite at elevated temperature. The micro-structure effects on the development of swelling pressure at elevated temperature are discussed based on the quantitative analysis.

It is known that the repulsion between double layers increases with increasing temperature based on the calculation of DDL theory, resulting in the increase of swelling capacity (Pusch et al., 1990; Ye et al., 2013). This is conflicting with the observations in a number of previous experimental investigations (Pusch et al.,1990; Villar et al., 2010; Tripathy et al., 2015, Lee et al., 2010). Therefore, an improved model to predict the swelling pressure at elevated temperature has been aimed to develop in this research and is presented in this chapter. Section 6.2 introduces the regular solid solution model and the proposed model for the characterisation of micro pores in compacted bentonite. Section 6.3 presents the method to obtain the thermodynamic

parameters of the solid solution model at elevated temperature. The comparisons between theoretical swelling and the measured swelling from experiments for different bentonite are presented. In Section 6.4, the discussion on the formation of clay stacks at elevated temperature for calcium and sodium type bentonite has been presented. The summary is presented in Section 6.5.

6.2. A model for the prediction of swelling pressure

This section presents the method of predicting swelling pressure at elevated temperature considering the effective void ratio. According to the solid solution model, the hydrous fraction of smectite can be estimated from the curves of suction and water content. Then, the effective void ratio for compacted bentonite is calculated from the hydrous smectite and applied for the estimation of swelling pressure.

6.2.1. Regular solid solution model

The interlayer hydration and dehydration of smectite can be described as a solid solution geochemical reaction between the interlayer water molecules and a symbolic hydrous and its homologous anhydrous counterparts of smectite (Ransom and Helgeson, 1995):

$$hydrous\ smectite \rightleftharpoons anhydrous\ smectite + n_c H_2O \tag{6.1}$$

where n_c represents the number of moles of water in the interlayer adsorption or desorption reaction, given as the moles of water per smectite half formula unit, i.e., $O_{10}(OH)_2$ (Ransom and Helgeson, 1994). The mass action law action for reaction can be written as:

$$K_{eq} = \frac{a_{as} * (a_{H_2O})^{n_c}}{a_{hs}} \tag{6.2}$$

where K_{eq} is the equilibrium constant for the reaction of the dehydration, a_{H_2O} is the activity of H_2O in the aqueous phase, and a_{as} and a_{hs} represent the activities of the anhydrous and hydrous smectite in the solid solution, respectively. The a_{as} and a_{hs} can be expressed as:

$$a_{as} = x_{as} * \lambda_{as} \tag{6.3}$$

$$a_{hs} = x_{hs} * \lambda_{hs} \tag{6.4}$$

In which x_{as} and x_{hs} mean mole fraction; λ_{as} and λ_{hs} denotes activity coefficients. Combined with Eqs. (6.3) and (6.4) into Eq. (6.2), the equilibrium constant can be described as:

$$log\ K_{eq} = log\left(\frac{1-X_{hs}}{X_{hs}}\right) + log(\lambda_{as}) - log(\lambda_{hs}) + n_c log\alpha_{H_2O} \tag{6.5}$$

In a regular binary solid solution, the excess mole Gibbs free energy of mixing (G_{xs}) is described by

$$G_{xs} = W_s X_{hs} X_{as} \tag{6.6}$$

where W_s (J/mol) denotes the Margules parameter for the binary regular solid solution of hydrous and anhydrous smectite components which is independent of temperature and pressure.

Vieillard et al. (2011) adopted two Margule parameters, W_{G1} and W_{G2}, with $W_{G1} \neq W_{G2}$. Therefore,

$$log(\lambda_{as}) = \frac{W_{G1}+2X_{as}(W_{G2}-W_{G1})}{2.303RT}(1-X_{as})^2 \tag{6.7}$$

$$log(\lambda_{as}) = \frac{W_{G2}+2X_{as}(W_{G1}-W_{G2})}{2.303RT}(1-X_{hs})^2 \tag{6.8}$$

The formulas of $log(\lambda_{as})$ and $log(\lambda_{as})$ were presented in the study by Ransom and Helgeson (1994) when $W_{G1} = W_{G2}$. In Eq. (6.5), it is assumed

$$\phi = log\left(\frac{1-X_{hs}}{X_{hs}}\right) + n_c log\alpha_{H_2O} \tag{6.9}$$

Substituting Eqs. (6.6), (6.7) and (6.8) into Eq. (5), then

$$\phi = logK_{eq} - (\frac{1}{2.303RT})[(X_{hs})^2 W_{G1} - (1-X_{hs})^2 W_{G2} + 2X_{hs}(1-X_{hs})(W_{G2} - W_{G1})] \tag{6.10}$$

Where R is gas constant (8.314 J·mol^{-1}·K^{-1}) and T is temperature (K). From the vapour adsorption isothermal data, the thermodynamic parameters of the reaction, including the Margules parameter W_{G1}, W_{G2}, and equilibrium constant ($logK_{eq}$) can be determined. These are calculated from a non-linear interpolation between ($\phi = log\left(\frac{1-X_{hs}}{X_{hs}}\right)$) and ($X_{hs}$) (Vieillard et al, 2011). By assuming that no more than two layers of water molecules are formed near the vicinity of clay surface in the interlayer space

(Sedighi and Thomas, 2014) and the activity of water a_{H_2O} is equal to 1, the fraction of hydrous smectite (X_{hs}) to substitute Eq. (6.9) into Eq. (6.10) can be obtained.

6.2.2. Prediction of the effective void ratio

In DDL theory presented in previous chapter, the simplified two clay platelet model was used to predict the swelling pressure by assuming that the clay particles consist of a single unit layer. It was assumed that the clay platelets are uniformly dispersed, and the distance between the clay platelets is identical. The formation of tactoids influences the surface area of montmorillonite as larger particles with the diffuse double layer only fully manifesting itself on the outside surfaces (Manassero et al, 2016). A possible reduction of the specific surface area due to the formation of the clay particles has been discussed in Chapter 5. The theoretical swelling pressure can be computed by:

$$p = 2n_0kT(\cosh u - 1) \tag{6.11}$$

$$\sqrt{(2\cosh z - 2\cosh u)} = \left(\frac{B}{S}\right)\sqrt{\frac{1}{2\varepsilon_0 D n_0 kT}} \tag{6.12}$$

$$\int_z^u \frac{1}{\sqrt{(2\cosh y - 2\cosh u)}}dy = -Kd \tag{6.13}$$

$$K = \sqrt{\frac{2n_0 v^2 e'^2}{\varepsilon_0 DkT}}\ (m^{-1}) \tag{6.14}$$

$$e_{macro} = G_s\gamma_w\frac{SSA_{tot}}{n_s}d \times 10^6 \tag{6.15}$$

where p is the swelling pressure (Pa), n_0 is the ionic concentration of the bulk fluid (number/m^3), k is Boltzmann's constant (1.38 × 10^{-23} J/K), T is the absolute temperature (K), u is the nondimensional midplane potential, x is the distance from the clay surface, y is the nondimensional potential at distance x from the clay surface, ξ is the distance function, z is the nondimensional potential at the clay surface, γ_w is the unit weight of water, SSA_{tot} is a constant which can be measured by experimental techniques such as EGME (Ethylene Glycol Monoethyl Ether), n_s is the stacked TOT layers of per particle. , B is the exchange capacity of the clay (meq/100 g), d is half the distance between clay layers (m), K is the diffuse double layer parameter (1/m), e' is the elementary electric charge (1.602 × 10^{-19} C), ε_0 is the permittivity of vacuum and

equal to $1/4\pi$ in the esu system (Partheniades, 2010), D is the relative dielectric constant of bulk fluid (80.4 for water), the n_0 (ionic concentration of bulk fluid) value is considered as 10^{-4} M, which refers to distilled water, e_{macro} is the macro pore ratio, G_s is the specific gravity. The calculation of the macro void ratio can be obtained by:

$$n = 1 - \frac{\rho_d}{G_s} \tag{6.16}$$

$$n_{micro} = X_{hs} \frac{n_c v_{il}}{m_{sm}} \rho_d^{sm} \tag{6.17}$$

$$\rho_d^{sm} = X_{sm} \rho_d [1 - (1 - X_{sm}) \frac{\rho_d}{\rho_{im}}]^{-1} \tag{6.18}$$

$$n_{macro} = n - n_{micro} \tag{6.19}$$

$$e_{macro} = \frac{n_{macro}}{1 - n_{macro}} \tag{6.20}$$

where n is porosity, G_s is the specific gravity of the clay, ρ_d represents the bulk dry density of the clay (kg/m^3). ρ_{im} denotes the density of the non-smectite minerals or impurities (kg/m^3). n_{macro} and n_{micro} are macro micro porosity of the soil, respectively. ρ_d^{sm} represents the bulk dry density of smectite (kg/m^3). v_{il} denotes the specific molar volume of the interlayer water (=17.22 m^3/mol). m_{sm} means the molar mass of dry smectite (=378.79 kg/mol). n_c means moles of the adsorbed interlayer water.

If the properties of bentonite (i.e., e, B, SSA_{tot}, n_0, and v) are known, the swelling pressure can then be calculated at different temperature as shown in Fig. 6.1. The steps of calculations include:

(1) To obtain the mole fraction of hydrous smectite X_{hs} through thermodynamic parameters W_{G1}, W_{G2} and $logK_{eq}$.

(2) Given that the smectite content is known, the micro porosity can be calculated from Eq. (6.17). The macro void ratio can then be calculated from Eq. (6.20).

(3) Due to the formation of the clay particles, the unit layer per particle n_s can be multiple. In this model, n_s is assumed to be integer, ranging from 2 to 5 for compacted bentonite. The half the distance between clay layers d can be obtained by Eq. (6.15).

(4) Based on the physical properties of bentonite the nondimensional midplane potential u and the nondimensional potential at the clay surface z can be calculated from Eq. (6.12) and Eq. (6.13).

(5) From Eq. (6.11), the swelling pressure can then be calculated.

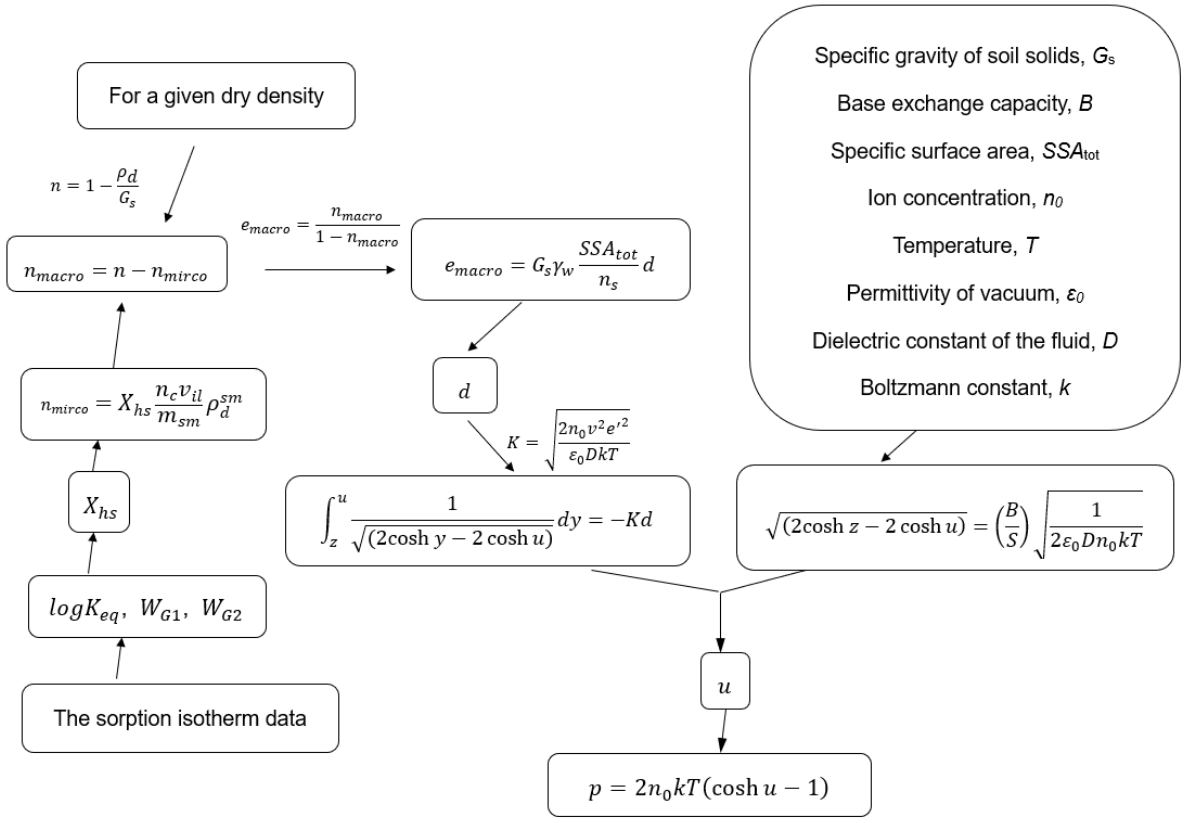

Fig. 6.1. Procedure for the determination of swelling pressure for a given dry density with the proposed method based on the diffuse double layer theory.

6.3. Validation of the model for swelling pressure of compacted bentonite at elevated temperature

This section presents the validation results of swelling pressure of compacted bentonite at elevated temperature from the proposed model. The thermodynamic parameters are determined from empirical equation and water/vapour adsorption experimental data. The comparisons with experimental data are showed for three different bentonite clays, and the evolution of micro/macro pore is presented.

6.3.1. Thermodynamic parameter for FEBEX bentonite and MX-80 bentonite

The behaviour of FEBEX bentonite at elevated temperature, including swelling pressure and sorption isotherm, has been well studied. The retention curves and swelling pressure obtained for different dry densities and temperatures have been reported by Lloret and Villar (2007) and Villar et al. (2010). The relationship between suction and water content can be expressed by the following empirical relationship (Lloret and Villar, 2007):

$$w = (a + bn)[1 + (\frac{s}{P_0 e^{-\eta(n-n_0^*)} e^{-\alpha(T-T_0)}})^{\frac{1}{1-\lambda}}]^{-\lambda} \quad (6.17)$$

where, w is the water content in percentage, n denotes the porosity, s means the suction in MPa, and T means the temperature in Celsius degree. The values of fitted parameters a, b, P_0, λ, η, n_0^*, α, and T_0 are 10.4, 41.89, 12.68 MPa, 0.211, 7.97, 0.4, 0.00647 °C^{-1} and 20°C, respectively 10.4.

Using the Equation (6.17), the predicted retention curves at 1.5 Mg/m^3, 1.6 Mg/m^3, 1.7 Mg/m^3 have been used for the rest of calculations. Temperature considered for testing the model varies from 20°C to 80°C. Therefore, the sorption isotherm data at different densities and temperature are obtained. Based on the Eq. (6.9) and Eq. (6.10), the variations of ϕ $(= log\left(\frac{1-X_{hs}}{X_{hs}}\right))$ and X_{hs} is presented as shown in Fig. 6.2. It is assumed that the activity of water is equal to 1. Then the fraction of hydrous smectite during saturation will be obtained. The thermodynamic parameters (W_{G1} and W_{G2}) are temperature independent. For compacted FEBEX bentonite, the thermodynamic parameters are obtained from the sorption isotherm data at 20°C and presented in Table 6.1. The dashed lines in Fig. 6.2 are plotted by Eq. (6.10). The R-square for fitting curves are ranging from 0.39 to 0.99. The fitting curves does not show a high correlation at relatively higher temperature. It is assumed that one molar mass of smectite constantly has two molar mass of absorbed interlayer water. The reason might lie on the decrease of micro pores as the loss of absorbed water at elevated temperature.

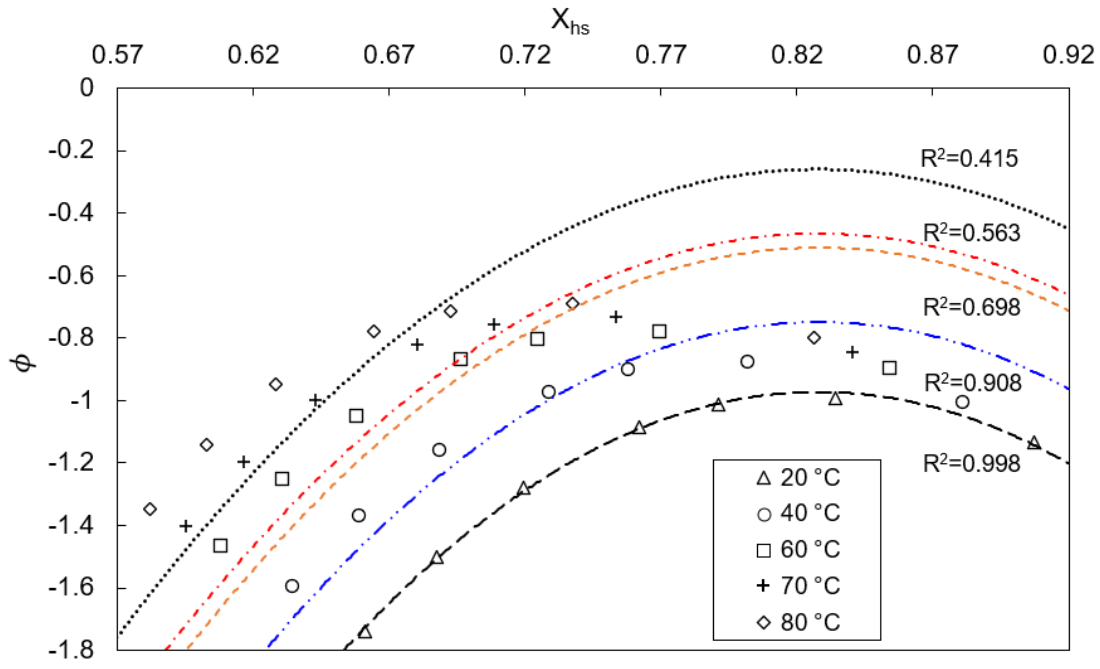
X_hs
0.57
0.62
0.67
0.72
0.77
0.82
0.87
0.92
0
-0.2
-0.4
-0.6
-0.8
-1
-1.2
-1.4
-1.6
-1.8
ϕ
R²=0.415
R²=0.563
R²=0.698
R²=0.908
R²=0.998
20 °C
40 °C
60 °C
70 °C
80 °C

(a)

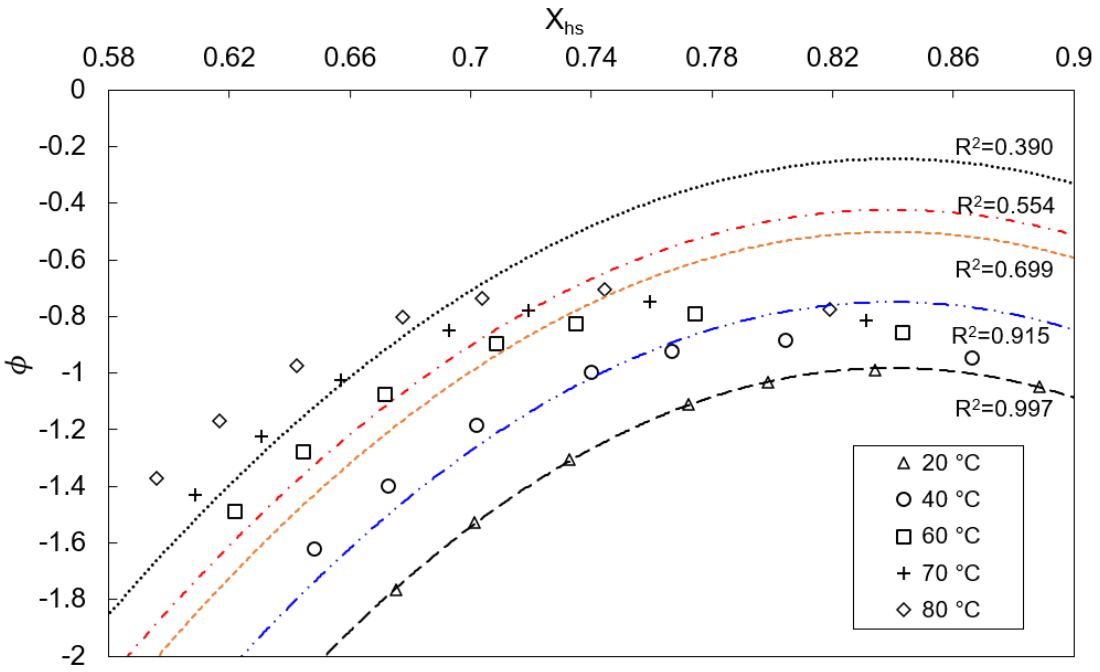
X_hs
0.58
0.62
0.66
0.7
0.74
0.78
0.82
0.86
0.9
0
-0.2
-0.4
-0.6
-0.8
-1
-1.2
-1.4
-1.6
-1.8
-2
ϕ
R²=0.390
R²=0.554
R²=0.699
R²=0.915
R²=0.997
20 °C
40 °C
60 °C
70 °C
80 °C

(b)

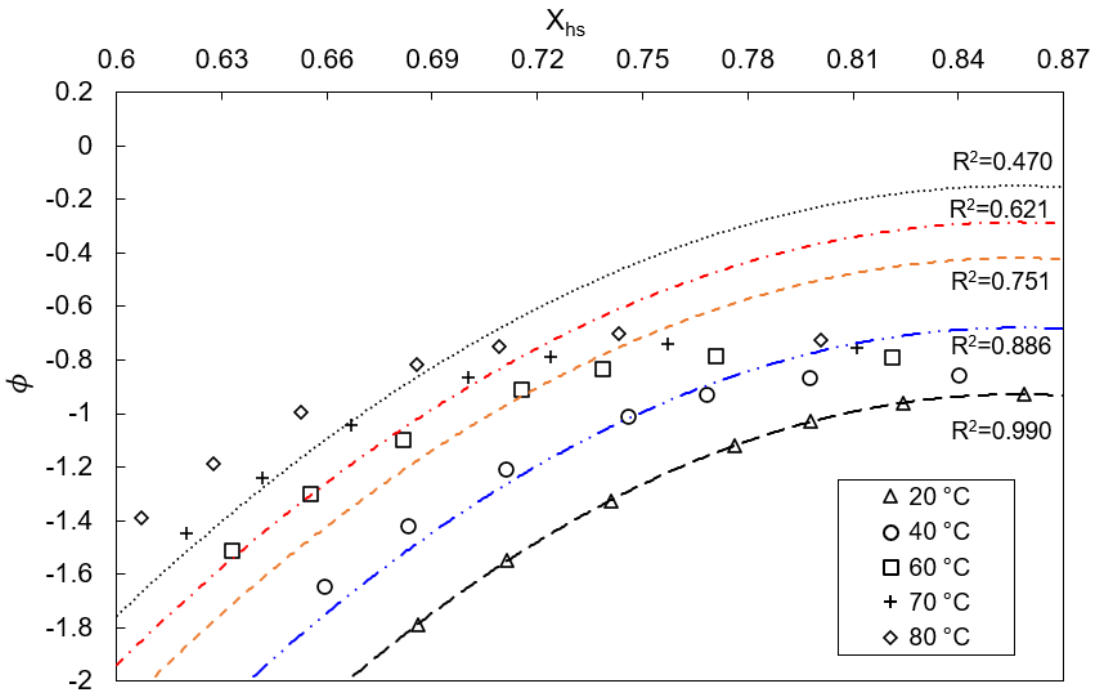

(c)

Fig. 6.2. Variations of ϕ with X_{hs} at different temperature for different dry densities of compacted FEBEX bentonite: (a) 1.5 Mg/m^3; (b)1.6 Mg/m^3; (c) 1.7 Mg/m^3. The dash lines are fitting curves by Eq. (10).

The physico-chemical properties of MX-80 bentonites are adopted from the study by Tripathy et al. (2014). The specific gravity, the montmorillonite content, clay fraction, cation exchangeable capacity, specific surface area, and weighted average valency were found to be 2.76, 76%, 84%, 88.44 meq/100g, 640 m^2/g, 1.47. The measured swelling pressure under temperature change was present in study of Tripathy et al. (2015).

The thermodynamic parameters of the solid-solution model, including the equilibrium constant of the reactions and Margules parameters are derived from water/vapour adsorption experimental data (Villar, 2005). The water retention curves of compacted MX-80 bentonite at dry densities of 1.5, 1.6, 1.7 Mg/m^{3}were taken at 20°C. As shown in Table, W_{G1} and W_{G2} are independent of temperature change. The thermodynamic parameters are obtained through Eq. (6.9) and Eq. (6.10). As the lack

of water retention curves of compacted MX-80 bentonite at different temperature, the equilibrium constant of the reaction at different temperature can be obtained by (Langmuir, 1997):

$$(logK_{eq})_T = \frac{\Delta H^0_{r,T_0}}{2.303R}\left(\frac{1}{T_0}-\frac{1}{T}\right)+\frac{\Delta C^0_p}{2.303R}\left(\frac{T_0}{T}-1\right)-\frac{\Delta C^0_p}{R}log\left(\frac{T}{T_0}\right)+(logK_{eq})_{T_0} \quad (6.18)$$

where $\Delta H^0_{r,T_0}$ (cal·mol^{-1}) is the standard enthalpy of reaction at reference temperature (T_0), and ΔC^0_p is the standard heat capacity of the reaction at constant pressure (c cal·mol^{-1}·K^{-1}). Temperatures T and T_0 are in Kelvin. The parameters X_{hs} and $logK_{eq}$ at 25 °C and 70 °C are calculated from Eq. (6.18) and shown in Table 6.2.

With the increase of temperature, the fraction of hydrous smectite (X_{hs}) decreases for both two kinds of bentonite. The relationship between suction and water content for compacted Voclay bentonite is presented in Table 3.2. Then Margules parameters W_{G1}, W_{G2} and $logK_{eq}$ at 25 °C can be obtained. Based on the equilibrium constant of the reaction at different temperature, $logK_{eq}$ at 40 °C, 60 °C, 80 °C can be calculated from Eq. (6.18). The thermodynamic parameters of compacted Voclay bentonite at different densities and temperature are presented in Table 6.3.

Table 6.1 The thermodynamic parameters of compacted FEBEX bentonite at different densities and temperature

Temperature	1.5 Mg/m^3				1.6 Mg/m^3				1.7 Mg/m^3			
(°C)	X_{hs}	*logK*eq	W_{G1}	W_{G2}	X_{hs}	*logK*eq	W_{G1}	W_{G2}	X_{hs}	*logK*eq	W_{G1}	W_{G2}
20	0.971	-6.140	-24490	-71520	0.963	-6.697	-27920	-81690	0.912	-7.099	-31270	-85990
40	0.853	-5.586			0.849	-6.099			0.833	-6.546		
60	0.783	-5.507			0.787	-5.530			0.783	-5.849		
70	0.773	-4.880			0.773	-5.305			0.763	-5.557		
80	0.736	-4.549			0.744	-4.987			0.743	-5.272		

Table 6.2 The thermodynamic parameters of compacted MX-80 bentonite at different densities and temperature

Dry density	1.5 Mg/m^3			1.6 Mg/m^3			1.7 Mg/m^3		
Temperature (°C)	20	25	70	20	25	70	20	25	70
X_{hs}	0.890	0.826	0.446	0.958	0.942	0.450	0.941	0.950	0.570
*logK*eq	-1.016	-0.941	-0.205	-1.081	-1.006	-0.270	-1.340	-1.265	-0.529
W_{G1}	1501			2639			246		
W_{G2}	-8183			-8251			-8743		

Table 6.3 The thermodynamic parameters of compacted Voclay bentonite at different densities and temperature

Temperature	1.1 Mg/m^3				1.4 Mg/m^3				1.7 Mg/m^3			
(°C)	X_{hs}	$logK$eq	W_{G1}	W_{G2}	X_{hs}	$logK$eq	W_{G1}	W_{G2}	X_{hs}	$logK$eq	W_{G1}	W_{G2}
25	0.96	-1.132	2853	-2340	0.97	-1.280	2167	-3056	0.98	-1.630	1265	-5638
40	0.94	-0.910			0.95	-1.058			0.97	-1.408		
60	0.82	-0.594			0.86	-0.742			0.93	-1.092		
80	0.54	-0.262			0.63	-0.410			0.79	-0.760		

6.3.2. Comparison between the experimental and theoretical swelling pressure

By assuming the values of the average number of layers per particle are ranging from 2 to 5, the calculated swelling pressure with a comparison of experimental data at different temperature are shown in Fig. 6.3, Fig. 6.4, and Fig. 6.5 for FEBEX bentonite, MX-80 bentonite, and Voclay bentonite, respectively. The red lines are the predicted results from Gouy-Chapman theory and unable to predict the swelling pressure at elevated temperature. The predicted swelling pressure increases with the increase of temperature according to Gouy-Chapman DDL theory, which conflicts with experimental observations. In the proposed model, the theoretical swelling pressure drops with increasing temperature which fits with the trend of experimental data. For a given void ratio, the increase of n_s leads to an increase of d according to Eq. (6.15). The larger the value of n_s, the lower swelling pressure can develop. Due to the uncertainty of n_s, it is assumed to be in the interval of 1 to 5 for compacted bentonite.

The temperature effects on the change of n_s is different because of the type of dominated cations. It can be concluded that the values of n_s increased with the increase of temperature compared with experimental swelling pressure for compacted FEBEX bentonite, ranging from 3 to 5. While for compacted MX-80 bentonite, the corresponding values of n_s shows a decrease.

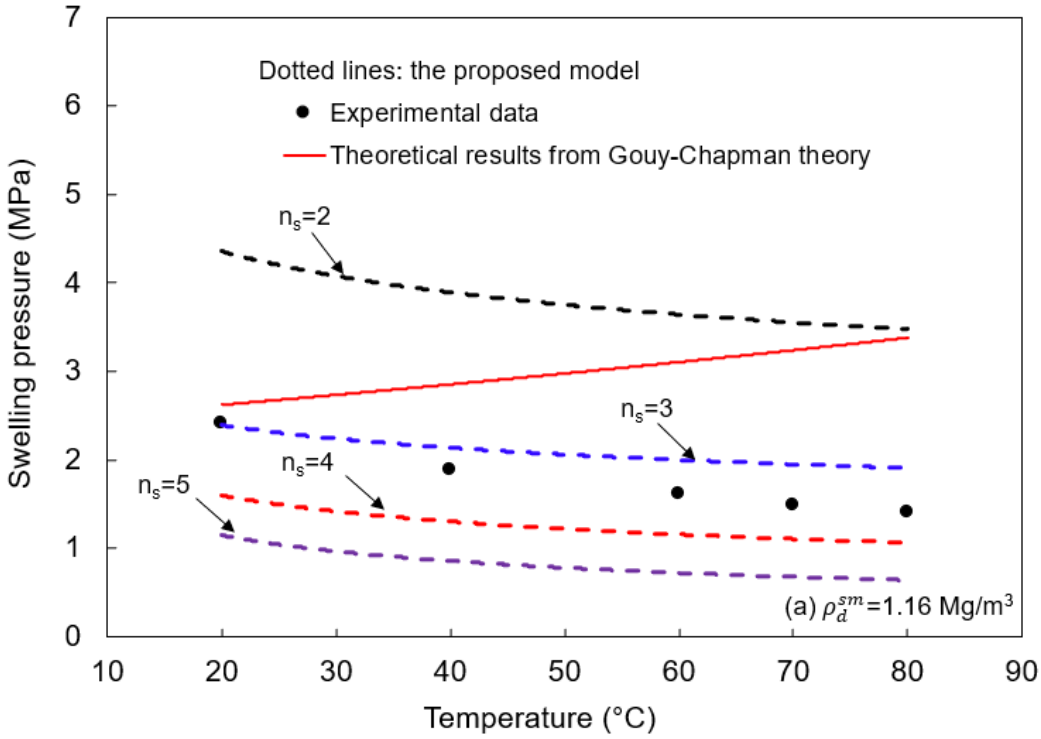
Dotted lines: the proposed model
Experimental data
Theoretical results from Gouy-Chapman theory
n_s=2
n_s=3
n_s=4
n_s=5
(a) ρ_d^{sm}=1.16 Mg/m^3
Swelling pressure (MPa)
Temperature (°C)

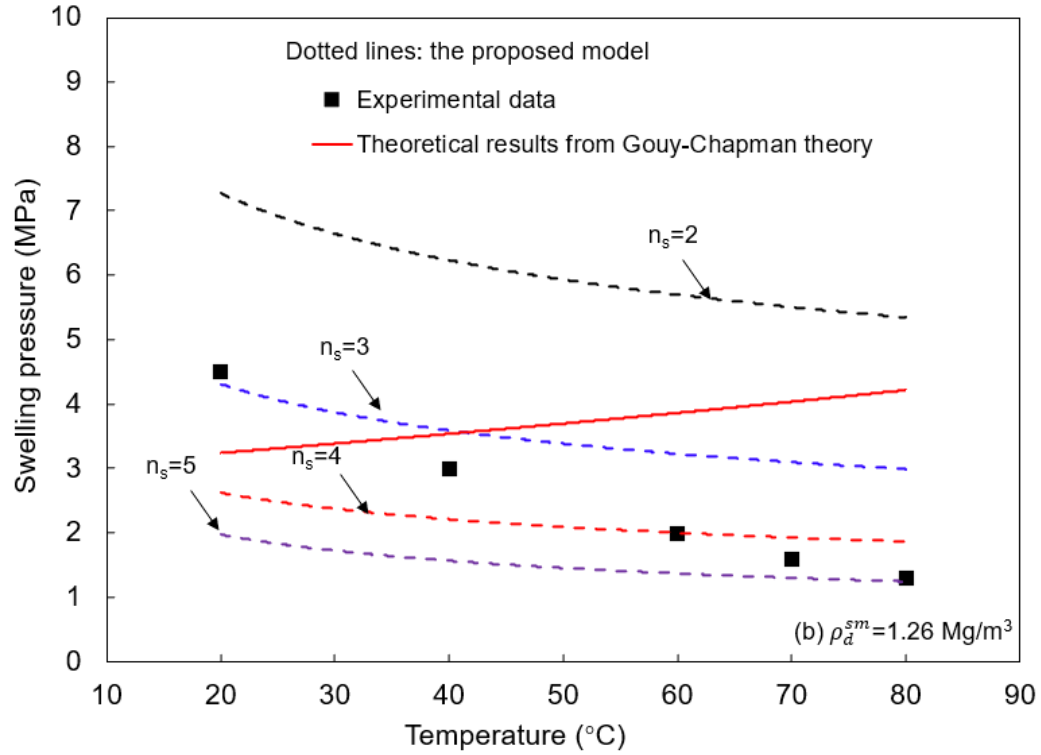
Dotted lines: the proposed model
Experimental data
Theoretical results from Gouy-Chapman theory
n_s=2
n_s=3
n_s=4
n_s=5
(b) ρ_d^{sm}=1.26 Mg/m^3
Swelling pressure (MPa)
Temperature (°C)

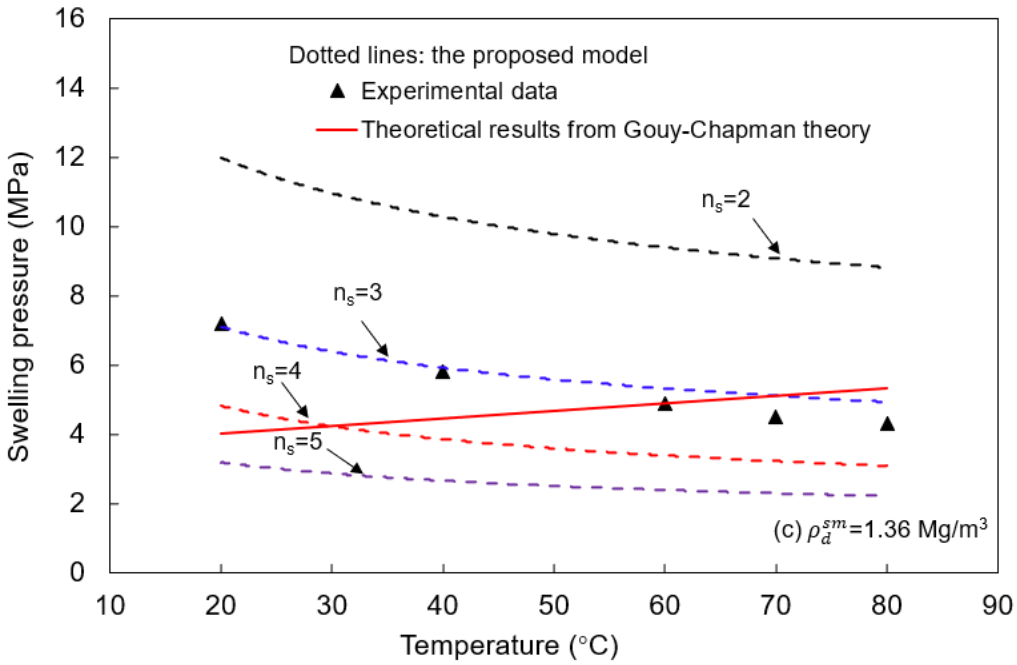

Fig. 6.3. Comparison of measured swelling pressure as a function of temperature with the predicted pressure for compacted FEBEX bentonite.

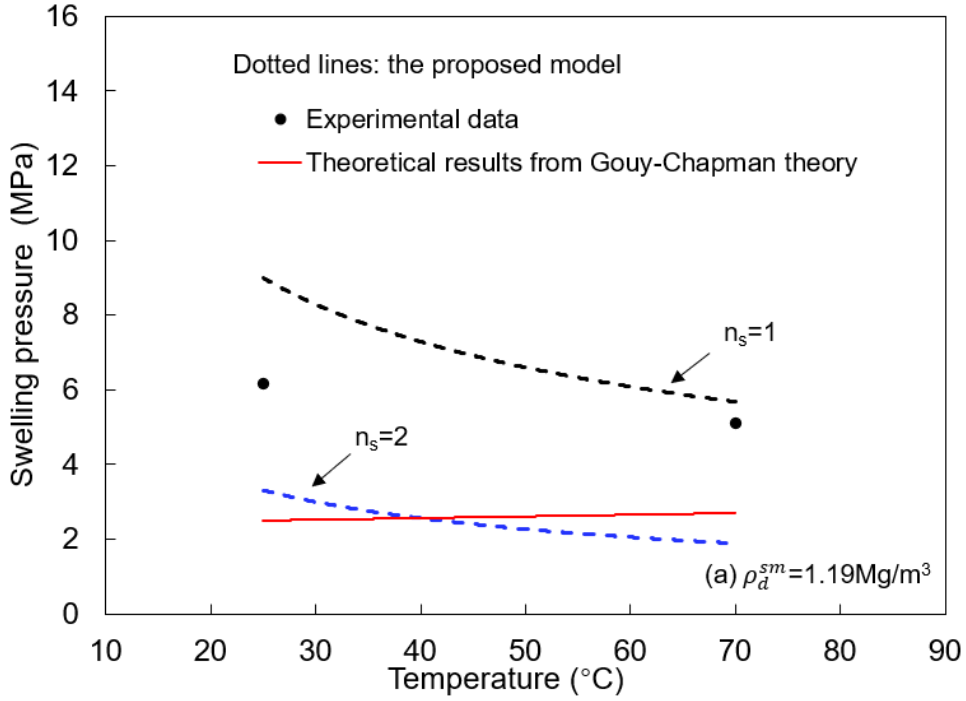

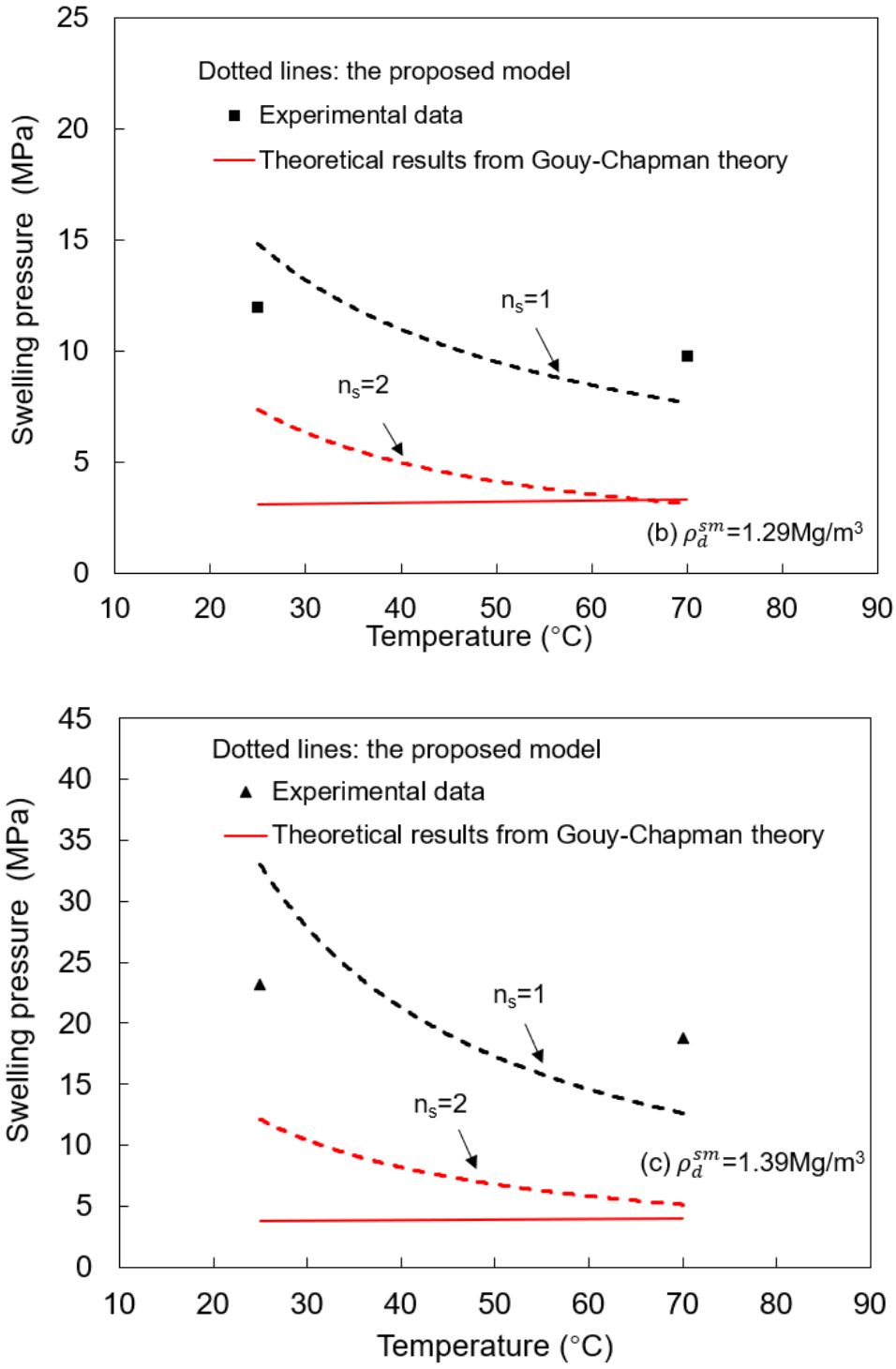

Fig. 6.4. Comparison of measured swelling pressure as a function of temperature with the predicted pressure for compacted MX-80 bentonite.

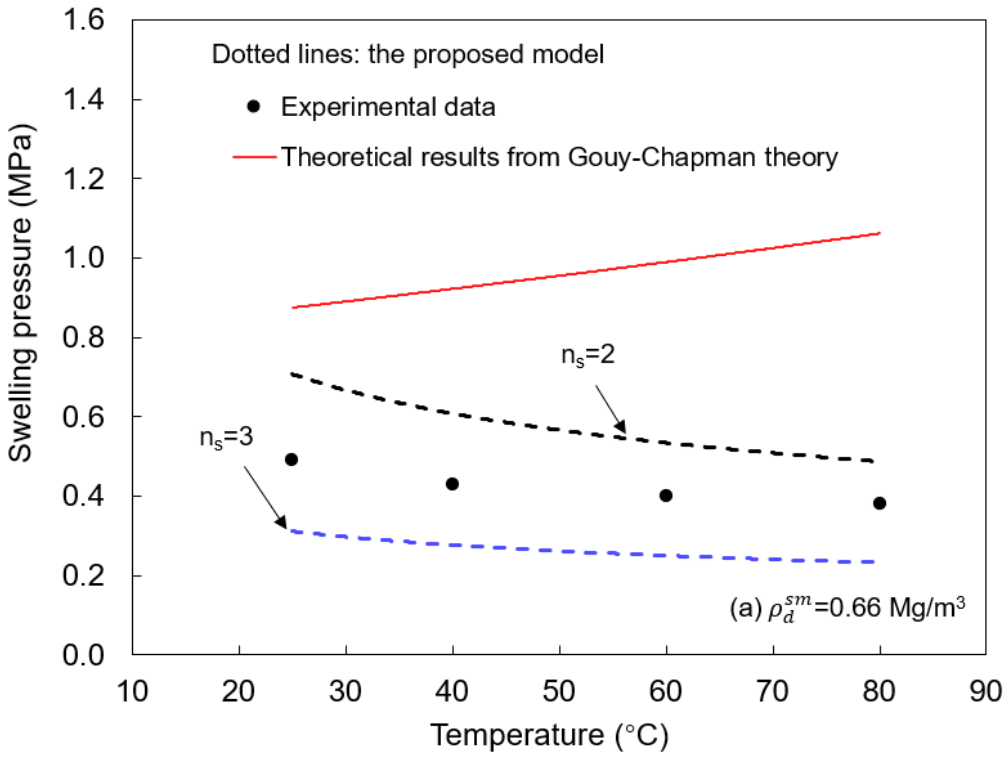
Dotted lines: the proposed model
Experimental data
Theoretical results from Gouy-Chapman theory
n_s=2
n_s=3
(a) ρ_d^{sm}=0.66 Mg/m^3
Swelling pressure (MPa)
Temperature (°C)
0.0
0.2
0.4
0.6
0.8
1.0
1.2
1.4
1.6
10
20
30
40
50
60
70
80
90

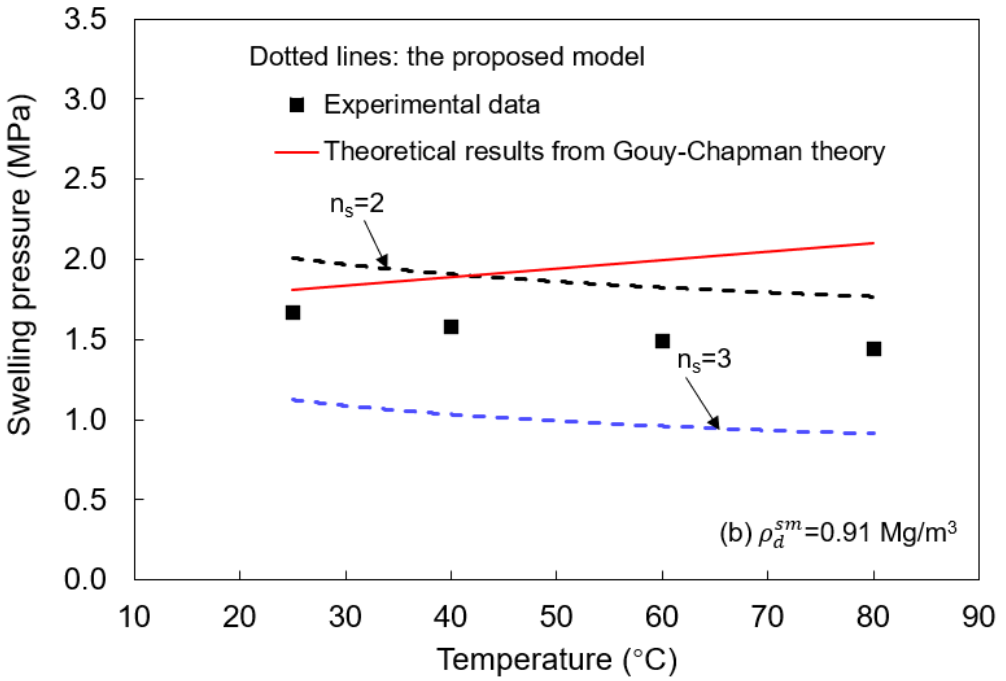
Dotted lines: the proposed model
Experimental data
Theoretical results from Gouy-Chapman theory
n_s=2
n_s=3
(b) ρ_d^{sm}=0.91 Mg/m^3
Swelling pressure (MPa)
Temperature (°C)
0.0
0.5
1.0
1.5
2.0
2.5
3.0
3.5
10
20
30
40
50
60
70
80
90

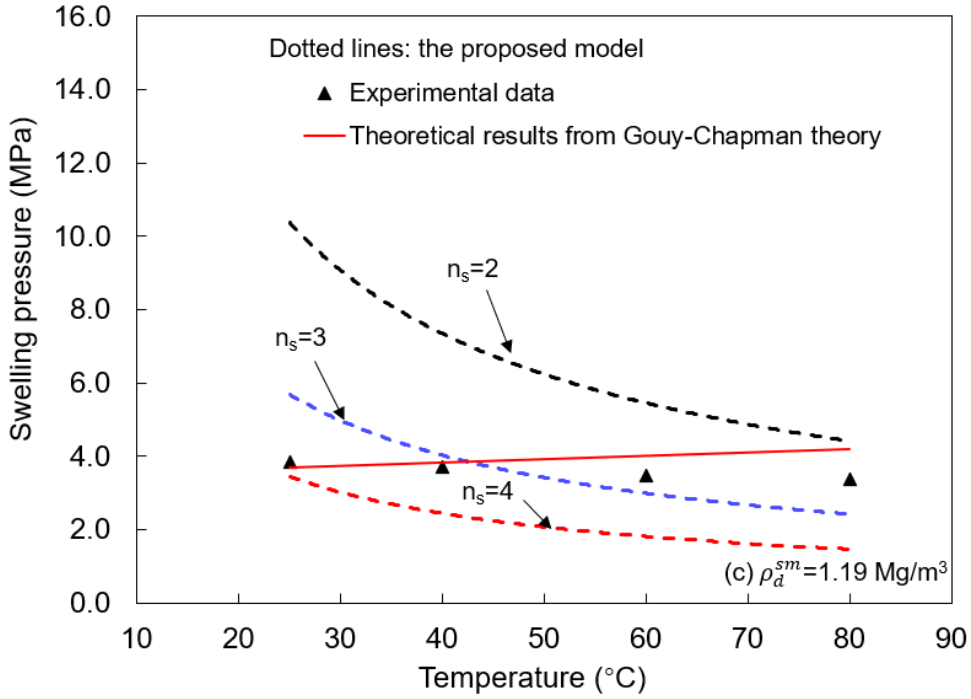

Fig. 6.5. Comparison of measured swelling pressure as a function of temperature with the predicted pressure for compacted Voclay bentonite.

Figure 6.6 shows the ratio of macro pores where osmotic pressure arises from increased with temperature. The theoretical results show that macro pore ratio shows a linearly increase by increasing temperature as plotted with dash lines in Fig. 6.6. The increase of macro pore has been explained as a consequence of the transfer of microstructural (interlayer) water to the macrostructure triggered by temperature (Villar and Lloret, 2004; Vidal and Dubacq, 2009). The mass of water in macro pores increases with temperature, which contributes to accelerate the movement of water. That is consistent with the observations of the change of hydraulic behaviour at elevated temperature for both sodium and calcium bentonite.

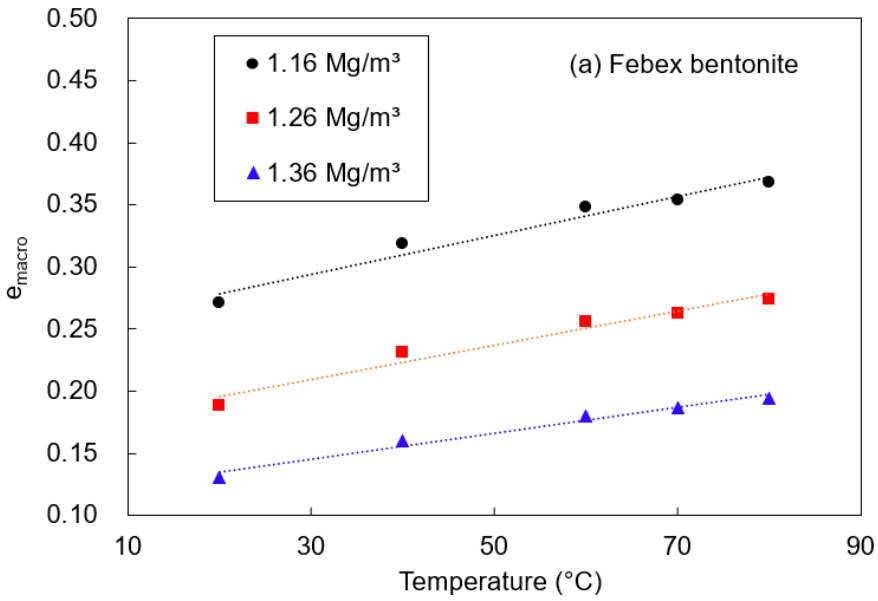
0.50
0.45
0.40
0.35
0.30
0.25
0.20
0.15
0.10
e_macro
1.16 Mg/m³
1.26 Mg/m³
1.36 Mg/m³
(a) Febex bentonite
10
30
50
70
90
Temperature (°C)

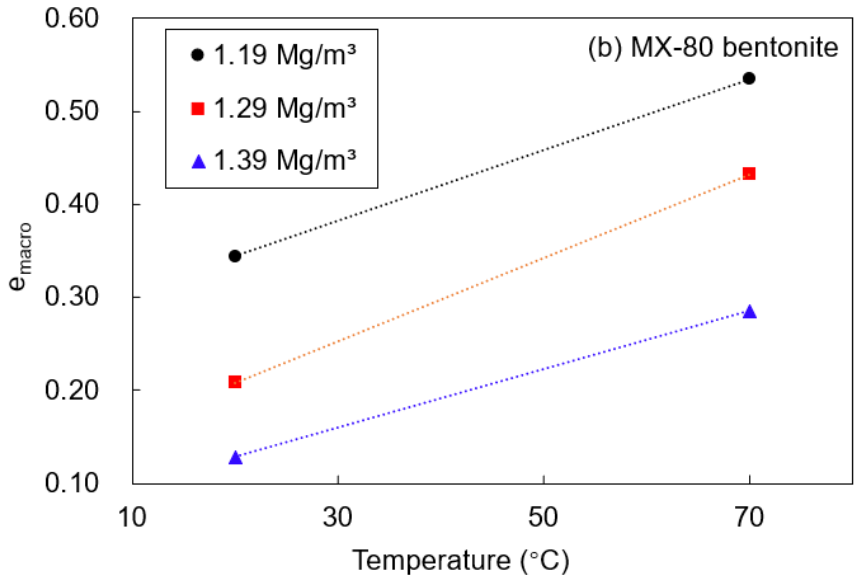
0.60
0.50
0.40
0.30
0.20
0.10
e_macro
1.19 Mg/m³
1.29 Mg/m³
1.39 Mg/m³
(b) MX-80 bentonite
10
30
50
70
Temperature (°C)

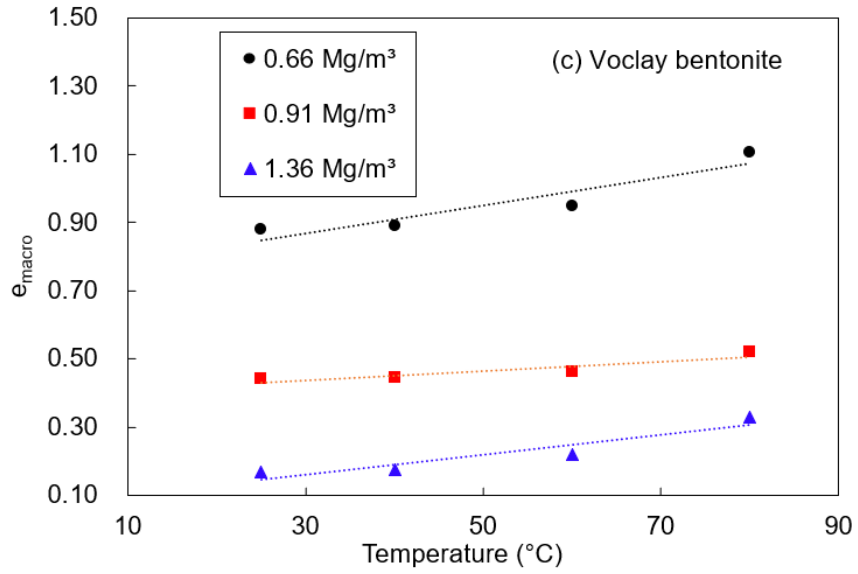
1.50
1.30
1.10
0.90
0.70
0.50
0.30
0.10
e_macro
0.66 Mg/m³
0.91 Mg/m³
1.36 Mg/m³
(c) Voclay bentonite
10
30
50
70
90
Temperature (°C)

Fig. 6.6 The evolution of macro pore ratio with temperature change for three kinds of compacted bentonite. The dash lines are fitting curves.

6.4. Discussion: Temperature effects on the formation of clay particles

The value of n_s is independent of temperature. The predicted swelling pressure decreases at elevated temperature which is consistent with the trend in experimental investigations for both types of bentonite clays. Compared with experimental data, n_s changes with increasing temperature. The formation of tactoids has influenced the surface area of the montmorillonite as a much larger particle with the diffuse double layer only fully manifesting itself on the outside surfaces (Schanz and Tripathy, 2009; Manassero et al, 2016).

The n_s values if the back calculations from experimental data of compacted FEBEX bentonite (Ca dominated) are used, ranging from 3 to 5 at different dry densities, are greater than those for compacted MX-80 bentonites (Na dominated). The average number of clay platelets or lamellae forming tactoids increases with an increase in the valence of cations in the soil solution (Manassero et al, 2016). Thuresson et al. (2017) found that the percentage of charged clay platelets which are neutralized by divalent cations was equal to or larger than 0.8, the increase in number of platelets per tactoid with temperature was observed both in simulations and experiments. That increase was getting smaller when temperature was up from 55°C to 90°C.

Due to the variation of the dominated force between particles, the particles of Ca-montmorillonite are generally made up of a larger number of stacked unit layers than Na dominated bentonites. For compacted sodium bentonite, the force between particles is more likely to being repulsive with monovalent cations. According to the trend in Fig. 8, n_s of experimental data showed a decrease with temperature. With monovalent counterions in the system solely, the electrostatic interaction between the particles is repulsive, whereas when multivalent counterions are introduced, the interaction can be attractive due to the electrostatic ion-ion correlation effects (Thuresson et al, 2017). The

enhanced attractive electrostatic ion-ion correlation interactions with temperature leads to a large aggregate and a reduced osmotic pressure (Thuresson et al, 2016). This can be understood from the observations in Fig.6.4 for compacted MX-80 bentonite. The use of Eq. (6.15) to estimate the external surface area at elevated temperature provides a new perspective in the DDL calculation. Further work needs to be on the assurance of n_s theoretically or experimentally.

Temperature effect on the formation of particles is likely to be different for different type of bentonite clays. The drop of swelling pressure was both found in experimental investigation. It can be concluded that the reduction of hydration force for between interlayer is mainly responsible for the decrease of swelling pressure. The denser the sample, the larger proportion of interlayer water is found (Pusch, 2015). The poor prediction of original DDL theory is attributed to the limited volume of DDL water, particularly at relatively high dry densities. The proposed model in this paper for the consideration of temperature effects on the fraction of hydrous smectite is necessary.

6.5. Conclusions

Based on DDL theory for the swelling pressure of compacted bentonite, an attempt was made to consider the effects of the formation of tactoids on the theoretical calculation. In addition, thermodynamic parameters were introduced to study the fraction of hydrous smectite due to the dominated hydration force between interlayer, particularly at relatively high dry densities. This approach was extended to investigate the evolution of swelling pressure at elevated temperature.

There are two reasons to explain the drop of swelling pressure when increasing temperature:

(1) The swelling pressure of compacted bentonite comprises of the hydration force between interlayers and the osmotic pressure between the particles. Temperature changes induces a water mass exchange between interlayer and intralayer/interparticle space. The interlayer volumetric water content reduced with increasing temperature,

and the dominated hydration force decreases consequently.

(2) The temperature affects the specific surface area due the formation of clay particles. For compacted FEBEX bentonite (calcium type montmorillonite), the number of stacked layers per particle increased due to the electrostatic ion-ion correlation effects. While for compacted MX-80 bentonite (sodium type montmorillonite), the number of stacked layers per particle decreased as the electrostatic interaction between the particles is repulsive increasing with temperature.

CHAPTER **SEVEN**

7. Temperature effects on the erosion of compacted bentonite

7.1. Introduction

Compacted bentonite clays can expand into the fractures of the surrounding rock (e.g., host rock repository) due to its high swelling capacity when it is subjected to water (saturation process). Clay colloidal particles are formed in contact with the groundwater in the fracture, leading to potential erosion of bentonite. The formation of colloidal particles and their release is one of the important factors that can potentially contribute to degradation of clay seal and enhanced migration of hazardous chemicals. Elevated temperature influences the interaction energy between colloidal particles. Temperature increase can enhance the colloid movement. Therefore, it is important to understand the extent at which the colloid generation can be enhanced at elevated temperature to assess the stability for sealing material.

In this chapter, the temperature effects on the formation of bentonite colloids are discussed. A set of experimental investigations were conducted for the effects of temperature of colloidal formation of compacted Voclay (SPV200) bentonite at 25°C and 60°C. Section 7.2 introduces the design of the experiments and procedures of measurements. In section 7.3, the results at different temperature from erosion tests and the discussion are presented. The conclusion of this chapter is presented in section 7.4.

7.2. Experimental programme

To investigate the temperature effect on the colloid generation, the erosion tests on compacted bentonite were conducted at 25°C and 60°C. In this experiment, the raw material of Voclay bentonite was used. Approximately 15.5 gram of Voclay bentonite powder with natural water content of 12% was compacted at the dry density of 1.4 Mg/m^3 for each specimen. The compaction procedures were same as that introduced in Chapter 3 (section 3.3). Applying deionised water, the inflow rate of the pressure pump

was set at 0.46 mm^3/s (water velocity of approximately 9×10^{-5} m/s). The volume of the outflow was around 40 mL/day. The setup is shown in Fig. 3.8, the dynamic experiments are conducted at constant temperature monitored by the internal thermal sensor. Inside of the cell of the bespoke oedometer, the bottom porous plate is replaced by sintered stainless-steel filters. The injected water was deionised with ionic strength of approximately 10^{-4} M (=10^{-4} mol/dm^3).

As described in Section 3.6, the turbidity of colloid solution was measured with the turbidimeter. Further, the concentrations of collected samples was measured by dynamic light scattering (DLS), which provided chemical analysis. A calibration curve was established by measuring the response of photomultiplier (cps, counts per second) at different and known concentrations of bentonite colloids. The known concentration of bentonite colloids was prepared in a magnetic stirrer for ten minutes at ambient temperature. For each data point, the average value was taken from three measurements. As presented in Fig. 7.1, the relationship between the concentration and the count rate in DLS measurement for bentonite colloids was found to be linear, which was consistent with the results in previous study by Missana et al. (2011). The dash lines are used as calibrated curves in literature and this study. Once the laser counts in DLS measurement are known, the bentonite concentration will be estimated from the calibrated curve. To obtain each data point, the average value of counts was taken from the same bottles of colloid by measuring three times.

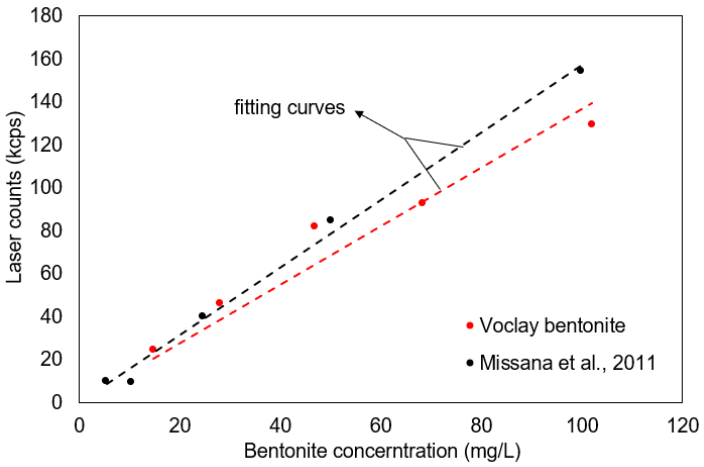

Fig. 7.1 The calibration curve to determine bentonite colloid concentration.

7.3. Results and discussion

7.3.1. DLS results

Fig. 7.2 shows the results of the turbidity measurements of the colloid solution (daily measurements). Fig. 7.3 presents the evolution of the bentonite colloid concentration converted from the DLS measurements. The plotted dash lines showed the change of concentration with temperature. It can be observed that the equilibrium concentration of colloidal solution was higher at elevated temperature (i.e., around 50 mg/L at 25°C, around 170 mg/L at 60°C). Correspondingly, the eroded mass increased from 2 mg/day to 7 mg/day with increasing temperature. The total calculated loss masses were 0.315g and 0.643g, respectively. Accordingly, the mass loss was 2% and 4.1% of the initial mass. The highest concentration among the daily collected samples was up to 320 mg/ L. After approximately 50 days, the system reached a steady-state at high temperature. The time taken to steady-state at low temperature was 60 days. This is consistent with the change of the turbidity variations shown in Fig. 7.2. At steady state, the value of the turbidity fluctuated between 20 NTU and 30 NTU at higher temperature, and between 3 NTU and 5 NTU at 25°C. Fig. 7.4 presents the mean size of the colloid particles at 25°C is 454 nm. The mean size of colloid particles at 60°C was smaller than that at 25°C, which was about 185 nm.

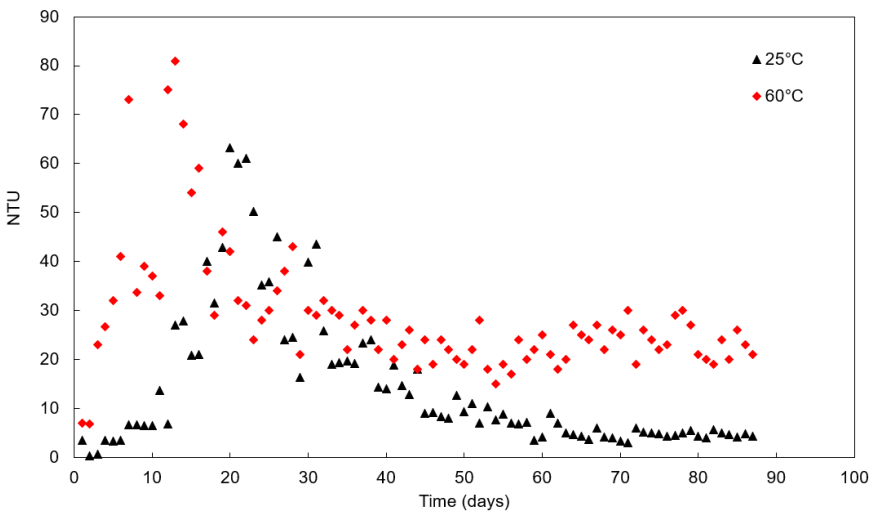

Fig. 7.2. The measured turbidity of colloids at different temperature.

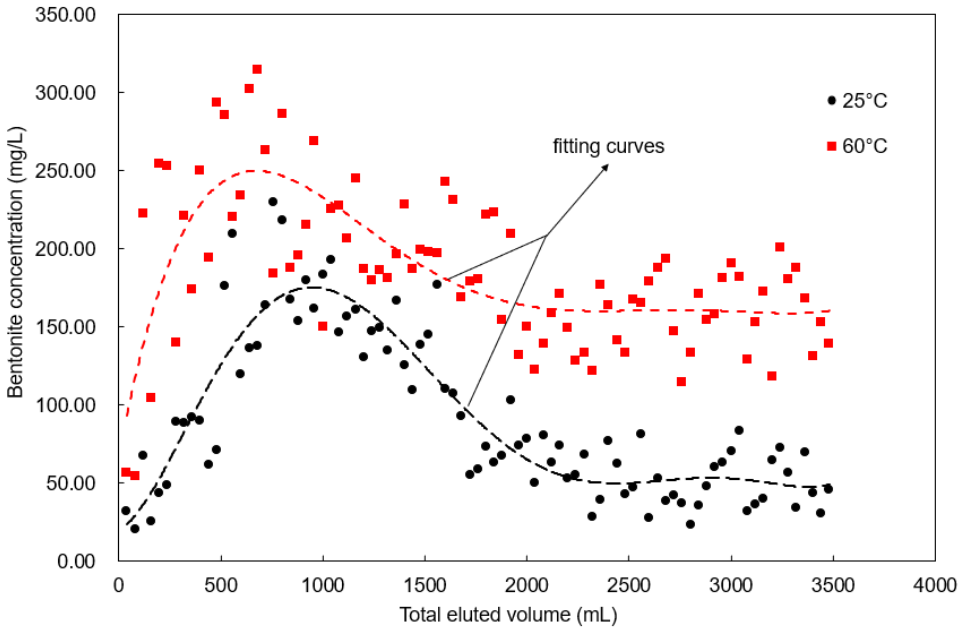

Fig. 7.3. The evolution of colloid concentration generated from compacted bentonite.

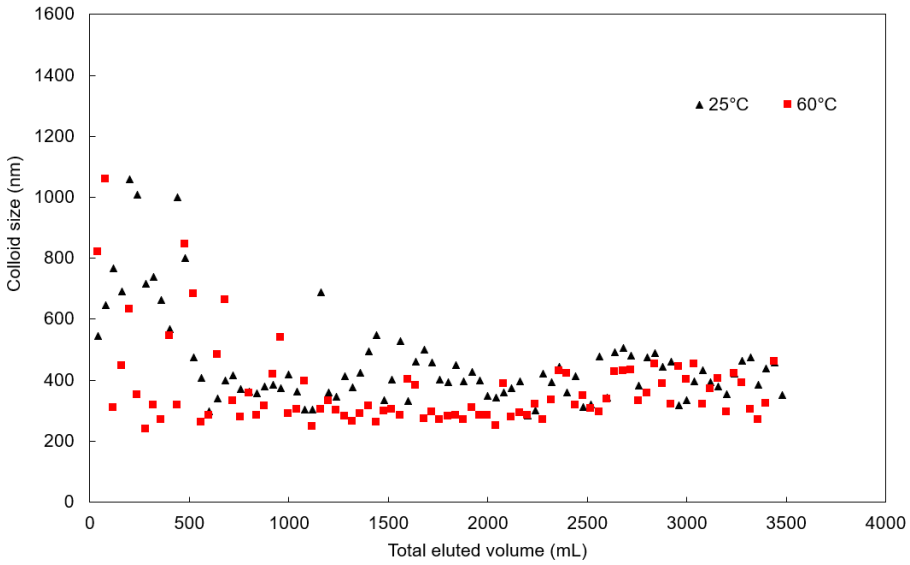

Fig. 7.4. Variation of the mean size of particles eroded with total eluted volume based on DLS measurements (the size change with time at different temperature is shown in the appendix).

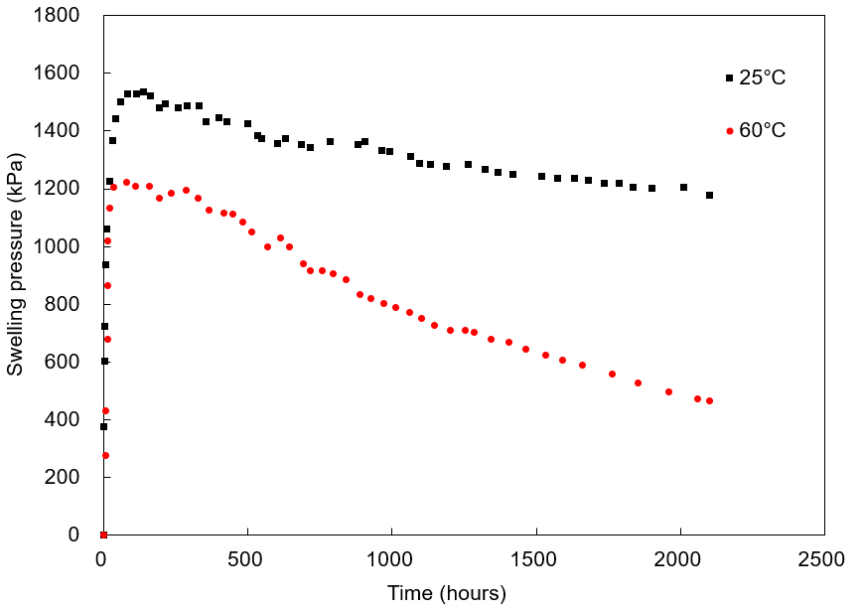

Fig. 7.5. The evolution of swelling pressure for compacted bentonite at a dry density of 1.4 Mg/m^3 at different temperature.

When water is injected into an unconfined specimen of bentonite, the repulsion forces between the bentonite layers decrease. This causes the specimen to swell until a new equilibrium is established with a lower internal swelling pressure. Another reason for the lower swelling pressure is erosion, which occurs when the force produces by flow along the bentonite surface exceeds the force bonding the clay particles (Pusch, 1999). Fig. 7.5 presents the evolution of swelling pressure of compacted bentonite with time. At the beginning of the experiments, the swelling pressure increases rapidly due to the water uptake. The rate of absorbing water is apparently larger than the rate of mass loss from erosion. The rising swelling pressure decreases due to the fully saturation. While the swelling pressure started to drop as the continuous of mass loss under constant inflowing water. The decrease of swelling pressure shows a constant rate until equilibrium. The time to reach the peak value is shortened at 60°C compared with that of at 25°C. The maximum values of swelling pressure are around 1500 kPa and 1200 kPa, respectively. With the continuous loss mass, the swelling pressure drops. For example, this value reduces from 1500 kPa to 1200 kPa at 25°C after 90 days, i.e., a 20% reduction. At higher temperature, the reduction is 62%, i.e., the swelling pressure

decreases from 1200 kPa to 460 kPa.

7.3.2. Temperature effects on the generation of colloids

A combination of the attractive van der Waals forces, repulsive electric diffuse layer forces, gravity and the act of gradient of chemical potential contribute to the movement of particles in water. Transport mechanism of particles in fractures has been discussed that can be classified into (Birgersson et al., 2009):

(1) Radial transport by repulsion of the bentonite particles in still water (swelling).

(2) Tangential transport by fluid flow driven by a water pressure gradient (viscous flow and erosion).

(3) Axial (vertical) transport driven by gravity (sedimentation)

The magnitude of erosion depends on the geochemical parameters of the groundwater. The higher concentration, the smaller loss mass will be eroded (Missana et al.,2011). Reaching the coagulation critical concentration (CCC), the bentonite will stop releasing particles (Neretnieks et al., 2009). The critical coagulation concentration (CCC) is the minimum concentration of electrolyte required to induce the coagulation of a stable colloidal suspension (Hsu and Kuo, 1997). Above the CCC, the clay forms a coherent gel that can resist the shear forces of the flowing water. At concentrations below CCC, the bentonite keeps expanding and releasing colloidal smectite particle. With the increase of distance, the hydration forces decrease, and the force between clay particles are weakening by diffusion. The expanding bentonite gel grows increasingly dilute, it becomes less viscous and can flow. At elevated temperature, the rate of releasing clay particles into water has increased. Due to the presence of DDL, temperature leads to an increase repulsion in the diffuse double layer (Pusch et al., 1990; Ye et al., 2013).

Bentonite erosion happens when the groundwater velocities are in a range of 10^{-5} to 10^{-4} m/s (Kurosawa et al., 1999). From physical models and experiments performed by Pusch (1999), it indicated a high flow rate could cause an erosion of a fully water saturated bentonite clay with the critical flow velocities of 10^{-4} m/s for tearing off 0.5

μm particles, and 10^{-6} μm/s for aggregates larger than 50 μm. Gravity produces frictional resistance for larger particles. The smaller particles with a diameter of 0.1 to 0.2 μm are less apt to be torn off than bigger aggregates. In this study, experimental results in Fig. 7.4 show that the average sizes of the bentonite particles in colloidal solution range from 237 nm to 1060 nm.

7.3.2. Temperature effects on physical stability of bentonite plugs in P&A

In this chapter, a simple calculation is conducted in the context of P&A. According to the average hydrodynamic diameter d_h of the particles, the diffusion rate D_r is calculated by using the Stokes-Einstein equation (Hiemenz and Rajagopalan, 1997):

$$D_r = \frac{kT}{12\pi\eta d_h} \tag{7.1}$$

where k is the Boltzmann constant, T is the absolute temperature, η is the viscosity of the water. The diffusion rates are 3.2 cm^2/year at 25°C and 3.9 cm^2/year at 60°C. The traditional length of cement plug is at least 20 m (Towler et al., 2020). Baik et al. (2007) assumed that 10 % of the host rock consists of a fracture pore space where bentonite particle might escape. Bentonite clay plugs as an alternative sealing material is assumed to be placed in an abandoned well with a diameter of 3.5 inches (=8.89 cm) (Tower et al., 2016). The possible loss mass after time t might be calculated with groundwater at a dilute density of C_0= 0.01 g/cm^3 (Grindrod et al., 1999):

$$\text{Emplaced mass (g)} \approx 1.4\pi r^2 h = 173795.5 \tag{7.2}$$

$$\text{Loss mass (g)} \approx 2C_0(D_r t/\pi)^{1/2}(2\pi r h)(0.1) \tag{7.3}$$

In terms of longevity, the sealing material is expected to perform for at least 1000 years as engineered barrier in the oil and gas industry (AMEC, 2014). Based on the assumption of t (=1000 years), the loss mass can be obtained from Eq. (7.3). The fraction of loss mass is estimated to be small (i.e., at 25°C 3564.7/173795.5=0.020; at 60°C, the loss fraction is up to 3935.6/173795.5=0.022). Furthermore, the fraction of loss mass after 10000 years is estimated to 0.114 and 0.126, respectively. Thus, the erosion of bentonite by a flowing groundwater would not significantly reduce the

physical stability. Compared with the weight of bentonite plugs, the magnitude of swelling pressure is negligible (Towler et al., 2020). To evaluate the mechanical stability of bentonite plugs, the failure mechanism of bentonite plugs is dependent on other factors, like the salinity of flowing water and pressure, which can be conducted.

7.5. Conclusions

The free swelling of bentonite leads to volume expansion due to water absorption, which in turn leads to colloid generation and density reduction of bentonite. Considering the geothermal conditions in a repository and the presence of hydraulically active fractures in the host rock, it is important to understand the temperature effects on colloid detachment. In this chapter, the temperature effects on the erosion of the bentonite surface were analysed.

Experimental results showed that surface erosion of bentonite was observed at the water flow rate used (40 mL/day). The swelling pressure contributed to the release of clay particles at the initial phase. Then a slower erosion rate was established with a constant decrease of swelling pressure. At higher temperature, the time taken to reach equilibrium state was shortened. Furthermore, temperature increased the colloid generation rate. The increase of repulsion possibly contributed to the reduction of the average colloid particle size at higher temperature. A simple simulation with in situ data was conducted for performance assessment of well plugging and abandonment. Although the swelling pressure showed a significant drop at elevated temperature with a loss of mass, the erosion of bentonite would not affect the physical stability of bentonite plugs. The change of hydraulic conductivity or chemical transport were suggested for further studies to underpin safety assessment.

CHAPTER **EIGHT**

8. Conclusions and further work

8.1. Conclusions

With the aim to advance the understanding of the hydro-mechanical behaviour of bentonite at elevated temperature, this work presented and discussed the results of several experimental and theoretical investigations.

A bespoke high pressure, high temperature constant strain rate oedometer was designed and commissioned to develop an understanding of i) the swelling pressure response of pre-saturated compacted bentonite to the increase of temperature and ii) the swelling pressure development during saturation at elevated temperature. The measurements were extended to evaluate the effects of elevated temperature on hydraulic conductivity of samples studied for both series of experiments.

The properties of the Voclay bentonite were determined according to the standard laboratory tests prior to experimental programme. The swelling pressure of compacted bentonite was measured by constant volume tests at different temperature. The effects of dry density, hydraulic gradients, and temperature on the swelling pressure of compacted bentonite were investigated. The microstructure effects on compacted bentonite at elevated temperature were studied.

The theoretical work based on the DDL theory was conducted for the estimation of swelling pressure of compacted bentonite at different temperature. An attempt was made to consider the effects of the formation of tactoids on the theoretical calculation. The proposed model to predict the swelling pressure of compacted bentonite was established by the combination of regular solid-solution theory and diffuse double layer theory. The thermodynamic parameters were introduced to study the fraction of hydrous smectite due to the dominated hydration force between interlayer, particularly at relatively high dry densities. The experiments on surface erosion of compacted bentonite at elevated temperature were conducted to explore thermal effects on the

colloid generation.

This program aimed to fully characterise the bentonite and provide the technical evidence to support the application for sealing repositories (i.e., HLW disposal and P&A). The knowledge of the effects of elevated temperature on porosity and pore-water in compacted bentonite is crucial for predicting the evolution of sealing materials during the operational phase. To undertake detailed technical assessments of performance under different conditions, it is of great significance to understand how the selection of sealing materials for their hydro-mechanical behaviour meet the need for desirable performance. Overall, the following conclusions are drawn.

(1) The swelling pressure of compacted Voclay (SPV200) bentonite increased with the increase of dry density of smectite. The swelling pressure decreased with increasing temperature from 25°C to 80°C for all three dry densities studied. The swelling pressure reduction was much larger for higher density samples, indicating a larger exchange of pore water in the microstructure system of the clay. The response of samples saturated at elevated temperature indicated an acceleration of the hydration rate to reach the new pressure equilibrium. The temperature effects on swelling pressure were limited in terms of mechanical stability in the applications of HLW disposal and P&A.

(2) An increase of hydraulic conductivity with temperature was consistently observed across the densities studied. Larger increase of hydraulic conductivity was observed for lower density samples. Increasing hydraulic conductivity was observed with increasing hydraulic gradient, which was further enhanced at elevated temperatures. These responses were explained with the rearrangement of pore water in the microstructure and with changes to water mobility due to changes of its physical and retention properties with temperature.

(3) An approach to predict the swelling pressure of compacted bentonite based on the diffuse double layer theory was presented. Modified equations were suggested in terms of the relationship between void ratio and the number of unit layers per particle of smectite. The computed swelling pressure and the reported experimental

data were presented for ten kinds of bentonite, and it was shown that the inclusion of microstructure characteristics in the DDL theory can significantly improve the accuracy of the prediction for a range of bentonite types and compaction degrees. Among the parameters studied, considerable impact, yet a level of uncertainty was found to be related to the specific surface area. By the modified DDL it was shown that the formation of clay particles had a significant influence on the swelling pressure. The relationship between size of aggregates and micro/macro pores was rebuilt. Due to the unlikely presence of DDL water in interlayer spaces, the variation of interaction forces between aggregates could be evaluated from knowledge of the fraction of macro pores.

(4) A combination of regular solid solution model and DDL model was introduced to characterise the development of swelling pressure of compacted bentonite at elevated temperature. In this new model, the swelling pressure of compacted bentonite comprises of the hydration force between interlayers and the osmotic pressure between the particles. The distance between aggregates was modified as the temperature effects on the properties of pore water. Through the estimation of pore change, it was found that temperature changes induced water mass exchange between interlayer and interparticle space. The interlayer volumetric water content decreased with increasing temperature, and the dominated hydration force decreased consequently. The advantage of this new model is that it provides the evolution of micro/macro pore with the change of temperature, which allows for better understanding the hydraulic and transport properties under temperature variations.

(5) The temperature affects the specific surface area due the formation of clay particles. For compacted FEBEX bentonite (calcium-montmorillonite), the number of stacked layers per particle increased due to the electrostatic ion-ion correlation effects. While for compacted MX-80 bentonite (sodium-montmorillonite), the number of stacked layers per particle decreased as the electrostatic interaction between the particles is repulsive increasing with temperature.

(6) The increase of temperature increased the eroded rate of compacted bentonite. The diffusion rate of clay particles increased at elevated temperature. The increase of repulsion contributed to the average particle size of colloid decreases at higher temperature.

Regarding to the application of Voclay (SPV) bentonite in HLW disposal and P&A of wells, a range of dry densities of compacted bentonite are considered. In HLW disposal, the lower boundary for saturated density of clay buffer is required to reach 1950 kg/m^3 (Posiva, 2009). The compacted Voclay bentonite at a dry density of 1.7 Mg/m^3 can be potentially applied as the hydraulic and mechanical properties meet the requirement of design. In P&A, the dry density of bentonite plug is estimated larger than 1.0 kg/m^3 from the field tests (Towler et al., 2016). The compacted Voclay bentonite at a dry density of 1.4 Mg/m^3 shows a much higher resilience under temperature change. Overall, for further evaluation, temperature effects must be considered to evaluate the colloid generation which can facilitate pollutants migration through rock fractures. In situ tests and chemical process are needed to better understand the effects of temperature in the sealing system from a long-term view.

8.2. Further work

As this research lays the focus on the applications of compacted bentonite in HLW disposal and P&A, future investigation among the areas are following:

(a) In sealing repositories, the compacted bentonite can be subjected to the intrusion of salinity water. Experimental work needs to be conducted with NaCl solution and $CaCl_2$ solution to assess the hydro-mechanical behaviour of compacted bentonite.

(b) The average number of unit layers per particle could be estimated by the hydraulic behaviour. The influence of pore changes at thermal effects on hydraulic conductivity needs to be studied theoretically with a comparison of hydraulic properties in previous studies.

(c) In the scenario of P&A, the shear strength and the lodgement pressure of compacted bentonite as plugs are crucial for the emplacement work. These mechanical properties depend on many factors such as the diameter of wells and the loading,

and require further experimental investigations.

(d) For the considerations of both sealing repositories (HLW disposal and P&A), the chemical effect on erosion of compacted bentonite needs to be considered for the stability of sealing material.

(e) The stability of generated colloids at elevated temperature can possibly influence the transport of radionuclides. In this area, work needs to be undertaken to understand the chemical processes at elevated temperatures This investigation can be extended for the application of HLW disposal for the safety assessment.

9. References

Achang, M., Yanyao, L., Radonjic, M., 2020. A review of past, present, and future technologies for permanent plugging and abandonment of wellbores and restoration of subsurface geologic barriers. Environmental Engineering Science, 37(6), 395-408.

AECL, 1994. Environmental Impact Statement on the Concept for Disposal of Canada's Nuclear Fuel Waste. AECL technical report AECL-10711.

Ahmed, S., Salehi, S., 2021. Failure Mechanisms of the Wellbore Mechanical Barrier Systems: Implications for Well Integrity. Journal of Energy Resources Technology, 143(7), 073007.

Agus, S. S., Schanz, T., 2008. A method for predicting swelling pressure of compacted bentonites. Acta Geotech. 3, 125–137.

Alabi, O. O., Popoola, O. I., Adegoke, J. A., 2012. Modification of Darcy's Law for Extremely Fine-Grained Soils. Electron. J. Geotech. Eng., 17, 1305-1321.

Albarran, N., Missana, T., Garcia-Gutierrez, M., Alonso, U., Mingarro, M., 2011. Strontium migration in a crystalline medium: effects of the presence of bentonite colloids. J. Contam. Hydrol. 122, 76–85.

Albarran, N., Degueldre, C., Missana, T., Alonso, U., García-Gutiérrez, M., López, T., 2014. Size distribution analysis of colloid generated from compacted bentonite in low ionic strength aqueous solutions. Appl. Clay Sci. 95, 284–293.

Al-Taie, L., Pusch, R.,g Knutsson, S., 2014. Hydraulic properties of smectite rich clay controlled by hydraulic gradients and filter types. Appl. Clay Sci. 87, 73–80.

Alonso, U., Missana, T., Fernández, A. M., García-Gutiérrez, M., 2018. Erosion behaviour of raw bentonites under compacted and confined conditions: Relevance of smectite content and clay/water interactions. Applied Geochemistry, 94, 11-20.

Amec Foster Wheeler., 2016. Sealing Site Investigation Boreholes: Phase 2. Task 5: Techniques used in the oil and gas industry for placing materials in boreholes. Potential application to generic sealing concepts for the RWM Siting Programme. Amec foster Wheeler.

Anderson, R. L., Ratcliffe, I., Greenwell, H. C., Williams, P. A., Cliffe, S., Coveney, P. V., 2010. Clay Swelling a Challenge in the Oilfield. Earth-Sci. Rev., 98, 201-216.

ANDRA ,2005. Dossier 2005 Argile: Architecture and management of a geological repository. ANDRA. Châtenay-Malabry, France.

Appelo, C.A.J., 2013. A review of porosity and diffusion in bentonite. Working report 2013-29, Posiva, Finland.

Bag, R., Rabbani, A., 2017. Effect of temperature on swelling pressure and compressibility characteristics of soil. Appl. Clay Sci. 136, 1–7.

Bag, R., 2011. Coupled thermo-hydro-mechanical-chemical behaviour of MX80 bentonite in geotechnical applications (Doctoral dissertation, Cardiff University).

Baik, M. H., Cho, W. J., Hahn, P. S., 2007. Erosion of bentonite particles at the interface of a compacted bentonite and a fractured granite. Engineering Geology, 91(2-4),

229-239.
Barnichon J.D., Deleruyelle F., 2009. Sealing experiments at the Tournemire URL. In:Towards convergence of technical nuclear safety practices in Europe, EUROSAFE.
Bel, J., Bernier, F., 2001. Temperature criterion related to clay-based backfill materials in the framework of a geological repository of heat producing radioactive waste. In: Proceedings of ICEM 2001, October 1–4, Bruges, 6 pp.
Bessho, K., Degueldre, C., 2009. Generation and sedimentation of colloidal bentonite particles in water. Appl. Clay Sci. 43, 253-259.
Birgersson, M., Boergesson, L., Hedstroem, M., Karnland, O., Nilsson, U., 2009. Bentonite erosion. Final report.
Bolt, G. H. Physico-chemical analysis of the compressibility of pure clays. Geotechnique 6, 86–93 (1956).
Bouby, M., Geckeis, H., Lützenkirchen, J., Mihai, S., Schäfer, T., 2011. Interaction of bentonite colloids with Cs, Eu, Th and U in presence of humic acid: a flow field-flow fractionation study. Geochim. Cosmochim. Acta 75, 3866–3880.
Bourg, I.C., Bourg, A.C.M., Sposito, G., 2003. Modeling diffusion and adsorption in compacted bentonite: a critical review. J. Contam. Hydrol. 61, 293–302.
Bourg, I.C., Sposito, G., Bourg, A.C.M., 2006. Tracer diffusion in compacted water-saturated bentonite. Clays Clay Miner. 54, 363–374.
Börgesson, L., Chijimatsu, M., Fujita, T., Nguyen, T. S., Rutqvist, J., Jing, L., 2001. Thermo-hydro-mechanical characterisation of a bentonite-based buffer material by laboratory tests and numerical back analyses. International Journal of Rock Mechanics and Mining Sciences, 38(1), 95-104.
Börgesson, L., Sandén, T., 2006. Piping and erosion in buffer and backfill materials. Current knowledge. (25) Laird, D. A. Influence of Layer Charge on Swelling of Smectites. Appl. Clay Sci. 2006, 34, 74−87.
BS 1377-2,1990. Soils for civil engineering purposes. Part 2: Classification tests. British Standards Instituition.
Bradbury, M. H., Baeyens, B., 2003. Porewater chemistry in compacted re-saturated MX-80 bentonite. J. Contam. Hydrol. 61, 329–338.
Bucher, F., Müller-Vonmoos, M., 1989. Bentonite as a containment barrier for the disposal of' highly radioactive wastes. Appl. Clay Sci. 4: 157-177.
Busby, J., 2010. Geothermal prospects in the United Kingdom.
Cadene, A., Durand-Vidal, S., Turq, P., Brendle, J., 2005. Study of individual Na-montmorillonite particles size, morphology, and apparent charge. Journal of Colloid and Interface Science, 285, 719-730
Carl, M.A. 2004. Final Closeout Report to Department of Energy, US Interstate Oil and Gas Compact Comission.
Cerato, A. B., Lutenegger, A. J.,2002. Determination of surface area of fine-grained soils by the ethylene glycol monoethyl ether (EGME) method. Geotechnical Testing Journal, 25(3), 315-321.
Celia, M., Bachu, S., Nordbotten, J., Kavetski, D. Gasda, S., 2005. Modeling Critical Leakage Pathways in a Risk Assessment Framework : Representation of

Abandoned Wells. 4th Annu. Conf. carbon capture sequestration DOE/NETL 1-9.
Chapman, L., 1913. A contribution to the theory of electrocapillarity. Philosophical Magazine Series 6 25 (148), 475–481
Chen, Y.G., Jia, L.Y., Li, Q., Ye, W.M., Cui, Y.J., Chen, B., 2017. Swelling deformation of compacted GMZ bentonite experiencing chemical cycles of sodium-calcium exchange and salinization-desalinization effect. Appl. Clay Sci. 141, 55–63.
Chen, T., Sedighi, M., Jivkov, A. P., Seetharam, S. C., 2020. A model for hydraulic conductivity of compacted bentonite–inclusion of microstructure effects under confined wetting. Géotechnique, 1-14.
China Atomic Energy Authority (CAEA), 2006. R&D guidelines for the geological disposal of high-level radioactive waste in China. Beijing: CAEA; (in Chinese).
Cho, W.J., Lee, J.O., Chun, K.S., 1999. The temperature effects on hydraulic conductivity of compacted bentonite. Appl. Clay Sci. 14, 47-58.
Cho, W.J., Lee, J.O., Kang, C.H., 2000. Influence of temperature elevation on the sealing performance of a potential buffer material for a high-level radioactive waste repository. Ann. Nucl. Energy 27, 1271-1284.
Cleall, P. J., Singh, R. M., Thomas, H. R., 2013. Vapour transfer in unsaturated compacted bentonite. Géotechnique, 63(11), 957-964.
Cui, Y. J., Sultan, N., Delage, P., 2000. A thermo-mechanical model for saturated clays. Can. Geotech. J. 37, No. 3, 607-620.
Cui, Y. J., 2017. On the hydro-mechanical behaviour of MX80 bentonite-based materials. Journal of Rock Mechanics and Geotechnical Engineering, 9(3), 565-574.
Daniels, K., Harrington, J., Zihms, S., Wiseall, A., 2017. Bentonite permeability at elevated temperature. Geosciences, 7(1), 3.
Daniels, K. A., Harrington, J. F., Sellin, P., Norris, S., 2021. Closing repository void spaces using bentonite: does heat make a difference?.Applied Clay Science,210, 106124.
Delage P., Sultan N., Cui Y.J., 2000. On the thermal consolidation of Boom clay. Can. Geotech. J. 37(2): 343–354.
Delage, P., Marcial, D., Cui, Y. J., Ruiz, X., 2006. Ageing effects in a compacted bentonite: A microstructure approach. Geotechnique 56, 291-304.
Delage P., Cui Y.J., Tang A.M., 2010. Clays in radioactive waste disposal. Journal of Rock Mechanics and Geotechnical Engineering; 2(2):111-23.
Davies, R. J. et al., 2014. Oil and gas wells and their integrity: Implications for shale and unconventional resource exploitation. Mar. Pet. Geol. 56, 239-254.
Dixon, D. A., Gray, M. N., Hnatiw, D., 1992. Critical gradients and pressures in dense swelling clays. Canadian Geotechnical Journal, 29(6), 1113-1119.
Dixon, D., Graham, J., Gray, M., 1999. Hydraulic conductivity of clays in confined tests under low hydraulic gradients. Can. Geotech. J. 36, pp. 815-825.
Du, J., Zhou, A., Lin, X., Bu, Y., Kodikara, J., 2021. Prediction of swelling pressure of expansive soil using an improved molecular dynamics approach combining diffuse double layer theory. Applied Clay Science, 203, 105998.
ENRESA, 2000. FEBEX project. Full-scale Engineered Barriers Experiment for a Deep

Geological Repository for High Level Radioactive Waste in Crystalline Host Rock. Final Report. Publicacion Tecnica ENRESA 1/2000, Madrid (354 pp.).

Englehardt, J., Wilson, M. J., & Woody, F. (2001). New Abandonment Technology New Materials and Placement Techniques. SPE Exploration and Production Environmental Conference. https://doi.org/10.2118/66496-MS

Faisal, H.M.N., Katti, K.S., Katti, D.R., 2020. Molecular mechanics of the swelling clay tactoid under compression, tension and shear. Appl. Clay Sci. In press. https://doi. org/10.1016/j.clay.2020.105908.

Fernández, A. M., Baeyens, B., Bradbury, M., Rivas, P., 2004. Analysis of the porewater chemical composition of a Spanish compacted bentonite used in an engineered barrier. Phys. Chem. Earth 29, 105–118.

Fernández, A. M., Rivas, P., 2005. Analysis and distribution of waters in the compacted FEBEX bentonite: pore water chemistry and adsorbed water properties. Advances in understanding engineered clay barriers, 257, 275.

Flopetrol., 2019. Plug and Abandonment (P&A) SandAband. Available at: https://www.flopetrol-wb.com/plug-and-abandonmentpa-sandaband.

Fredlund, D.G.,2006. Unsaturated soil mechanics in engineering practice. J. Geotech. Geoenviron. 132:286-321.

Gatabin, C., Talandier, J., Collin, F., Charlier, R., Dieudonne, A.C., 2016. Competing effects of volume change and water uptake on the water retention behaviour of a compacted MX-80 bentonite/sand mixture. Appl. Clay Sci. 121-122, 57-62.

Gates, W. P., Bouazza, A., Churchman, G. J., 2009. Bentonite clay keeps pollutants at bay. Elements, 5(2), 105-110.

Gens, A., Alcoverro, J., Blaheta, R., Hasal, M., et al., 2021. HM and THM interactions in bentonite engineered barriers for nuclear waste disposal. International Journal of Rock Mechanics and Mining Sciences,137, 104572.

Gens, A., Alonso, E., 1992. A framework for the behavior of unsaturated clay. Canadian Geotechnical Journal 29, 1013–1032.

Gouy, G. 1910. Electric charge on the surface of an electrolyte. Journal of Physics, 4(9): 457. Chapman, D.L. 1913. A contribution to the theory of electro- capillarity. Philosophical Magazine, 25: 475–481.

Grindrod, P., Peletier, M., Takase, H., 1999. Mechanical interaction between swelling compacted clay and fractured rock, and the leaching of clay colloids. Eng. Geol. 54, 159–165.

Hausmannova, L., Vasicek, R., 2014. Measuring hydraulic conductivity and swelling pressure under high hydraulic gradients. Geological Society, London, Special Publications, 400(1), 293-301.

Hensen, E. J., Smit, B., 2002. Why clays swell. The Journal of Physical Chemistry B, 106(49), 12664-12667.

Hiemenz, P.C., Rajagopalan, R., 1997. Principles of Colloid and Surface Chemistry, 3rd ed. Marcel Dekker, New York.

Hsiao, Y. W., Hedström, M., 2017. Swelling pressure in systems with Na-montmorillonite and neutral surfaces: a molecular dynamics study. The Journal of Physical Chemistry C,121(47), 26414-26423.

Hsu, J. P., Kuo, Y. C., 1997. The critical coagulation concentration of counterions: Spherical particles in asymmetric electrolyte solutions. Journal of colloid and interface science, 185(2), 530-537.

Holmboe, M., Wold, S., Jonsson, M., 2012. Porosity investigation of compacted bentonite using XRD profile modeling. Journal of Contaminant Hydrology, 128(1-4), 19-32.

Holl, H. G., Scheuermann, A., 2018. Characterisation of geomechanical properties of bentonite clay used for plug and abandonment operations of coal seam gas wells. Journal of Minerals and Materials Characterization and Engineering, 6(2), 218-234.

Holl, H. G., 2019. Hydraulic testing of compacted bentonite used for plug and abandonment operations. Journal of Minerals and Materials Characterization and Engineering, 7(5), 261-278.

Hopmans, J. W., Dane, J. H. ,1986. Temperature Dependence of Soil Hydraulic Properties. Soil Science Society of America Journal, 50(1), 4-9.

IEAE, 1983. Geoenvironment and waste disposal.

Idemitsu, K., Tachi, Y., Furuya, H., Inagaki, Y., Arima, T., 1996. Diffusion of uranium in compacted bentonites in the reducing condition with corrosion products of iron. Mater. Res. Soc. Symp. Proc. 412, 683-690.

Imbert, C., Villar, M.V., 2006. Hydro-mechanical response of a bentonite pellets/powder mixture upon infiltration. Appl. Clay Sci. 32, 197–209.

Jacinto, A. C., Villar, M. V., Gómez-Espina, R., Ledesma, A., 2009. Adaptation of the van Genuchten expression to the effects of temperature and density for compacted bentonites. Appl. Clay Sci. 42, 575-582.

Jacinto, A. C., Villar, M. V., Ledesma, A., 2012. Influence of water density on the water-retention curve of expansive clays. Geotechnique 62, 657-667.

James, M.C., 1996. Using coarse ground bentonite to plug abandoned holes. Water Well Journal 50, 44.

Jia, L. Y., Chen, Y. G., Ye, W. M., Cui, Y. J., 2019. Effects of a simulated gap on anisotropic swelling pressure of compacted GMZ bentonite. Engineering Geology,248, 155-163.

Johnson, L.H., Leneveu, D.M., Shoesmith, D.W., Oscarson, D.W., Gray, M.N., Lemire, R.J., Garisto, N.C., 1994. The vault model for postclosure assessment. AECL Research Report, AECL-10714, Canada, 404 pp.

JNC, 2000. H12: Project to Establish the Scientific and Technical Basis for HLW Disposal in Japan, Project Overview Report. JNC Technical Report TN1410 2000-001, Japan Nuclear Cycle Development Institute, Tokaimura, Japan.

Juvankoski, M., 2010. Description of Basic Design for Buffer (Working Report 2009–131). Technical Report Eurajoki, Finland.

Kalea, R.C., Ravi, K., 2019. Influence of thermal history on swell pressures of compacted bentonite, Process Safety and Environmental Protection, 123, 199-205.

Kallay, N., Barouch, E., Matijevic, E., 1987. Diffusional detachment of colloidal particles from solid7solution interfaces. Adv. Colloid Interface Sci. 27, 1-42.

Khan, M. I., 2012. Hydraulic conductivity of moderate and highly dense expansive

clays.
Kang, M., Christian, S., Celia, M. A., Mauzerall, D. L., Bill, M., Miller, A. R., et al., 2016. Identification and characterization of high methane-emitting abandoned oil and gas wells. Proceedings of the National Academy of Sciences of the United States of America, 113(48), 13636–13641.
Karnland, O., 1997. Bentonite swelling pressure in strong NaCl solutions. Correlation between model calculations and experimentally determined data. SKB Tech. Rep. 30, 30.
Karnland, O., Nilsson, U., Weber, H., Wersin, P., 2008. Sealing ability of Wyoming bentonite pellets foreseen as buffer material–Laboratory results. Physics and Chemistry of the Earth, Parts A/B/C, 33, S472-S475.
Karnland, O., 2010. Chemical and Mineralogical Characterization of the Bentonite Buffer for the Acceptance Control Procedure in a KBS-3 Repository; SKB TR-10-60.
Katti, K., Katti, D., 2001. Effect of clay-water interactions on swelling in montmorillonite clay. Department of Civil Engineering and Construction North Dakota State University, Fargo.
Kjellander, R., Marcelja, S., Pashley, R. M., Quirk, J. P., 1988. Double-layer ion correlation forces restrict calcium-clay swelling. The Journal of Physical Chemistry, 92(23), 6489-6492.
Komine, H., Ogata, N., 1994. Experimental study on swelling characteristics of compacted bentonite, Can. Geotech. J., 31, 478–490.
Komine, H., Ogata, N., 1996. Prediction for swelling characteristics of compacted bentonite. Canadian Geotechnical Journal,33(1), 11-22.
Komine, H., Ogata, N., 1999. Experimental study on swelling characteristics of sand-bentonite mixture for nuclear waste disposal. Soils and foundations, 39(2), 83-97.
Komine, H., 2004. Simplified evaluation for swelling characteristics of bentonites. Eng. Geol. 71, 265–279.
Komine, H., 2008. Theoretical equations on hydraulic conductivities of bentonite-based buffer and backfill for underground disposal of radioactive wastes. J. Geotech. Geoenviron. Eng. 134(4), 497-508.
Kozaki, T., Liu, J., Sato, S. (2008). Diffusion mechanism of sodium ions in compacted montmorillonite under different NaCl concentration. Physics and Chemistry of the Earth, Parts A/B/C, 33(14-16), 957-961.
Kiran, R., Teodoriu, C., Dadmohammadi, Y., Nygaard, R., Wood, D., Mokhtari, M., Salehi, S., 2017. Identification and evaluation of well integrity and causes of failure of well integrity barriers (A review).m Journal of Natural Gas Science and Engineering, 45, 511-526.
Kurosawa, S., Kato, H., Ueta, S., Yokoyama, K., Fujihara, H., 1999. Erosion properties and dispersion-flocculation behavior of bentonite particles. Mater. Res. Soc. Symp. Proc. 556, 679–686.
Lajudie, A., Raynal, J., Petit, J.-C., Toulhoat, P., 1994. Clay-based materials for engineered barriers: a review. In: Proc. XVIII Int. Symp. Sci. Basis Nucl. Waste Manage., MRS'94, Kyoto, Japan, vol. 353, pp. 221-230.

Laird, D. A., 2006. Influence of layer charge on swelling of smectites. Applied clay science, 34(1-4), 74-87.

Lee, J.H., Lee, M.S., Choi, H.J., Choi, J.W. Temperature Effect on the Swelling Pressure of a Domestic Compacted Bentonite Buffer. J. Nucl. Fuel Cycle Waste Technol. 8, 207–213 (2010).

Lee, J. O., Lim, J. G., Kang, I. M. & Kwon, S., 2012. Swelling pressures of compacted Ca-bentonite. Eng. Geol. 129-130, 20-26.

Li, X.L., Bastiaens, W., Van, M.P., Verstricht J., Chen G.J., Weetjens, E., Sillen, X., 2010. Design and development of large-scale in-situ PRACLAY heater test and horizontal high-level radioactive waste disposal gallery seal test in Belgian HADES. Journal of Rock Mechanics and Geotechnical Engineering; 2(2):103-10.

Li, X. M., WANG, Y. H., 2003. Regressive analysis of swelling and shrinkage deformationrule of expansive soils. Journal of Xiangtan Mining Institute.

Li, T., Rutqvist, J., Hu, M., 2021. TOUGH-RFPA: Coupled thermal-hydraulic-mechanical Rock Failure Process Analysis with application to deep geothermal wells. International Journal of Rock Mechanics and Mining Sciences, 142, 104726.

Lingnau, B. E., Graham, J., Yarechewski, D., Tanaka, N., Gray, M. N., 1996. Effects of temperature on strength and compressibility of sand-bentonite buffer. Engineering Geology, 41(1-4), 103-115.

Liu, J., Yamada, N., Kozaki, T., Sato, S., Ohashi, H., 2003. Effect of silica sand on activation energy for diffusion of sodium ions in montmorillonite and silica sand mixture. J. Contam. Hydrol. 61, 85-93.

Liu, L., 2013. Prediction of swelling pressures of different types of bentonite in dilute solutions. Colloids Surfaces A Physicochem. Eng. Asp. 434, 303–318.

Low, P. F., Margheim, J. F., 1979. The swelling of clay: I. Basic concepts and empirical equations. Soil Science Society of America Journal,43(3), 473-481.

Low, P.F., 1991. Structural and other forces involved in swelling of clays. In the proceedings of NATO advanced workshop on clay swelling and expansive soils, Cornell University Ithaca, New York.

Lloret, A., Villar, M. V., Sanchez, M., Gens, A., Pintado, X., Alonso, E. E., 2003. Mechanical behaviour of heavily compacted bentonite under high suction changes. Géotechnique, 53(1), 27-40.

Lloret, A., Villar, M.V., 2007. Advances on the knowledge of the thermo-hydromechanical behaviour of heavily compacted FEBEX bentonite. Physics and Chemistry of the Earth 32 (8-14), 701-715.

Ma, C., Hueckel, T., 1992. Stress and pore pressure in saturated clay subjected to heat from radioactive waste: a numerical simulation. Can. Geotech. J. 29, 1087.

Ma C., Hueckel T. Thermomechanical effects on adsorbed water in clays around a heat source. International Journal for Numerical and Analytical Methods in Geomechanics, 1993, 17 (3): 175–196.

Madsen, F. T., Müller-Vonmoos, M., 1989. The swelling behaviour of clays. Applied Clay Science, 4(2), 143-156.

Madsen, F.T., 1998. Clay mineralogical investigations related to nuclear waste disposal. Clay Miner. 33, 109-129.

Manassero, M., Dominijanni, A., Fratalocchi, E., Mazzieri, F., Pasqualini, E., & Boffa, G., 2016. About the state parameters of active clays. In Geoenvironmental Engineering (pp. 99-110).

Malmberg C. G., Maryott A. A., 1956. Dielectric Constant of Water from 0°C to 100 °C. J. Res. Natl. Bur. Stand., 56.1.

Marcial, D., Delage, P., Cui, Y. J., 2002. On the high stress compression of bentonites. Canadian Geotechnical Journal, 39(4), 812-820.

Martin, P.L., Barcala, J.M., Huertas, F., 2006. Large-scale and long-term coupled thermo-hydro-mechanic experiments with bentonite: the febex mock-up test. J. Iber. Geol. 32 (2), 259–282.

Massat, L., Cuisinier, O., Bihannic, I., Claret, F., Pelletier, M., Masrouri, F., Gaboreau, S., 2016. Swelling pressure development and inter-aggregate porosity evolution upon hydration of a compacted swelling clay. Appl. Clay Sci. 124-125, 197-210.

Melkior, T., et al., 2009. Na^+ and HTO diffusion in compacted bentonite: Effect of surface chemistry and related texture. Journal of Hydrology, 370(1-4), 9-20.

Meleshyn, A., Bunnenberg, C., 2005. The gap between crystalline and osmotic swelling of Na-montmorillonite: A Monte Carlo study. The Journal of chemical physics, 122(3), 034705.

Michot, L. J., Bihannic, I., Porsch, K., Maddi, S., Baravian, C., Mougel, J., Levitz, P., 2004. Phase diagrams of Wyoming Na-montmorillonite clay. Influence of particle anisotropy. Langmuir, 20(25), 10829-10837.

Michot, L. J., et al., 2013. Coagulation of Na-montmorillonite by inorganic cations at neutral pH. A combined transmission X-ray microscopy, small angle and wide angle X-ray scattering study. Langmuir, 29(10), 3500-3510.

Missana, T., Alonso, Ú., Turrero, M. J., 2003. Generation and stability of bentonite colloids at the bentonite/granite interface of a deep geological radioactive waste repository. Journal of Contaminant Hydrology, 61(1-4), 17-31.

Missana, T., Alonso, Ú., García-Gutiérrez, M., Mingarro, M., 2008. Role of bentonite colloids on Europium and Plutonium migration in a granite fracture. Appl. Geochem. 23, 1484–1497.

Missana, T., Alonso, U., Albarran, N., García-Gutiérrez, M., Cormenzana, J. L., 2011. Analysis of colloids erosion from the bentonite barrier of a high level radioactive waste repository and implications in safety assessment. Physics and Chemistry of the Earth, Parts A/B/C, 36(17-18), 1607-1615.

Mitchell, J.K., 1993. Fundamentals of Soil Behavior, 2nd ed. Wiley, New York 236–271.

Mitchell, J. K., Soga, K., 2005. Fundamentals of soil behavior (Vol. 3). New York: John Wiley & Sons.

Möri, A., Alexander, W.R., Geckeis, H., Hauser, W., Schäfer, T., Eikenberg, J., Fierz, T., Degueldre, C., Missana, T., 2003. The colloid and radionuclide retardation experiment at the Grimsel Test Site: influence of bentonite colloids on radionuclide migration in a fractured rock. Colloid. Surface. A. 217, 33-47.

NAGRA, 2002. Project Opalinus Clay Safety Report: Demonstration of disposal feasibility for spent fuel, vitrified high-level waste and long-lived intermediate-

level waste (Entsorgungsnachweis) NAGRA Tech. Rep. 02-05, NAGRA, Wettingen, Switzerland.
Navarro, V., De la Morena, G., Yustres, Á., González-Arteaga, J., Asensio, L., 2017. Predicting the swelling pressure of MX-80 bentonite. Applied Clay Science, 149, 51-58.
NDA, 2010. Geological Disposal: Steps Towards Implementation. Nuclear Decommissioning Authority Report NDA/RWMD/013.
Neretnieks, I., Liu, L., Moreno, L., 2009. Mechanisms and models for bentonite erosion.
Norwegian Petroleum Directorate Guidance for Drilling and Well Activity. NORSOK D-010 standard Rev.3 August 2004.
Partheniades, E., 2010. Cohesive Sediments in Open Channels: Properties,Transport, and Applications, Elsevier, New York.
Pandey, S. N., Chaudhuri, A., Kelkar, S., 2017. A coupled thermo-hydro-mechanical modeling of fracture aperture alteration and reservoir deformation during heat extraction from a geothermal reservoir. Geothermics, 65, 17-31.
Pedarla, A., Puppala, A. J., Hoyos, L. R., Vanapalli, S. K., Zapata, C., 2012. SWRC modelling framework for evaluating volume change behavior of expansive soils. In Unsaturated soils: Research and applications (pp. 221-228). Springer, Berlin, Heidelberg.
Pogacnik, J., Elsworth, D., O'Sullivan, M., & O'Sullivan, J., 2016. A damage mechanics approach to the simulation of hydraulic fracturing/shearing around a geothermal injection well. Computers and Geotechnics, 71, 338-351.
Posiva Oy. Image Gallery. Available online: http://posiva.fi/en/media/image_gallery?gfid_2061=92#gallery_2061(accessed on 18 March 2020)
Pusch, R., 1980a. Swelling pressure of highly compacted bentonite. SKBF/KBS technical report: No.80-13
Pusch, R., 1980b. The Permeability of Highly Compacted Bentonite. Swedish Nuclear Fuel and Waste Management Company, Technical Report 80-16.
Pusch, R., 1982. Mineral-water interactions and their influence on the physical behaviour of highly compacted Na bentonite, Can. Geotech. J., 19, 381-387.
Pusch, R., 1983. Stability of Bentonite Gels in Crystalline Rock — Physical Aspects. SKBF/KBS TR-83-04. Swedish Nuclear Fuel and Waste Management Co., Stockholm.
Pusch, R., Karnland, O., Hokmark, H., 1990. GMM a general microstructural model for qualitative and quantitative studies of smectite clays. SKB Technical Report 90–43.
Pusch, R., 1999. Clay Colloid Formation and Release from MX-80 Buffer. SKB TR-99-31. Swedish Nuclear Fuel and Waste Management Co., Stockholm.
Pusch, R., 2001. The microstructure of MX-80 clay with respect to its bulk physical properties under different environmental conditions (No. SKB-TR--01-08). Swedish Nuclear Fuel and Waste Management Co.
Pusch, R., Bluemling, P., Johnson, L., 2003. Performance of strongly compressed MX-80 pellets under repository-like conditions. Appl. Clay Sci. 23, 239-244.
Pusch, R., 2006. Clays and nuclear waste management. In: Bergaya F, Theng BKG,

Lagaly G (eds) Handbook of Clay Science. Developments in Clay Science volume 1, Elsevier, Amsterdam, pp 703-716.
Pusch, R., Yong, R. N., 2006. Microstructure of smectite clays and engineering performance. CRC Press.
Pusch, R., 2008. Geological Storage of Highly Radioactive Waste. Current Concepts and Plans for Radioactive Waste Disposal. Springer.
Pusch, R., 2015. Bentonite clay: environmental properties and applications. CRC Press.
Romero, E., Gens, A., Lloret, A., 2001. Temperature effects on the hydraulic behaviour of an unsaturated clay. Geotech. Geol. Eng. 19, 311–332.
Romero, E., Della Vecchia, G., Jommi, C., 2011. An insight into the water retention properties of compacted clayey soils. Geotechnique 61, 313–328.
Rutqvist, J., Börgesson, L., Chijimatsu, M., Nguyen, T. S., Jing, L., Noorishad, J., Tsang, C. F., 2001. Coupled thermo-hydro-mechanical analysis of a heater test in fractured rock and bentonite at Kamaishi Mine - comparison of field results to predictions of four finite element codes. International Journal of Rock Mechanics and Mining Sciences, 38(1), 129–142.
Salles, F., Douillard, J.M., Denoyel, R., Bildstein, O., Jullien, M., Beurroies, I., Van Damme, H., 2009. Hydration sequence of swelling clays: evolutions of specific surface area and hydration energy. J. Colloid Interface Sci. 333 (2), 510–522.
Saiyouri, N., Hicher, P. Y., Tessier, D., 2000. Microstructural approach and transfer water modelling in highly compacted unsaturated swelling clays. Mechanics of Cohesive-frictional Materials: An International Journal on Experiments, Modelling and Computation of Materials and Structures, 5(1), 41-60.
Saiyouri, N., Tessier, D., Hicher, P. Y., 2004. Experimental study of swelling in unsaturated compacted clays. Clay minerals, 39(4), 469-479.
Sato, H., 2008. Thermodynamic model on swelling of bentonite buffer and backfill materials. Physics and Chemistry of the Earth, Parts A/B/C,33, S538-S543.
Schaefer, T., Huber, F., Seher, H., Missana, T., Alonso, U., Kumke, M., Eidner, S., Claret, F., Enzmann, F., 2012. Nanoparticles and their influence on radionuclide mobility in deep geological formations. Appl. Geochem. 27, 390-403.
Schatz, T., Kanerva, N., Martikainen, J., Sane, P., Olin, M., Seppälä, A., Koskinen, K., 2013. Buffer erosion in dilute groundwater (No. POSIVA--12-44). Posiva Oy.
Schanz, T., Tripathy, S., 2009. Swelling pressure of a divalent-rich bentonite: Diffuse double-layer theory revisited. Water Resour. Res. 45, 1–9.
Schanz, T., Khan, M.I., Al-Badran, Y., 2013. An alternative approach for the use of DDL theory to estimate the swelling pressure of bentonites. Appl. Clay Sci. 83–84, 383–390.
Schanz, T., Al-Badran, Y., 2014. Swelling pressure characteristics of compacted Chinese Gaomiaozi bentonite GMZ01. Soils Found. 54, 748–759.
Sedighi, M., 2011. An investigation of hydro-geochemical processes in coupled thermal, hydraulic, chemical and mechanical behaviours of unsaturated soils, PhD Thesis, Cardiff University. http://orca.cf.ac.uk/54236/.
Sedighi, M., Thomas, H. R., 2014. Micro porosity evolution in compacted swelling clays - A chemical approach. Appl. Clay Sci. 101, 608–618.

Sedighi, M., Thomas, H. R., Vardon, P. J., 2018. Reactive transport of chemicals in compacted bentonite under nonisothermal water infiltration. Journal of Geotechnical and Geoenvironmental Engineering, 144(10), 04018075.

Sellin, P., Leupin, O. X., 2013. The use of clay as an engineered barrier in radioactive-waste management–a review. Clays and Clay Minerals, 61(6), 477-498.

Segad, M., Jönsson, B., Cabane, B., 2012. Tactoid Formation in Montmorillonite. J. Phys. Chem. C., 116, 25425−25433.

SKB, 2006. Long-term safety for KBS-3 repositories at Forsmark and Laxemar – a first evaluation, in: Main Report of the SR-Can Project, SKB Technical Report TR- 06-09, Swedish Nuclear Fuel and Waste Management Co., Stockholm, Sweden.

SKB, 2011. Environmental Impact Statement, Interim storage, encapsulation and final disposal of spent nuclear fuel, March 2011, ISBN 978-91-978702-5-2.

Skipper, N.T., Refson, K., McConnell, J.D.C., 1991. Computer simulation of interlayer water in 2:1 clays. J. Chem. Phys. 94 (11), 7434-7445.

Sing, R. M., Thyagaraj, T., Thomas, H. R., 2006. Swelling of compacted clay under osmotic gradients. Géotechnique, 56(10), 707-713.

Singh, R. M., 2007. Experimental and numerical investigation of heat and mass movement in unsaturated clays. Cardiff University (United Kingdom).

Singhal, S., Houston, S.L., Houston W.N., 2014. Swell pressure, matric suction, and matric suction equivalent for undisturbed expansive clays. Can. Geotech. J. 52:356-366

Shirazi, S. M., Kazama, H., Salman, F. A., Othman, F., Akib, S., 2010. Permeability and swelling characteristics of bentonite. Int. J. Phys. Sci. 5, 1647–1659.

Smith, D. E., Wang, Y., Chaturvedi, A., Whitley, H. D., 2006. Molecular Simulations of the Pressure, Temperature, and Chemical Potential Dependencies of Clay Swelling. J. Phys. Chem. B, 110, 20046−20054.

Sposito, G., 1972. Thermodynamics of swelling clay-water systems. Soil Science,114(4), 243-249.

Sridharan, A., Jayadeva, M. S., 1982. Double layer theory and compressibility of clays. Géotechnique, 32(2), 133-144.

Sridharan, A., Choudhury, D., 2002. Swelling pressure of sodium montmorillonites. Géotechnique, 52(6), 459-462.

Sun, W. J., Wei, Z. F., Sun, D. A., Liu, S. Q., Fatahi, B., Wang, X. Q., 2015. Evaluation of the swelling characteristics of bentonite–sand mixtures. Engineering Geology, 199, 1-11.

Sun, H., 2017. Prediction of Swelling Pressure of Compacted Bentonite with Respect to Void Ratio Based on Diffuse Double Layer Theory. In International Congress and Exhibition. Sustainable Civil Infrastructures: Innovative Infrastructure Geotechnology (pp. 89-104). Springer, Cham.

Tang, A. M., Cui, Y. J., Barnel, N., 2008. Thermo-mechanical behaviour of a compacted swelling clay. Géotechnique 58(1), 45-54.

Tang C.S., Tang A.M., Cui Y.J., Delage P., Barnichon J.D., Shi B., 2011. A study of the hydromechanical behaviour of compacted crushed argillite. Engineering Geology;118(3-4):93-103.

Tiller, K. G. and Smith, L. H., 1990. Limitations of EGME Retention to Estimate Surface Area of Soils. Australian Journal of Soil Science, Vol. 28, pp. 1–26.

Thuresson, A., Karnland, O., Jönsson, B., 2016. Anomalous temperature behavior in clay swelling due to ion-ion correlations. EPL (Europhysics Letters),114(3), 38002.

Thuresson, A., Jansson, M., Plivelic, T. S., Skepö, M., 2017. Temperature Response of Charged Colloidal Particles by Mixing Counterions Utilizing Ca2+/Na+ Montmorillonite as Model System. J. Phys. Chem. C 121, 7951–7958.

Tournassat, C., Neaman, A., Villiéras, F., Bosbach, D., Charlet, L., 2003. Nanomorphology of montmorillonite particles: Estimation of the clay edge sorption site density by low-pressure gas adsorption and AFM observations. American Mineralogist, 88. 1989-1995.

Towler, B., Hywel-Evans, D., Firouzi, M., 2020. Failure modes for hydrated bentonite plugs used in well decommissioning operations. Applied Clay Science, 184, 105385.

Towler, B., Firouzi, M., Mortezapour, A., Hywel-Evans, P., 2016. Field trials of the use of hydrated bentonite for decommissioning oil and gas wells. The APPEA Journal 56, 561.

Tripathy, S., Sridharan, A., Schanz, T., 2004. Swelling pressures of compacted bentonites from diffuse double layer theory. 450, 437–450.

Tripathy, S., Bag, R., Thomas, H. R., 2014. Effects of post-compaction residual lateral stress and electrolyte concentration on swelling pressures of a compacted bentonite. Geotechnical and Geological Engineering,32(4), 749-763

Tripathy, S., Bag, R., Thomas, H.R., 2015. Enhanced isothermal effect on swelling pressure of compacted MX80 bentonite. Eng. Geol. for society and territory. 6, 537–539.

Tu, H.Y., Vanapalli, S.K., 2016. Prediction of the variation of swelling pressure and one-dimensional heave of expansive soils with respect to suction using the soil-water retention curve as a tool. Can. Geotech. J. 53:1213-1234.

Uddin, F., 2018. Montmorillonite: An introduction to properties and utilization (pp. 3-23). London: IntechOpen.

van Olphen, H., 1964. An introduction to clay colloid chemistry. Soil Science,97(4), 290.

Viani, B. E., Low, P. F., Roth, C. B., 1983. Direct measurement of the relation between interlayer force and interlayer distance in the swelling of montmorillonite. J. Colloid Interface Sci. 96, 229-244 (1983).

Vieillard, P., Blanc, P., Fialips, C. I., Gailhanou, H., Gaboreau, S., 2011. Hydration thermodynamics of the SWy-1 montmorillonite saturated with alkali and alkaline-earth cations: A predictive model. Geochimica et Cosmochimica Acta 75(19):5664-5685.

Vidal, O., Dubacq, B., 2009. Thermodynamic modelling of clay dehydration, stability and compositional evolution with temperature, pressure and H2O activity. Geochimica et Cosmochimica Acta, 73(21), 6544-6564.

Villar, M.V., Lloret, A., 2004. Influence of temperature on the hydro-mechanical behaviour of a compacted bentonite. Appl. Clay Sci. 26, 337-350.

Villar, M.V., 2005. MX-80 Bentonite. Thermo-Hydro-Mechanical characterisation performed at CIEMAT in the context of the Prototype Project. Informes Técnicos CIEMAT, vol. 1053. Madrid. 39 pp.

Villar, M. V., Lloret, A., 2008. Influence of dry density and water content on the swelling of a compacted bentonite. Applied Clay Science, 39(1-2), 38-49.

Villar, M. V., Gómez-Espina, R., Lloret, A., 2010. Experimental investigation into temperature effect on hydro-mechanical behaviours of bentonite. J. Rock Mech. Geotech. Eng. 2, 71-78.

Villar, M. V., Gómez-Espina, R., & Gutiérrez-Nebot, L. (2012). Basal spacings of smectite in compacted bentonite. Applied clay science, 65, 95-105.

Wang, Q., Tang, A. M., Cui, Y.J., Delage, P., Gatmiri, B., 2012. Experimental study on the swelling behaviour of bentonite/claystone mixture. Engineering Geology; 124:59-66.

Wang, Q., Tang, A. M,. Cui Y.J., Barnichon, J. D,. Delage, P., Ye, W.M., 2013. The effects of technological voids on the hydro-mechanical behaviour of compacted bentonite-sand mixture. Soils and Foundations; 53(2):232-45.

Wang, Q., Cui, Y. J., Minh Tang, A., Xiang-Ling, L., Wei-Min, Y., 2014a. Time- and density-dependent microstructure features of compacted bentonite. Soils Found. 54, 657–666.

Wang, X., Shao, H., Hesser, J., Zhang, C., Wang, W., Kolditz, O., 2014b. Numerical analysis of thermal impact on hydro-mechanical properties of clay. Journal of Rock Mechanics and Geotechnical Engineering, 6(5), 405-416.

Wang, X., Shao, H., Wang, W., Hesser, J., Kolditz, O.,2015. Numerical modeling of heating and hydration experiments on bentonite pellets. Eng. Geol. 198, 94-106.

Wersin, P., Curti, E., Appelo, C. A. J., 2004. Modelling bentonite–water interactions at high solid/liquid ratios: swelling and diffuse double layer effects. Applied Clay Science, 26(1-4), 249-257.

Wheaton, J.R., Regele, S., Bohman, R., Clark, D., Reiten, J.C., 1994. Experiments in subsurface applications of bentonite in Montana. Montana Bureau of Mines and Geology. Memoir 66, 43.

Wilson, M. J., Wilson, L., 2014. Clay mineralogy and shale instability: an alternative conceptual analysis. Clay Minerals, 49(2), 127-145.

Ye, W.M., Wan, M., Chen, B., Chen, Y.G., Cui, Y.J., Wang, J., 2013. Temperature effects on the swelling pressure and saturated hydraulic conductivity of the compacted GMZ01 bentonite. Environ. Earth Sci. 68, 281–288.

Ye, W. M., Zheng, Z. J., Chen, B., Chen, Y. G., Cui, Y. J., Wang, J., 2014. Effects of pH and temperature on the swelling pressure and hydraulic conductivity of compacted GMZ01 bentonite. Appl. Clay Sci.,101, 192-198.

Yong, R.N., Warkentin, B.P. 1975. Soil properties and behaviour. Elsevier, Amsterdam.

Yong, R.N., Mulligan, C.N., Fukue, M., 2006. Geoenvironmental Sustainability. CRC Press, Taylor and Francis.

Zagorščak, R., Sedighi, M., Thomas, H. R., 2016. Effects of thermo-osmosis on hydraulic behavior of saturated clays. International Journal of Geomechanics, 17(3), 04016068.

Zhang, F., Zhang, Z. Z., Low, P. F., Roth, C. B., 1993 The Effect of Temperature on the Swelling of Montmorillonite. Clay Miner., 28, 25−31.

Zhu, C. M., Ye, W. M., Chen, Y. G., Chen, B., Cui, Y. J., 2013. Influence of salt solutions on the swelling pressure and hydraulic conductivity of compacted GMZ01 bentonite. Eng. Geol. 166, 74–80.

Zihms, S. G., Harrington, J. F., 2015. Thermal cycling: impact on bentonite permeability. Mineralogical Magazine,79(6), 1543-1550.

Appendix: the evolution of size distribution of the eroded solutions at elevated temperature

The following figures show the result of size distribution of the collected solutions at 25°C and 60°C in DLS measurements. At 25°C, the presence of larger particles (> 1000nm) can be found before 50 days when the concentration of the collected eroded solutions reaches stable. After 50 days, the size of particles in solutions are basically less than 1000 nm. While at 60°C, the variation of the fraction of larger particles seems to be insignificant. Increasing temperature tends to change the fraction of particles whose sizes is ranging from 100 to 1000 nm.

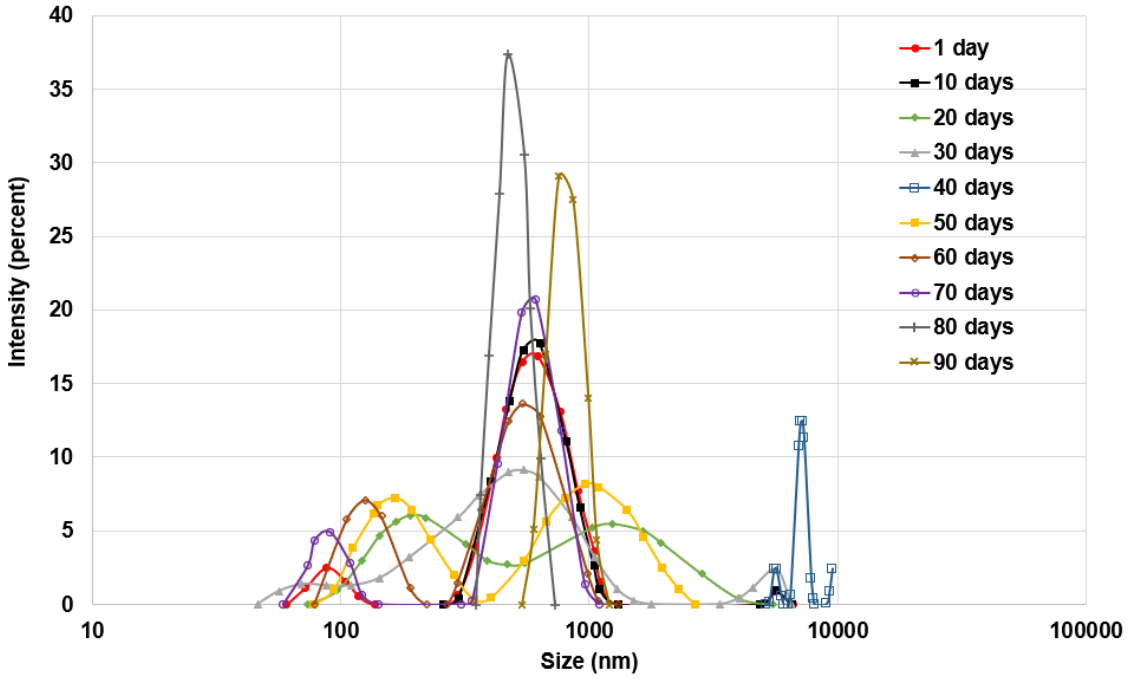

(a) The size fraction of eroded particles conducted at 25°C.

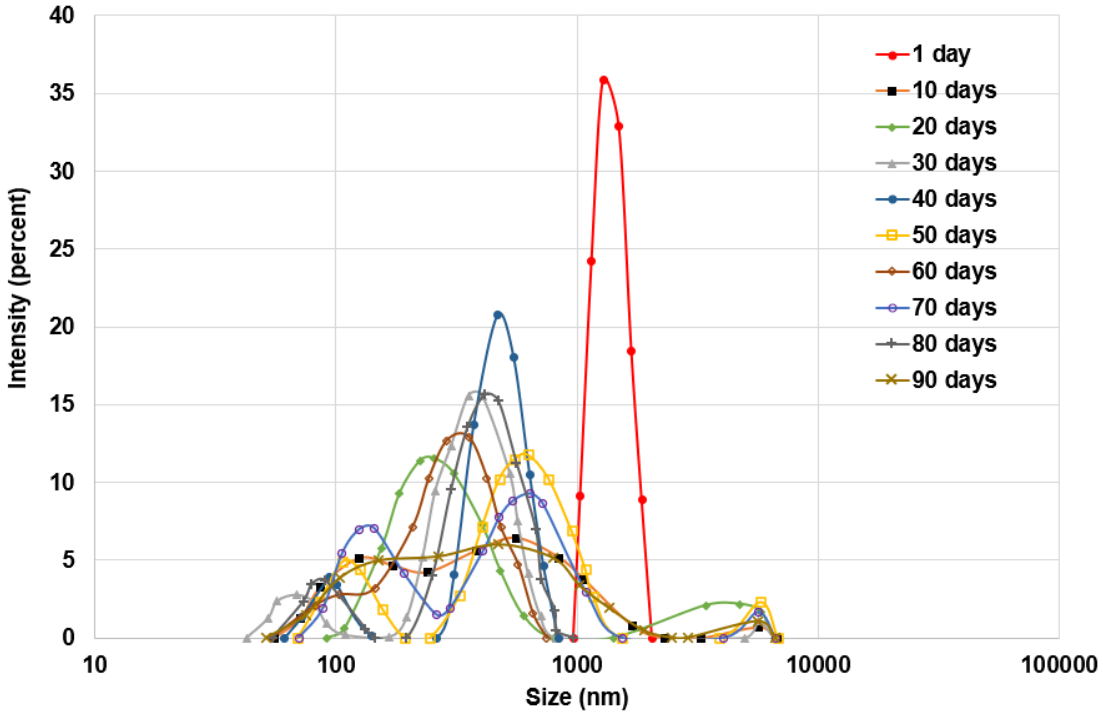

(b) The size fraction of eroded particles conducted at 60°C.